

Doctoral Dissertation (Shinshu University)

**Preparation and characterization of Electrospun Nanofibers
for Apparel and Medical Application**

Doctor of Engineering Thesis

Zeeshan Khatri

**Department of Bioscience and Textile Technology
Interdisciplinary Graduate School of Science and Technology
Shinshu University**

ABSTARCT

Preparation and characterization of Electrospun Nanofibers for Apparel and Medical Application

September 2013

ZEESHAN KHATRI

Dr.Eng. Thesis, Shinshu University

Directed by: Prof. Ick-Soo Kim

The growing application of nanofibers in various fields led the nanofibers research intense in terms of exploring multifunctional properties. Nanofibers in medical have received a great deal of interest especially in tissue engineering scaffold, biosensor and drug delivery applications. Although, the current research is intensively underway that addressing problems associated with nanofiber applications in medical, however, the need is to develop materials really based on nanoscale so that the full advantage of nanotechnology can be taken. Beside, nanofiber technical application, a few patents and papers on nanofibers apparel have been appeared recently. All nanofibers apparel so far reported have demonstrated functional properties but lack the aesthetic properties. Providing aesthetic appealing nanofibers with functional properties, we conducted series of experiments and developed nanofibers for apparel application. This thesis reports the aesthetic and functional properties of nanofibers. The aesthetic properties cover by

investigating dyeability of nanofibers with various dye class and functional properties covers by developing nanofibers substrate for biosensor and nanofiber tubes for nerve guide.

Fashion and casual apparel of cellulose based have widely been used by a consumer due to its outstanding properties of breathability, air permeability, hygroscopicity, no static electricity, biodegradability and show interesting physical properties such as a low density together with high mechanical characteristics. The cellulosic apparels are marketed in the form of white, dyed or printed according the end-user's requirement. We investigated aesthetic properties by producing colored cationic-cellulose nanofibers for the very first time for the potential application of apparel use. The cellulose acetate nanofibers were electrospun followed by deacetylation and cationization to produce functional cationic-cellulose nanofibers and then dyed with anionic reactive dyes. The spectrophotometric measurement of dyed samples was carried out to determine color coordinates and color yield values. The cationic-cellulose nanofibers showed enhanced color yield and dye fixation without addition of an electrolyte in comparison to cellulose nanofibers. The cationization of cellulose nanofibers significantly enhanced the color yield values of around 76% at dye concentrations of 5%. Excellent color fastness results demonstrate that these new colored and breathable materials can potentially be considered as future apparel for casual or fashion.

In another study, webs of cellulose acetate nanofiber were electrospun and dyed with a high energy level CI Disperse Red 167:1 dye and a low energy level CI Disperse Blue 56 dye using the continuous pad-dry-bake method. Results revealed that the high energy level dye produced better color yield than the lower energy level dye. The dyed cellulose acetate nanofibers

produced acceptable colorimetric values, color yield and color fastness. Young's modulus of dyed nanofibers increased by threefold in comparison to the undyed cellulose acetate nanofibers. Scanning electron microscopy images showed good morphology with the smooth surface of the dyed cellulose acetate nanofibers.

The study of functional and dyeing properties of the electrospun nanofibers has recently gained substantial interest. However, the dyeing of nanofibers still in transition phase and faces problem of lower color yield. Owing to the higher surface area of cellulose nanofibers, the color yield obtained is nearly four to five times lower than the conventional cotton fiber. The present work reports on dyeing of cellulose nanofibers with CI reactive black 5 dye via a simple and dual padding method to improve color yield and dye fixation. The color yields were determined by K/S values and color coordinates using spectrophotometer and the results were compared between single and dual padding methods. The dyed cellulose nanofibers were characterized by FTIR, WAXD and FE-SEM. X-ray diffraction studies revealed that the dyed cellulose nanofibers having Cellulose II form and show a better crystallinity than the undyed cellulose nanofibers.

Cellulose Acetate (CA) nanofibers have unique absorption properties and therefore they have been considered a suitable candidate to be used as substrate for biosensor. CA nanofibers webs deserve a special attention because of their very good water retention properties. CA nanofibers based biosensor in certain application come into contact with various liquids and requires high degree of wicking rate to transport liquid to its destination. Cellulose acetate (CA)/ poly vinyl alcohol (PVA) blended nanofibers were prepared via co-electrospinning using double nozzle for jetting cellulose acetate and poly vinyl alcohol independently. The CA/PVA blend nanofibers webs were deacetylated in aqueous alkaline solution to convert CA in to regenerated cellulose and to

remove PVA nanofibers from the raw web. The resultant nanofibers webs were characterized by wicking rate, water contact angle, SEM and FTIR analysis. The results revealed that by varying concentration of PVA solution enhances the wicking rate. Such a nanofibers web may be used in biosensor strip and other medical applications where the high wicking rates are desired.

Recently attempts have been made to develop nanofibers tubes suitable for nerve regeneration made of biodegradable nanofibers. Among all polymeric nanofibers poly (ϵ -caprolactone) (PCL) is distinctively known for better mechanical stability and poly (L-lactic acid) (PLLA) for relatively faster biodegradability. Our purpose of study is to investigate their blending compatibility and the ability to form nanofibers tubes via electrospinning. We electrospun the PCL-PLLA nanofiber tubular using different blend ratios of PCL-PLLA. The electrospun nanofibers were continuously deposited over high speed rotating mandrel to fabricate nanofibers tubes having inner diameter of 2 mm and the wall thickness of 55-65 μm . The diameters of nanofibers were between 715-860 nm. The morphologies of PCL-PLLA nanofibers tubes were examined under Scanning Electron Microscope (SEM), showed better structural stability and formability than the neat PLLA nanofibers. Fourier transform infrared spectroscopy (FTIR) study revealed that the PCL-PLLA blend nanofiber exhibit characteristic peaks of both PCL and PLLA and was composition dependent. Raman and X-ray diffraction studies showed that the increasing PCL ratio in the PCL-PLLA blend increased crystallinity of PCL-PLLA blends. Differential Scanning Calorimetry (DSC) revealed recrystallization peaks in PCL-PLLA blends ratio of 1:2 and 1:1. Based on characterization, the electrospun PCL-PLLA nanofibers tubes is considered to be a better candidate for further in-vivo or in-vitro investigation, and resolve biocompatibility issues in tissue engineering.

ACKNOWLEDGEMENTS

All praises and thanks are to Allah, the Lord of the worlds, the most beneficent, the most merciful for helping me accomplish this work. I would like to thank to my Advisor, Prof Ick Soo Kim for encouragement, kind support, enthusiastic attention, critical discussions, valuable advice and guidance. I would like also thank to our Dr. Kai Wei for his valuable suggestions and kind help during research. Mr Nakashima Ryu deserves special thanks for assisting me in Japanese that made my life very easy in Japan.

I can't forget to praise my mother and father, who gave me the vision to pursue for higher studies and provided a ground to succeed in my life; it's more than the words of acknowledgement. I would like to thank my wife for her love and support during my PhD. My sincerest thanks are due to the past members of our lab Dr Byoung Suhk Kim, Kyu-Oh Kim, Yujin Lee for their help, support and guidance. I also thank to all my Lab colleagues for their technical assistance and allow me to work in a very friendly environment. I am highly indebted to Global COE program for financial support, without which, my PhD would not be possible.

Zeeshan Khatri
Shinshu University
September 2013

Table of Contents

ABSTARCT	ii
ACKNOWLEDGEMENTS	vi
TABLES OF CONTENTS	vii
LIST OF TABLES	xii
LIST OF FIGURES	xiii
LIST OF SCHEMES	xvi
CHAPTER 1 Introduction	1
1.1 BACKGROUND	1
1.1.1 Nanofibers Textile Apparel.....	2
1.1.2 Medical Applications	3
1.1.3 Tissue Engineering	4
1.1.4 Wound Healing	5
1.1.5 Drug Release Based on Nanofibers	5
1.2 SCOPE AND OVERVIEW	6
1.2.1 Dyed nanofibers	6
1.2.2 Electrospun Tubes for Nerve Regeneration	7
1.3 REFERENCES	8
CHAPTER 2 Effect of Deacetylation on Wicking Behavior of Co-electrospun Cellulose Acetate/ Polyvinyl Alcohol Nanofibers Blend	12
2.1 INTRODUCTION	12
2.2 EXPERIMENTAL	14
2.2.1 Materials	14
2.2.2 Co-electrospinning	14

2.2.3. Deacetylation -----	15
2.2.4 Wicking rate -----	15
2.2.5 Water Contact Angle -----	16
2.2.6 Diameter of Nanofibers -----	16
2.2.7 Nanofibers Web Thickness -----	17
2.2.8. Scanning Electron Microscope -----	17
2.2.9 FT-IR spectroscopy -----	17
2.3 RESULTS AND DISCUSSION -----	17
2.3.1 Effect of deacetylation on wicking behavior of nanofiber webs-----	17
2.3.2 Effect of deacetylation on morphology of nanofibers and webs ---	24
2.3.3 Structural changes of deacetylated nanofibers webs -----	26
2.4 CONCLUSION -----	27
2.5 REFERENCES -----	28

CHAPTER 3 Cationic-Cellulose Nanofibers: Preparation and Dyeability with Anionic Reactive Dyes for Apparel Application -----32

3.1 INTRODUCTION -----	32
3.2 EXPERIMENTAL -----	35
3.2.1 Materials -----	35
3.2.2 Preparation of cationic-cellulose nanofibers -----	37
3.2.3 Dyeing of cellulose and cationic-cellulose nanofibers -----	38
3.2.4 Color measurements -----	38
3.2.5 FTIR spectroscopy -----	39
3.2.6 FE-SEM -----	39
3.2.7 Color fastness tests -----	39
3.3. RESULTS AND DISCUSSION -----	40
3.3.1 Effect of temperature on color yield and dye fixation -----	40

3.3.2 Effect of time on color yield and dye fixation -----	41
3.3.3 Comparison of build-up property and dye fixation -----	42
3.3.4 Colorimetric data of dyed nanofibers -----	45
3.3.5 Structural feature of nanofibers -----	49
3.3.6 Surface morphology of nanofibers -----	51
3.3.7 Color fastness performance of nanofibers -----	53
3.4. CONCLUSION -----	54
3.5 REFERENCES -----	55
CHAPTER 4 Pad dyeing of cellulose acetate nanofibers with disperse dyes -----	61
4.1 INTRODUCTION -----	61
4.2 EXPERIMENTAL -----	62
4.2.1 Materials -----	62
4.2.2 Electrospinning -----	63
4.2.3 Dyeing of nanofibers -----	64
4.2.4 Measurements -----	64
4.3 RESULTS AND DISCUSSION -----	65
4.3.1 Effect of baking temperature -----	65
4.3.2 Effect of baking time -----	66
4.3.3 Effect of dye concentration -----	67
4.3.4 Color fastness properties -----	69
4.3.5 Morphology of dyed CA nanofibers -----	70
4.3.6 Mechanical property -----	69
4.4. CONCLUSION -----	72
4.5 REFERENCES -----	73

CHAPTER 5 Dyeing of cellulose nanofibers for improving color yields by dual padding method	78
5.1 INTRODUCTION	78
5.2. EXPERIMENTAL	80
5.2.1. Materials	80
5.2.2. Preparing Cellulose nanofibers	80
5.2.3. Dyeing of nanofibers	81
5.2.4. Color measurement and testing	82
5.2.5. Characterization	82
5.3. RESULTS AND DISCUSSION	83
5.3.1. Effect of dye concentration in single padding	83
5.3.2. Effect of dye concentration in dual padding	85
5.3.3. Color fastness properties	87
5.3.4. Chemical structure of nanofibers	89
5.3.5. Morphology of Nanofibers	90
5.4. CONCLUSION	91
5.5 REFERENCES	91
CHAPTER 6 Electrospun Polycaprolactone/Poly(L-Lactic Acid) nanofibers tubes for nerve regeneration	95
6.1 INTRODUCTION	95
6.2 EXPERIMENTAL	97
6.2.1 Materials	97
6.2.2 Method	98
6.2.3 Characterization	94
6.3 RESULTS AND DISCUSSION	99
6.3.1 Morphology and structure of nanofibers tubes	99

6.3.2 Chemical structure of PCL-PLLA nanofibers tubes-----	101
6.3.3 Crystallinity of PCL-PLLA nanofibers tubes -----	103
6.3.4 Differential scanning calorimetry -----	105
6.4. CONCLUSION -----	107
6.5 REFERENCES -----	107
SUMMARY -----	113
ACCOMPLISHMENTS -----	116

LIST OF TABLES

Table 2.1 Water Contact angle (<i>degrees</i>) before and after deacetylation-----	23
Table 2.2 Nanofibers diameter and Nanofibers web thickness-----	23
Table 3.1 Color fastness to washing test ISO 105/C03 and color fastness to light test ISO 105/BO2 -----	53
Table 4.1 Color fastness of dyed nanofibers-----	70
Table 5.1 Effect of dye concentration on colorimetric values-----	85
Table 5.2 Color fastness to light test ISO 105-BO2 and color fastness to washing test ISO 105-C10:2006-----	88
Table 6.1 Tube wall thickness-----	99

LIST OF FIGURES

Figure 2.1	Wicking rate for CA without PVA, before and after deacetylation -----	19
Figure 2.2	Wicking rate for CA with 10% PVA, before and after deacetylation-----	19
Figure 2.3	Wicking rate for CA with 15% PVA, before and after deacetylation-----	20
Figure 2.4	SEM images taken after wicking ceased or time up. (a), (b) and (c) before deacetylation and (d), (e) and (f) after deacetylation. (a) and (d) CA without PVA, (b) and (e) CA/PVA 10% and, (c) and (f) CA/PVA 15% -----	21
Figure 2.5	SEM images (a), (b) and (c) before deacetylation and (d), (e) and (f) after deacetylation. (a) and (d) CA without PVA, (b) and (e) CA/PVA 10% and, (c) and (f) CA/PVA 15% -----	25
Figure 2.6	FTIR for CA without PVA, before and after deacetylation -----	25
Figure 2.7	FTIR for CA/ PVA (10%), before and after deacetylation-----	26
Figure 2.8	FTIR for CA/ PVA (15%), before and after deacetylation-----	26
Figure 3.1	Dye structures of reactive dyes. -----	36
Figure 3.2	Effect of temperature (a) and effect of time (b) on color strength (K/S) and dye fixation (%F) of CI reactive black 5 (dyeing time 80 min, dye concentration 1% omw). -----	41
Figure 3.3	Build-up and dye fixation (%F) of three dyes each at (1%; 3%; 5% omw) dye concentrations obtained for cellulose and cationic-cellulose nanofibers (dyeing temperature 60 °C and dyeing time 60 min) -----	42
Figure 3.4 (a)	Color difference for CI reactive black 5. (b) Color difference for CI reactive blue 19. (c) Color difference for CI reactive red 195. -----	46
Figure 3.5	FTIR spectra: (a) CA, (b) CA-DA, (c) cationic cellulose, (d) cellulose dyed with CI reactive black 5, (e) cationic-cellulose dyed with CI reactive black 5- -----	50
Figure 3.6	SEM images (a, c, e and g) cellulose and (b, d, f and h) cationic-cellulose nanofibers; inset are FE-SEM images; (a and b) undyed, (c and d) dyed with	

	CI reactive black 5, (e and f) dyed with CI reactive blue 19 and (g and h) dyed with CI reactive red 195-----	52
Figure 4.1	Dye structures of (a) CI Disperse Red 167:1 and (b) CI Disperse Blue 56---	63
Figure 4.2	Effect of baking temperature on (a) color yield (K/S), (b) lightness (L*) and (c) chroma (C*). For those plots with two y-axes, the right scale corresponds to CI Disperse Blue 56 measurements, the left scale corresponds to CI Disperse Red 167:1 measurements -----	66
Figure 4.3	Effect of baking time on color yield-----	67
Figure 4.4	Effect of dye concentration on color yield and colorimetric values. For those plots with two y-axes, the right scale corresponds to CI Disperse Blue 56 measurements, the left scale corresponds to CI Disperse Red 167:1 measurements-----	69
Figure 4.5	SEM images of cellulose acetate nanofibers: (a) without dye, (b) dyed with CI Disperse Red 167:1 and (c) dyed with CI Disperse Blue 56. Inset images are macroscopic photographs of dyed webs of cellulose acetate nanofibers -----	71
Figure 4.6	Young's moduli of undyed, blank and dyed Cellulose acetate nanofibers-	72
Figure 5.1	Dye structure of CI reactive black 5 -----	80
Figure 5.2	Effect of dye concentration on color yield and dye fixation-----	83
Figure 5.3	Effect of double padding on color yield -----	84
Figure 5.4	Reflectance curves of CI reactive black 5 -----	87
Figure 5.5	FTIR spectra of cellulose nanofibers without dye (A), CI reactive black 5 dye (B) and cellulose nanofibers dyed with CI reactive black 5 (C) -----	90
Figure 5.6	FESEM images of cellulose acetate nanofibers (A), cellulose nanofibers without dye (B) and cellulose nanofibers dyed with CI reactive black 5 (C)-- -----	91
Figure 6.1	SEM images for nanofiber tubes (A) neat PCL, (B) PCL-PLLA, 2:1, (C) PCL-PLLA, 1:1, (D) PCL-PLLA, 1:2 and (E) neat PLLA; the images F-E are corresponding tube wall surface. -----	100
Figure 6.2	FT-IR spectra for (a) neat PCL, (b) PCL-PLLA, 2:1, (c) PCL-PLLA, 1:1, (d) PCL-PLLA, 1:2 and (e) neat PLLA.-----	102

Figure 6.3 Raman spectra for neat PCL, neat PLLA and their blends -----**104**

Figure 6.4 XRD patterns for neat PCL, neat PLLA and their blends-----**104**

LIST OF SCHEMES

- Scheme 3.1** Reactions of CHPTAC showing cationization of cellulose nanofibers-----**35**
- Scheme 5.1** Reaction mechanism of CI reactive black 5 with cellulose -----**79**

CHAPTER 1

INTRODUCTION

1.1 BACKGROUND

Research in polymer nanofibers has undergone significant progress in the last one decade. One of the main driving forces for this progress is the increasing use of these polymer nanofibers for biomedical and biotechnological applications. The essence of nanotechnology is in the creation and utilization of materials and devices at the level of atoms, molecules, and supramolecular structures, and in the exploitation of unique properties and phenomena of matters with size in nanometers [1].

Electrospinning is currently the only technique that allows the fabrication of continuous fibers with diameters down to a few nanometers. The method can be applied to synthetic and natural polymers, polymer alloys, and polymers loaded with chromophores, nanoparticles, or active agents, as well as to metals and ceramics. Fibers with complex architectures, such as core-shell fibers or hollow fibers, can be produced by special electrospinning methods. It is also possible to produce structures ranging from single fibers to ordered arrangements of fibers. Electrospinning is not only employed in university laboratories, but is also increasingly being applied in industry. The scope of applications, in fields as diverse as optoelectronics, sensor technology, catalysis, filtration, apparels and medical, is very broad.

1.1.1 Nanofibers Textile Apparel

Nonwovens composed of nanofibers can be used in combination with conventional textiles (for example, as interlinings) to modify the properties of the textiles. The objective can be to increase the wind resistance, to regulate the water-vapor permeability, to optimize the thermal insulation behavior, or to give the textile a specific functionality (such as the lotus effect, aerosol filtering, or protection against chemical or biological hazards).

The transition from microfiber to nanofiber nonwovens leads to significant changes in the transport processes of the material as a result of the dramatic reduction in the pore dimensions and the large increase in the inner surface area. For example, in the case of gas diffusion, which is important with respect to thermal insulation, there is a transition from the normal diffusion regime (in which the diffusion path is determined by impacts between the gas particles) to the Knudsen regime (in which the diffusion path is mainly determined by impacts between the gas particles and the fibers). This topic has been extensively studied using Monte Carlo simulations.[2] The situation is similar for the viscous permeation of liquids through nonwovens: the permeation coefficient is directly correlated to the average fiber radius. Gas-transport properties are of great importance to textile applications.[3, 4] Experimental findings have shown that the airflow (wind) resistance of nanofiber nonwovens is increased by up to three orders of magnitude in comparison to conventional textiles, which leads to a significant thermal effect. The wind resistance improves immensely with decreasing pore dimensions and, given identical pore sizes and fiber dimension, can be varied over a large range by adjusting the coverage ($1m$; the mass of deposited nanofibers per unit area). The wind resistance typically increases by a factor 1000 if the coverage is increased from 0.1 to 10 gm^2 . The coverage of 10 gm^2 corresponds to a nonwoven thickness of up to 20 mm (for a porosity of 60%). At the same time, the permeability of the nonwovens to water vapor is very high (comparable to that of PTFE

membranes) and can be influenced by the chemical nature of the fiber material (for example, hydrophilic or hydrophobic). The thermal insulation of nonwovens is mainly a result of the limited diffusion of air molecules in the materials. The thermal insulation increases significantly with decreasing pore size if the pore diameter of the nonwoven is 10–100 times smaller than the mean free path of the gas molecules (about 70 nm for air at normal pressure).

The aerosol-filtering properties of nanofiber nonwovens have also been investigated. The filter efficiency of a textile increases significantly with increasing coverage by a nanofiber nonwoven. An efficiency of 100% can be achieved at a coverage of only 1 gm². [5] The use of nanofiber nonwovens for protection against chemical and biological hazards has been discussed as well. This application is based on the functionalization of the nonwoven with a catalyst (for example, an enzyme) that can decompose harmful substances. [3, 5] The large inner surface area that is available for these catalytic processes is a great advantage of nanofiber nonwovens.

1.1.2 Medical Applications

Nanostructured polymer systems of natural or synthetic origin—in the form of nanofibers, hollow nanofibers, core– shell nanofibers, nanotubes, or nanorods—have a multitude of possible applications in medicine and pharmacy. A main reason for this wide applicability is that the nanoscale is particularly relevant for biological systems, because proteins, viruses, and bacteria have dimensions on this order. Many viruses, for example, the tobacco mosaic virus or the Marburg virus, have the shape of a nanotube. In the following, we present some current activities in the use of nanosystems in tissue engineering, wound healing, and drug delivery.

1.1.3 Tissue Engineering

One rapidly developing field of application for electrospun polymer nanofibers is regenerative medicine. The tissues that are targets for regeneration include cartilage, bone, skin tissue, blood vessels, lymphatic vessels, lung tissue, and heart tissue.[6] One approach in tissue engineering is the use of scaffolds or carrier matrices onto which stem cells or human body cells can be seeded. The job of the matrix is to facilitate the anchorage, migration, and proliferation of the cells, to reproduce the three-dimensional structure of the tissue to be replaced, and to support a differentiation along different cell lines, if stem cells are seeded first. This type of carrier matrix has to fulfill a diverse range of requirements with respect to biocompatibility, biodegradability, morphology, sterilizability, porosity, ability to incorporate and release drugs, and mechanical suitability. The morphologies of the matrices and materials used are diverse. One of the important requirements is that the scaffolds are porous enough to allow cells to grow in their depths while being provided with the necessary nutrients and growth factors. The degree of porosity and the average pore dimensions are significant factors for cell proliferation and the formation of three-dimensional tissues.[6,7]

A further prerequisite for a scaffold is a sufficient mechanical compatibility. Cartilage, for example, is characterized by a Young's modulus of about 130 MPa, a maximum deformation stress of about 20 MPa, and a maximum deformation of 20–120%; the corresponding values for skin tissue are 15–150 MPa, 5–30 MPa, and 35–115%.[8]

1.1.4 Wound Healing

An interesting application of electrospun nanofibers is the treatment of large wounds such as burns and abrasions.[9, 10] It is found that these types of wounds heal particularly rapidly and without complications if they are covered by a thin web of nanofibers, in particular, of biodegradable polymers. Such nanowebs have enough pores to assure the exchange of liquids and gases with the environment, but have dimensions that prevent bacteria from entering. Mats of electrospun nanofibers generally show very good adhesion to moist wounds.[11] Furthermore, the large specific surface area of up to $100 \text{ m}^2 / \text{g}$ is very favorable for the adsorption of liquids and the local release of drugs on the skin, making these materials suitable for application in hemostatic wound closure.[12] Compared to conventional wound treatment, the advantage is that scarring is prevented by the use of nanofibers.[13]

1.1.5 Drug release based on nanofibers

Nanofiber systems for the release of drugs (or functional compounds in general) are of great interest for tumor therapy, as well as for inhalation and pain therapy. The nanostructured carriers must fulfill diverse functions. For example, they should protect the drugs from decomposition in the bloodstream, and they should allow the controlled release of the drug over a chosen time period at a release rate that is as constant as possible. They should also be able to permeate certain membranes (for example, the blood–brain barrier), and they should ensure that the drug is only released in the targeted tissue. It may also be necessary for the drug release to be triggered by a stimulus (either external or internal) and to continue only as long as necessary for the treatment. For some time, nanoparticles (of lipids or biodegradable polymers, for example) have been extensively investigated with respect to the transport and release of

drugs.[453, 454] A variety of methods have been used for the fabrication of such nanoparticles, including spraying and sonification, as well as self-organization and phase-separation processes. Such nanoparticles are primarily used for systemic treatment. However, experiments are currently being carried on the targeting and enrichment of particular tissues (vector targeting) by giving the nanoparticles specific surface structures (for example, sugar molecules on the surface).

1.2 SCOPE AND OVERVIEW

1.2.1 Dyed Nanofibers

As one of the most abundant renewable polymer resources, cellulose has been widely used for fibers and films. Recently, the electrospinning of cellulose nanofibers has attracted a great deal of attention due to their good thermal stability, chemical resistance, biodegradability, etc. These properties will ensure that they find a broad range of applications in affinity membranes, biosensors, chemo sensors, protective cloths, reinforced nano composites, etc. Cellulose nanofibers have been prepared by the direct electrospinning of cellulose solution in N-methyl morpholine-N-oxide (NMMO) hydrate [14,15], which is known as one of the most promising cellulose solvents. However, the cellulose/NMMO hydrate solutions have to be electrospun at elevated temperatures in the range of 80-130 °C, due to the high melting temperature of NMMO hydrate, and the resulting cellulose nanofibers are relatively less uniform and have to be carefully washed with water in order to completely remove the residual NMMO. As an alternative to the direct electrospinning of cellulose solution, the electrospinning and subsequent deacetylation of cellulose acetate (CA) is more convenient and viable method. CA nanofibers based biosensor [16,17] in certain application come into contact with various liquids and require high degree of wicking rate to transport liquid to its destination [6]. As a matter of fact that the CA nanofibers

have limited water wicking due to presence of acetyl groups, therefore CA nanofibers are converted into regenerated cellulose (RC) to obtain satisfactory degree of wicking [18].

The current research trend in nanofibers as apparel use is increasing gradually. The past research was mainly focused within the functional properties only and to the best of our knowledge aesthetic properties of cellulose nanofibers are not investigated to date. Therefore, the need is to produce colored nanofiber and investigate into the aesthetic properties.

1.2.2 Electrospun Tubes for Nerve Regeneration

Although many nerve prostheses have been proposed in recent years, in the case of consistent loss of nervous tissue peripheral nerve injury is still a traumatic pathology that may impair patient's movements by interrupting his motor-sensory pathways. In the last few decades tissue engineering has opened the door to new approaches; however most of them make use of rigid channel guides that may cause cell loss due to the lack of physiological local stresses exerted over the nervous tissue during patient's movement. Electrospinning technique makes it possible to spin microfiber and nanofiber flexible tubular scaffolds composed of a number of natural and synthetic components, showing high porosity and remarkable surface/volume ratio. With the great efforts in ecological environment protection, various biodegradable polymers have been created and studied. Poly(L-lactic acid) (PLLA) is one of the most promising biodegradable polymers owing to its mechanical properties, thermoplastic processibility, biocompatibility, and biodegradability [19]. With many unique features, PLLA has been increasingly used as commodity plastics in packaging, agricultural products and disposable materials. It also has great potential of applications in medicine, surgery and tissue engineering because of its biocompatibility and

biodegradability [20, 21]. PLLA nanofibers have also attracted great attention in recent years because of its potential applications in medicine, tissue engineering and filtration [22].

The fabricated conduits reported in the literature thus far usually possess a solid rigid structure. The present work deals with the fabrication of electrospun fibrous tubular constructs to act as nerve guidance channels. It is not rigid and consequently well adaptable to the living system. Electrospinning represents an attractive approach to the fabrication of fibrous biomaterials, which can mimic the size scales of fibers composing the extracellular matrix of native tissues and organs. Hence, this method represents an attractive approach to the fabrication of fibrous biomaterials for tissue engineering purposes [23].

Poly(ϵ -caprolactone) (PCL) is an FDA-approved biodegradable polymer with excellent biocompatibility and flexibility, which has attracted increasing interest in many areas such as biodegradable packaging materials, implantable biomaterials and microparticles for drug delivery [24]. However, several disadvantages of PCL were also recognized, for example, (i) it degraded much slower than other known biodegradable polymers, which restricted their practical application range; (ii) the mechanical properties of the PCL scaffolds with high porosity were poor, which limited their use in hard tissue engineering. To overcome these shortcomings.

1.3 REFERENCES

[1] Zhang, Y., Lim, C. T., Ramakrishna, S., & Huang, Z. M. (2005). Recent development of polymer nanofibers for biomedical and biotechnological applications. *Journal of Materials Science: Materials in Medicine*, 16(10), 933-946.

- [2] Tomadakis, M. M., & Sotirchos, S. V. (2004). Ordinary and transition regime diffusion in random fiber structures. *AIChE Journal*, 39(3), 397-412.
- [3] Singh, A., Lee, Y., & Dressick, W. J. (2004). Self - Cleaning Fabrics for Decontamination of Organophosphorous Pesticides and Related Chemical Agents. *Advanced materials*, 16(23 - 24), 2112-2115.
- [4] Tsai, P. P., Schreuder-Gibson, H., & Gibson, P. (2002). Different electrostatic methods for making electret filters. *Journal of Electrostatics*, 54(3), 333-341.
- [5] Gibson, P., Schreuder-Gibson, H., & Rivin, D. (2001). Transport properties of porous membranes based on electrospun nanofibers. *Colloids and Surfaces A: Physicochemical and Engineering Aspects*, 187, 469-481.
- [6] Langer, R., Vacanti, J. P. (1993). *Science*, 260(5110), 920 – 926.
- [7] Kim, B. S., & Mooney, D. J. (1998). Development of biocompatible synthetic extracellular matrices for tissue engineering. *Trends in biotechnology*, 16(5), 224-230.
- [8] Li, W. J., Laurencin, C. T., Caterson, E. J., Tuan, R. S., & Ko, F. K. (2002). Electrospun nanofibrous structure: a novel scaffold for tissue engineering. *Journal of biomedical materials research*, 60(4), 613-621.
- [9] Nair, L. S., Bhattacharyya, S., & Laurencin, C. T. (2004). Development of novel tissue engineering scaffolds via electrospinning. *Expert opinion on biological therapy*, 4(5), 659-668.
- [10] Khil, M. S., Bhattarai, S. R., Kim, H. Y., Kim, S. Z., & Lee, K. H. (2004). Novel fabricated matrix via electrospinning for tissue engineering. *Journal of Biomedical Materials Research Part B: Applied Biomaterials*, 72(1), 117-124.

- [11] Venugopal, J., & Ramakrishna, S. (2005). Applications of polymer nanofibers in biomedicine and biotechnology. *Applied biochemistry and biotechnology*, 125(3), 147-157.
- [12] Huang, Z. M., Zhang, Y. Z., Kotaki, M., & Ramakrishna, S. (2003). A review on polymer nanofibers by electrospinning and their applications in nanocomposites. *Composites science and technology*, 63(15), 2223-2253.
- [13] Zong, X., Kim, K., Fang, D., Ran, S., Hsiao, B. S., & Chu, B. (2002). Structure and process relationship of electrospun bioabsorbable nanofiber membranes. *Polymer*, 43(16), 4403-4412.
- [14] Han, S. O., Youk, J. H., Min, K. D., Kang, Y. O., & Park, W. H. (2008). Electrospinning of cellulose acetate nanofibers using a mixed solvent of acetic acid/water: Effects of solvent composition on the fiber diameter. *Materials Letters*, 62(4), 759-762.
- [15] Kulpinski, P. (2005). Cellulose nanofibers prepared by the N-methylmorpholine-N-oxide method. *Journal of applied polymer science*, 98(4), 1855-1859.
- [16] Wang, X., Kim, Y. G., Drew, C., Ku, B. C., Kumar, J., & Samuelson, L. A. (2004). Electrostatic assembly of conjugated polymer thin layers on electrospun nanofibrous membranes for biosensors. *Nano Letters*, 4(2), 331-334.
- [17] Shuiping, L., Lianjiang, T., Weili, H., Xiaoqiang, L., & Yanmo, C. (2010). Cellulose acetate nanofibers with photochromic property: Fabrication and characterization. *Materials Letters*, 64(22), 2427-2430.
- [18] Callegari, G., Tyomkin, I., Kornev, K. G., Neimark, A. V., & Hsieh, Y. L. (2011). Absorption and transport properties of ultra-fine cellulose webs. *Journal of colloid and interface science*, 353(1), 290-293.

- [19] Liu, H., & Hsieh, Y. L. (2002). Ultrafine fibrous cellulose membranes from electrospinning of cellulose acetate. *Journal of Polymer Science Part B: Polymer Physics*, 40(18), 2119-2129.
- [20] Gupta, B., Revagade, N., & Hilborn, J. (2007). Poly (lactic acid) fiber: An overview. *Progress in polymer science*, 32(4), 455-482.
- [21] Bhattarai, S. R., Bhattarai, N., Yi, H. K., Hwang, P. H., Cha, D. I., & Kim, H. Y. (2004). Novel biodegradable electrospun membrane: scaffold for tissue engineering. *Biomaterials*, 25(13), 2595.
- [22] Yang, F., Murugan, R., Wang, S., & Ramakrishna, S. (2005). Electrospinning of nano/micro scale poly (L-lactic acid) aligned fibers and their potential in neural tissue engineering. *Biomaterials*, 26(15), 2603-2610.
- [23] Yoshimoto, H., Shin, Y. M., Terai, H., & Vacanti, J. P. (2003). A biodegradable nanofiber scaffold by electrospinning and its potential for bone tissue engineering. *Biomaterials*, 24(12), 2077-2082.
- [24] Cho, H., & An, J. (2006). The effect of ϵ -caproyl/d,l-lactylunit composition on the hydrolytic degradation of poly(d,l-lactide-ran- ϵ -caprolactone)-poly(ethylene glycol)-poly(d,l-lactide-ran- ϵ -caprolactone). *Biomaterials*, 27(4), 544-552.

CHAPTER 2

Effect of Deacetylation on Wicking Behavior of Co-electrospun Cellulose Acetate/ Polyvinyl Alcohol Nanofibers Blend

2.1 INTRODUCTION

Producing nanofibers via electrospinning is not new. However, blending different polymers and attempts are being undertaken towards the development of multi characteristic nanofibers to fulfill stringent requirements. Cellulose Acetate (CA) nanofibers webs deserve a special attention because of their very good water retention properties. The water retention per fibrous mass for the electrospun CA nanofibers web is nearly ten times higher than that for fabrics [1]. CA - a widely studied and characterized in terms of affinity membrane and filtration [2,3], capillary absorption models [4], deacetylation of nanofibers [5]. Electrospun fibrous webs have wide applications as bio-materials for tissue engineering and scaffolds [6-8].

CA nanofibers based biosensor [9,10] in certain application come into contact with various liquids and require high degree of wicking rate to transport liquid to its destination [4]. As a matter of fact that the CA nanofibers have limited water wicking due to presence of acetyl groups, therefore CA nanofibers are converted into regenerated

cellulose (RC) to obtain satisfactory degree of wicking [1]. The process of CA conversion into RC by deacetylation is very common that may be carried by treating CA nanofibers either in aqueous NaOH/EtOH solution for shorter period [1] or aqueous NaOH solution for longer time span [4]. The degree of substitution has been reported to complete by both methods. Yaser E. Greish et al., investigated the effect of thermal treatment of CA nanofibrous membranes at temperatures up to 208 °C in various conditions, followed by deacetylation for conversion of CA into RC nanofibers using 0.5M NaOH aqueous solution [11]. To enhance even high wicking rate of RC nanofibers, the CA nanofibers and blended with Poly Vinyl Alcohol (PVA) nanofibers were co-electropun simultaneously, followed by deacetylation to remove PVA nanofibers and convert CA into RC nanofibers. PVA is extremely hydrophilic and soluble in water [12]. The PVA itself readily reacts with different cross-linking agents to form a gel [13]. The water solubility is dependent on degrees of hydrolysis (DH). The effect of various DH on electrospinning has been discussed [14]. The fabrication and characterization of CA/PVA blends nanofiberous nonwoven mats have been studied by [15](Ding B. et al., 2004) in terms of their morphologies and mechanical properties.

The aim of this research was to enhance the wicking rate and to investigate the effect of deacetylation on wicking behaviour of CA/ PVA nanofibers webs. PVA nanofibers were produced from two concentrations 10% and 15% (wt%), each was co-electrospun with 17% (wt%) CA nanofibers and collected on same collector/drum. The use of PVA nanofibers were interim since the CA/ PVA blend nanofiber webs were deacetylated to remove PVA component and convert CA nanofibers into RC nanofibers. The resultant

nanofibers webs were characterized by wicking rate, water contact angle, FTIR and SEM analysis and compared to untreated nanofibers webs.

2.2 EXPERIMENTAL

2.2.1 Materials

Cellulose Acetate, CA, (39.8% acetyl content having average Mw = 30 kDa) and Polyvinyl Alcohol, PVA, (87–89% hydrolyzed, average Mw = 124–186 kDa) were obtained from Aldrich Chemical Company, and used without further purification.

2.2.2 Co-electrospinning

A high-voltage power supply (Har-100*12, Matsusada Co., Tokyo, Japan), capable of generating voltages up to 100 kV, was used as the source of the electric field. The concentration of CA was 17% by weight and prepared in Acetone/ Dimethyl formamide (DMF) with 2:1 by weight, while the PVA solutions were prepared in distilled water with two concentrations 10% and 15% by weight. CA and PVA solutions were co-electrospun independently and simultaneously onto a rotating metallic drum/collector at room temperature. Each solution was supplied through a plastic syringe attached to a capillary tip with an inner diameter of 0.6mm. The copper wire connected to a positive electrode (anode) was inserted into the polymer solution, and a negative electrode (cathode) was attached to a metallic collector. The voltage was fixed at 12.5 kV for CA and 12 kV for PVA. The distance between the capillary tip and the collector was fixed to be 15cm for both CA and PVA, and the plastic syringes were placed at an angle of 10° from the horizontal direction. Three types of nanofiber webs were prepared 1. CA nanofiber

without PVA nanofibers, 2. CA nanofibers with 10% PVA nanofibers and 3. CA nanofibers with 15% PVA nanofibers. Electrospinning was continued till the thickness of nanofiber web was achieved between 40 μm – 60 μm range. All nanofiber webs were air dried for at least 48 hours and then subjected to deacetylation.

2.2.3 Deacetylation

In order to remove acetyl groups from the CA nanofibers and remove PVA content from the CA nanofibers webs, deacetylation was carried out by aqueous hydrolysis [4] in 0.05M NaOH solution for 30 hours at room temperature and thoroughly rinsed off in distilled water until the pH of nanofiber webs reached to 7, followed by drying at 50°C for 4 hours. Additionally, pure PVA 10% nanofibers and pure PVA 15% nanofibers were dissolved separately to ensure their solubility in 0.05M NaOH solution for deacetylation of CA/PVA nanofibers blend.

2.2.4 Wicking rate

Wicking rate (the increase in height of wicking front per second) was assessed by hanging samples vertically over the petry dish containing dye solution. 1 % (w/v) dye solution was prepared with CI Reactive Blue 19 (Sumfix Brilliant Blue R, Sumitomo Chemicals, Japan) dissolved in distilled water. The sample size of nanofibers web was cut into 20 mm height and 5 mm width and fixed in an upright stationary clamp, beneath, a petry dish containing dye solution was kept on the jack movable up and down. The lower end of sample was 5 mm below the liquid surface during the wicking test and remaining 15 mm

was observed for wicking rise. The stop watch started as soon as the surface layer of dye solution touched the bottom edge of the vertically suspended sample. Simultaneously, a Camera (Canon with 8 megapixels) capable of capturing multiple shots at the rate of one shot per second was also started. The wicking test was lasted for either maximum 90 seconds or the wicking front reaches the height of maximum 15 mm, whichever reached first. The reason for setting up two different sets of conditions was that some samples having very high wicking could reach 15 mm height in less than 90 seconds and some of the samples, due to lack of wicking property, could not reach the height of 15 mm in more than 90 seconds. The multishot images were further evaluated by using Adobe Photoshop CS5.1 for calculating the height of wicking front per second. Since, the multishot interval was known, i.e. one shot per second, so it was easier to calculate the wicking rate.

2.2.5 Water Contact Angle

The static water contact angle (WCA) was determined by Sessile drop measurements using a Contact Shape Analyzer, DSA100 (Krüss, Hamburg, Germany).

2.2.6 Diameter of Nanofibers

The average diameters of nanofibers were analyzed by using Keyence Digital Microscope VH –Z500R at x5000 magnification.

2.2.7 Nanofibers Web Thickness

The average thickness of all nanofiber webs were measured by Digital Micrometer MCD130- 25 with measuring sensitivity of 1 μ m.

2.2.8. Scanning Electron Microscope

SEM (S-3000N by Hitachi, Japan) was used to study morphology of nanofiber before and after deacetylation.

2.2.9 FT-IR spectroscopy

The change in chemical structure of CA nanofibers with and without blending of PVA nanofibers, before and after deacetylation, was analysed on FTIR spectroscopy. (IR Prestige-21 by Shimadzu, Japan).

2.3 RESULTS AND DISCUSSION

2.3.1 Effect of deacetylation on wicking behavior of nanofiber webs

The Figures 2.1-2.3 demonstrates the wicking rate of CA and CA/PVA blend nanofibers webs, before and after deacetylation. Figure 1 shows CA nanofibers web before and after deacetylation, almost linear with slightly decrease in wicking rate after 40 seconds but over all less than after deacetylation over the time. The wicking rate of deacetylated CA nanofibers web was too high initially that reached wicking front height of 7 mm within 10 seconds and then started decreasing slowly until 10 mm wicking front height and

decreased more until the 15 mm wicking front height was reached. It can be seen that two third of wicking height was achieved in 25 seconds which is almost five times faster wicking rate than the remaining wicking rate and one and a half times enhanced wicking rate compared to that of the CA nanofibers web before deacetylation. The reason for the higher wicking rate is due to substitution of acetate groups with OH groups [1]. This affirms the behaviour of CA nanofibers after deacetylation shown in Figure 8 at 3400 cm^{-1} .

Figure 2 and 3 illustrate some change in wicking behaviour of CA/PVA (10%) and CA/PVA (15%) nanofiber webs before deacetylation. Wicking front height of maximum 2.5 mm and 3 mm could reach in 90 seconds for both PVA nanofiber samples. The reason for this decreased wicking is mainly attributed to the gel formation of PVA nanofibers that resist the liquid to flow through the web during wicking [13]. This fact is confirmed from the SEM images shown in Figure 2.4 (a-f), which were taken after wicking ceased. The SEM images in Figure 2.4 (b) and (c) clearly show gel formation in CA/PVA (10%) and CA/PVA (15%) nanofiber webs before deacetylation. This behaviour mainly attributed to the property of PVA nanofibers that have a tendency to gel formation [13]. The inset images shown in figure (a-f) are real pictures exposed during the wicking rate experiment done on all nanofiber web samples. The wicking front height of CA/PVA (15%) in Figure 4 (c) inset is relatively higher than the wicking front height of CA/PVA (10%) nanofiber web shown in Figure 2.4 (b). This slight enhancement is due to more PVA content in terms of nanofiber diameter resulting into many OH groups of PVA available to absorb liquid at initials wicking stage.

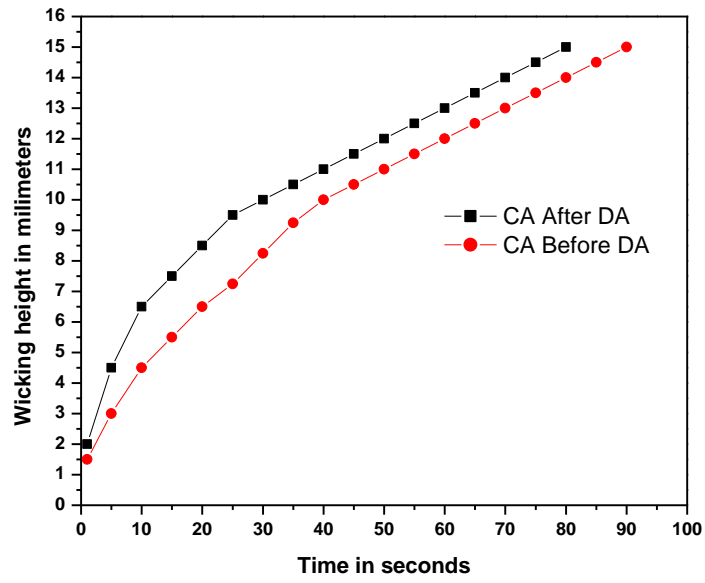


Figure 2.1 Wicking rate for CA without PVA, before and after deacetylation.

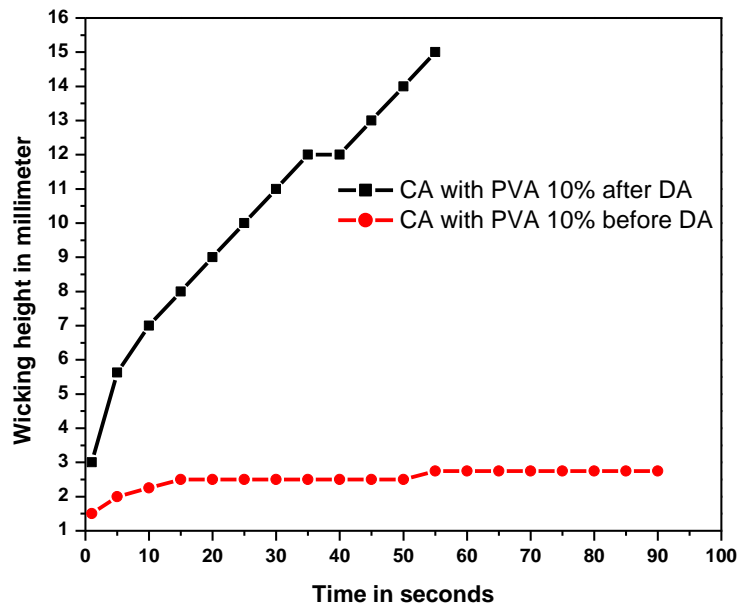


Figure 2.2 Wicking rate for CA with 10% PVA, before and after deacetylation

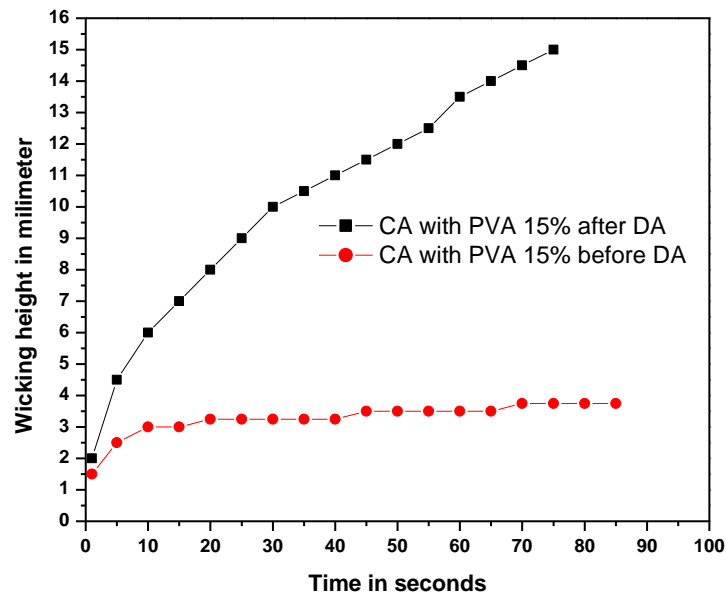


Figure 2.3 Wicking rate for CA with 15% PVA, before and after deacetylation

The PVA nanofibers were removed by deacetylation and wicking was compared before and after deacetylation. Figure 2.2 and 2.3 depict that the wicking rate of CA/ PVA (10%) and CA/ PVA (15%) was significantly enhanced after deacetylation. In case of CA/PVA (10%) deacetylated nanofibers web, the wicking rate was initially too high, similar to that of the CA deacetylated nanofibers web, reaching 7 mm wicking front height within 10 seconds and a continuous increment up to 15 mm wicking front height within 65 seconds (Figure 2.2). Overall, wicking was uniform and 20% faster than that of the CA deacetylated nanofibers web. In contrast to phenomenon of increased porosity in deacetylated CA nanofibers web that contributes to wicking enhancement [4]; the nanofiber web structure became denser and shrunk after the PVA component removed by deacetylation. The network of the nanofibers web was increased that provided

opportunity for liquid to flow through the nanofibers web smoothly and rapidly. In addition, substitution of acetate groups of the CA with OH groups, as depicted by FTIR analysis, was also one of the main contributing factors in the enhancement of wicking front height. The CA/ PVA (15%) deacetylated, on the other hand, was found to have 20% slower wicking rate than the CA/PVA (10%) deacetylated nanofibers web, in spite of more shrinkage in the nanofibers web structure . It is evident from the wicking rate data that the CA/PVA (10%) deacetylated nanofibers web had very good wicking profile.

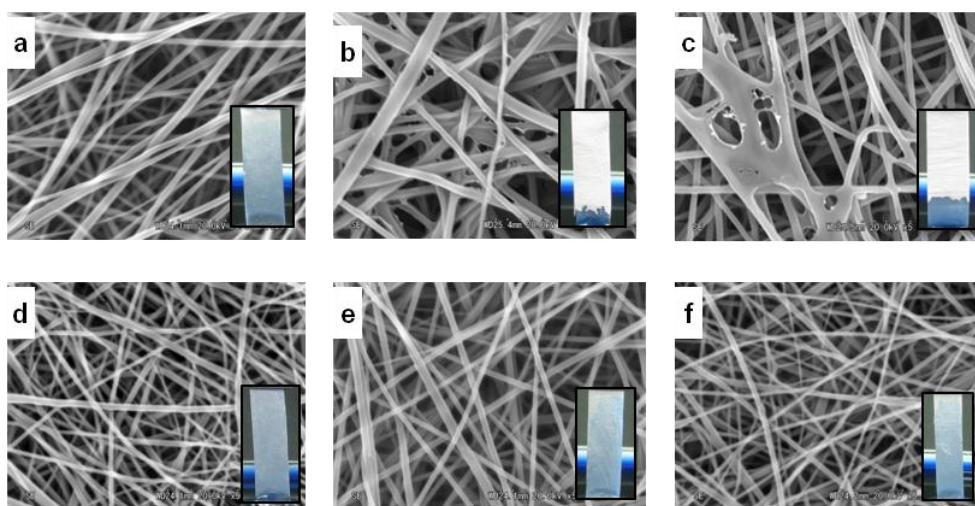


Figure 2.4 SEM images taken after wicking ceased or time up. (a), (b) and (c) before deacetylation and (d), (e) and (f) after deacetylation. (a) and (d) CA without PVA, (b) and (e) CA/PVA 10% and, (c) and (f) CA/PVA 15%

Another method to determine the wicking behavior is water contact angle (WCA) as reported by other researchers [1,10,16]. WCA was also performed for all samples and the results tabulated in Table 1.1. The results obtained for all three types of samples were quite different from results obtained earlier using vertical capillary method for wicking. Very high average WCA of around 111.8° was obtained in case of CA nanofibers web before deacetylation. This may be attributed to the acetyl groups in CA nanofibers. This may also be due to the protruding nanofibers that resist and delay penetration of water drop into the CA nanofiber web [17], therefore considered to be less hydrophilic. In contrast, the CA nanofiber web showed a significant increase in wicking rate provided hydrophilicity in the sample as shown in Figure 1. The differences in obtained results are mainly due to the method principles upon which they are based. The effect of deacetylation was very significant and obvious, the WCA decreased down to 4° , nearly undetectable. The reason for this significant change was due to the acetyl group substitution with hydrophilic OH groups. The WCA of CA/PVA (10%) and CA/PVA (15%) nanofibers webs before deacetylation decreased significantly in comparison to CA nanofibers web, i.e. about nine times and ten times respectively. Table 1 depicts no significant effect of deacetylation on WCA were observed in both CA/PVA (10%) and CA/PVA (15%) nanofibers webs. To understand the wicking behavior of nanofibers webs, the vertical capillary method provides a better means instead of Water Contact Angle, because the later method depends on the surface penetration only while the capillary method takes the whole nanofibers structure into account.

Table 2.1 Water Contact angle (*degrees*) before and after deacetylation







Before deacetylation			After deacetylation		
CA	111.8°		CA	04°	
CA/PVA (10%)	13.6°		CA/PVA (10%)	11.3°	
CA/PVA (15%)	7.9°		CA/PVA (15%)	6.7°	

Table 2.2 Nanofibers diameter and Nanofibers web thickness

Nanofibers web type	Average Nanofiber diameter, (μm)		Average Web thickness before deacetylation, (μm)	Average Web thickness after deacetylation, (μm)
	CA	PVA		
CA without PVA	0.74	--	44	38
CA with 10% PVA	0.74	0.34	58	49
CA with 15% PVA	0.74	0.71	60	50

2.3.2 Effect of deacetylation on morphology of nanofibers and webs

The average diameter of nanofibers and average nanofiber web thicknesses are tabulated in Table 2.2. The electrospinning time for each sample was around twelve hours in order to achieve 40 μm – 60 μm range of thickness. The average diameter of CA nanofibers was obtained 0.74 μm , half than the average diameter of 10% PVA nanofibers and double than the average diameter of 15% PVA nanofibers. The diameter of PVA nanofiber is dependent upon the concentration of PVA used [18]. The Table 2.2 shows the diameter of nanofibers produced from 15% PVA was increased to almost double than the diameter of nanofibers produced from 10% PVA when the PVA concentration was increased. The effect of deacetylation on nanofiber web thickness was quite significant as shown in Table 2.2. Overall, the thickness of nanofibers webs was reduced after deacetylation due to shrinkage. The amount of thickness shrunk after deacetylation was around 13.6% of CA, 15.5% of CA/PVA (10%) and 16.5% of CA/PVA (15%) nanofiber webs. Slightly higher reduction in thickness after deacetylation of CA/PVA (15%) nanofiber web was due to the removal of relatively thicker diameter of 15% PVA nanofibers as compared to the diameter of 10% PVA nanofibers. In addition, sample shrinkage after deacetylation may also be the reason of overall thickness reduction. The SEM images of all nanofibers webs were studied in terms of the effect of deacetylation on the nanofibers morphologies. The Figure 5.5 (a-f) shows a significant change observed in nanofibers surface morphology after deacetylation. As reported earlier, shrinkage and increased structure density is obvious from SEM images after deacetylation.

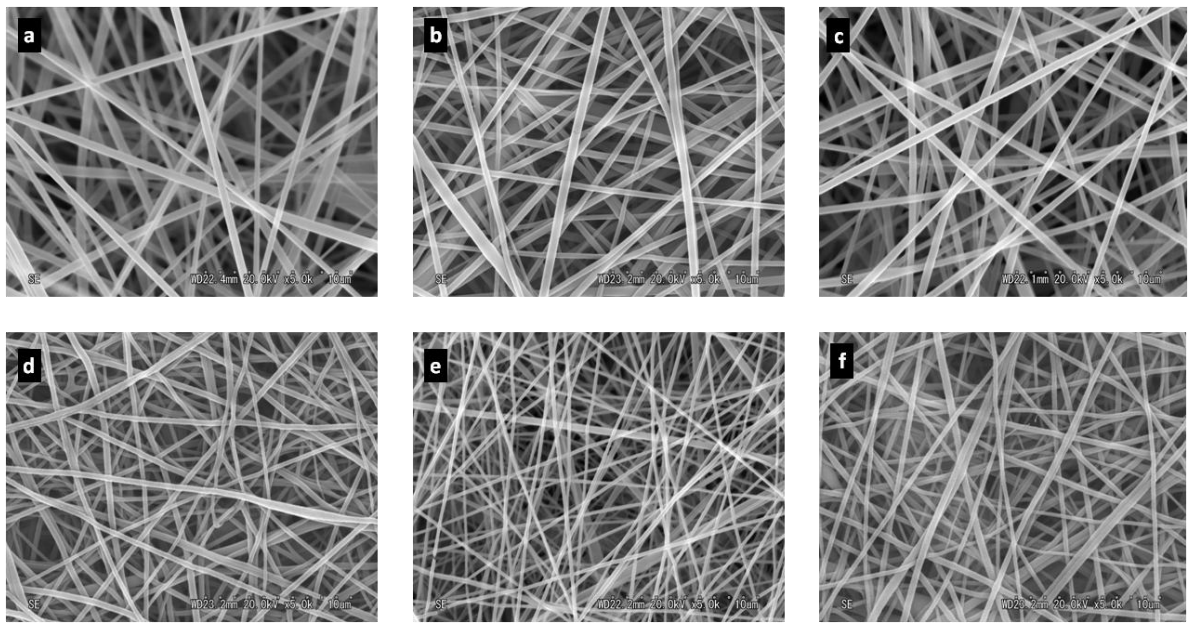


Figure 2.5 SEM images (a), (b) and (c) before deacetylation and (d), (e) and (f) after deacetylation. (a) and (d) CA without PVA, (b) and (e) CA/PVA 10% and, (c) and (f) CA/PVA 15%

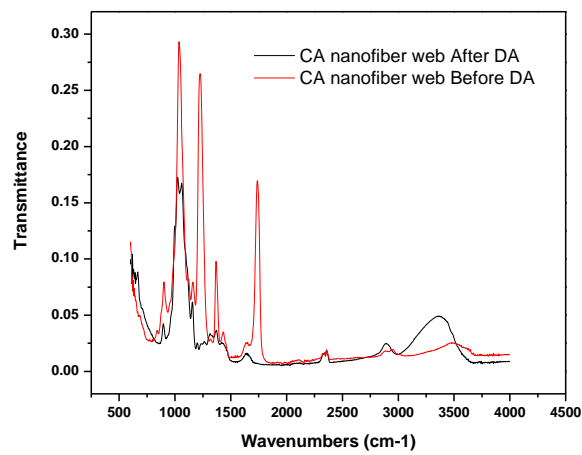


Figure 2.6 FTIR for CA without PVA, before and after deacetylation

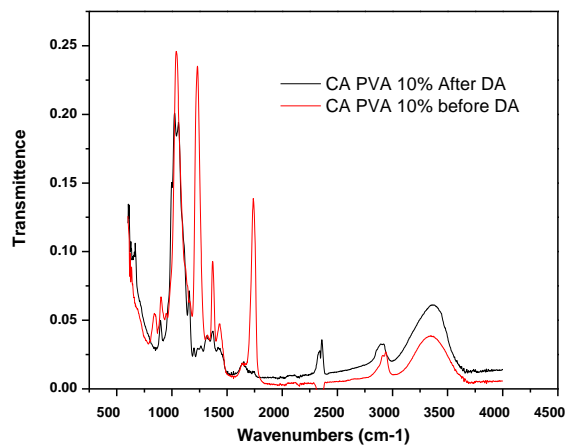


Figure 2.7 FTIR for CA/ PVA (10%), before and after deacetylation

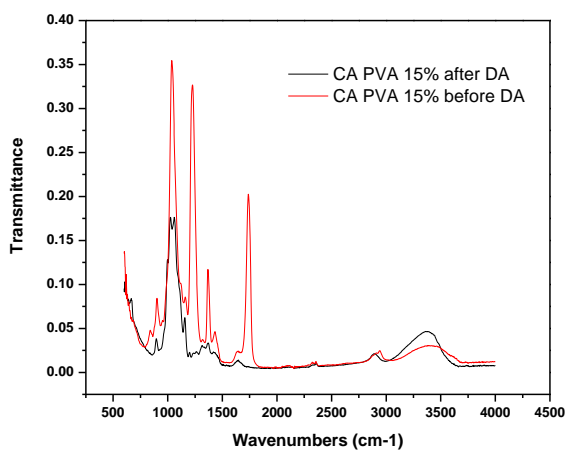


Figure 2.8 FTIR for CA/ PVA (15%), before and after deacetylation

2.3.3 Structural changes of deacetylated nanofibers webs

Figures 2.6-2.8 display changes in the FTIR spectra before and after deacetylation. The intensities of characteristic adsorption peaks attributed to the vibrations of the

acetate group at 1745 ($\nu_{C=O}$), 1375 (ν_{C-CH_3}) and 1235 cm^{-1} (ν_{C-O-C}), decreased and finally disappeared. On the contrary, an absorption peak at 3500 cm^{-1} (ν_{O-H}) is increased, as shown in Figure 2.7 and 2.8.

The PVA nanofiber has characteristic bands at around 860 cm^{-1} (ν_{C-O}), 110 cm^{-1} , 1450 cm^{-1} , 2900 cm^{-1} (ν_{-CH_2}) and 3400 cm^{-1} (ν_{O-H}) [15]. The characteristics bands at 1450 cm^{-1} , 2900 cm^{-1} (ν_{-CH_2}) and 3400 cm^{-1} (ν_{O-H}) became weaker and bands at 869 cm^{-1} and 110 cm^{-1} completely disappeared as result of deacetylation [15]. This suggests that the PVA nanofibers after deacetylation were removed. No new peaks were observed other than common characteristic peaks of CA and PVA nanofibers, it can therefore be said that there was no chemical reaction between CA and PVA nanofibers but simply a physical blending.

2.4 CONCLUSION

The effect of deacetylation was evaluated with respect to wicking rate. Three nanofibers webs were prepared, out of which the CA/PVA (10%) nanofibers blend demonstrates faster and more uniform wicking rate as compared to the CA/PVA (15%) nanofibers blends and CA without PVA nanofibers webs. The blending of PVA nanofibers significantly decreases the wicking rate if not deacetylated. After deacetylation, all types of nanofibers webs used in this study showed overall enhanced wicking rate. The vertical capillary method provides a better understanding of wicking behavior than the water contact angle of nanofibers webs. FTIR data showed no chemical reaction between CA

nanofibers and PVA nanofibers. The deacetylation had significantly affected the nanofibers web thickness, which brought a positive change in terms of increase in nanofibers network as study showed by SEM analysis. Such type of nanofibers webs can be used where the faster wicking is desired such as, biosensor strips and other medical applications.

2.5 REFERENCES

[1] Liu, H., & Hsieh, Y. L. (2002). Ultrafine fibrous cellulose membranes from electrospinning of cellulose acetate. *Journal of Polymer Science Part B: Polymer Physics*, 40(18), 2119-2129.

[2] Ma, Z., Kotaki, M., & Ramakrishna, S. (2005). Electrospun cellulose nanofiber as affinity membrane. *Journal of membrane science*, 265(1), 115-123.

[3] Ma, Z., & Ramakrishna, S. (2008). Electrospun regenerated cellulose nanofiber affinity membrane functionalized with protein A/G for IgG purification. *Journal of Membrane Science*, 319(1), 23-28.

[4] Callegari, G., Tyomkin, I., Kornev, K. G., Neimark, A. V., & Hsieh, Y. L. (2011). Absorption and transport properties of ultra-fine cellulose webs. *Journal of colloid and interface science*, 353(1), 290-293.

[5] Son, W. K., Youk, J. H., Lee, T. S., & Park, W. H. (2003). Electrospinning of ultrafine cellulose acetate fibers: Studies of a new solvent system and deacetylation of ultrafine cellulose acetate fibers. *Journal of Polymer Science Part B: Polymer Physics*, 42(1), 5-11.

[6] Du, J., & Hsieh, Y. L. (2008). Nanofibrous membranes from aqueous electrospinning of carboxymethyl chitosan. *Nanotechnology*, 19(12), 125707.

[7] Du, J., & Hsieh, Y. L. (2009). Cellulose/chitosan hybrid nanofibers from electrospinning of their ester derivatives. *Cellulose*, 16(2), 247-260.

[8] Katti, D. S., Robinson, K. W., Ko, F. K., & Laurencin, C. T. (2004). Bioresorbable nanofiber-based systems for wound healing and drug delivery: Optimization of fabrication parameters. *Journal of Biomedical Materials Research Part B: Applied Biomaterials*, 70(2), 286-296.

[9] Wang, X., Kim, Y. G., Drew, C., Ku, B. C., Kumar, J., & Samuelson, L. A. (2004). Electrostatic assembly of conjugated polymer thin layers on electrospun nanofibrous membranes for biosensors. *Nano Letters*, 4(2), 331-334.

[10] Shuiping, L., Lianjiang, T., Weili, H., Xiaoqiang, L., & Yanmo, C. (2010). Cellulose acetate nanofibers with photochromic property: Fabrication and characterization. *Materials Letters*, 64(22), 2427-2430.

- [11] Greish, Y. E., Meetani, M. A., Al Matroushi, E. A., & Shamsi, B. A. (2010). Effects of thermal and chemical treatments on the structural stability of cellulose acetate nanofibers. *Carbohydrate Polymers*, 82(3), 569-577.
- [12] Tsukada, M., Freddi, G., & Crighton, J. S. (2003). Structure and compatibility of poly (vinyl alcohol)-silk fibroin (PVA/SA) blend films. *Journal of Polymer Science Part B: Polymer Physics*, 32(2), 243-248.
- [13] Hodge, R. M., Edward, G. H., & Simon, G. P. (1996). Water absorption and states of water in semicrystalline poly (vinyl alcohol) films. *Polymer*, 37(8), 1371-1376.
- [14] Park, J. C., Ito, T., Kim, K. O., Kim, K. W., Kim, B. S., Khil, M. S., ... & Kim, I. S. (2010). Electrospun poly (vinyl alcohol) nanofibers: effects of degree of hydrolysis and enhanced water stability. *Polymer journal*, 42(3), 273-276.
- [15] Ding, B., Kimura, E., Sato, T., Fujita, S., & Shiratori, S. (2004). Fabrication of blend biodegradable nanofibrous nonwoven mats via multi-jet electrospinning. *Polymer*, 45(6), 1895-1902.
- [16] Liu, H., & Tang, C. (2006). Electrospinning of cellulose acetate in solvent mixture N, N-dimethylacetamide (DMAc)/acetone. *Polymer Journal*, 39(1), 65-72.

[17] Mason, C. R., Maynard-Atem, L., Al-Harbi, N. M., Budd, P. M., Bernardo, P., Bazzarelli, F., ... & Jansen, J. C. (2011). Polymer of intrinsic microporosity incorporating thioamide functionality: preparation and gas transport properties. *Macromolecules*, 44(16), 6471-6479.

[18] Jia, Y. T., Gong, J., Gu, X. H., Kim, H. Y., Dong, J., & Shen, X. Y. (2007). Fabrication and characterization of poly (vinyl alcohol)/chitosan blend nanofibers produced by electrospinning method. *Carbohydrate polymers*, 67(3), 403-409.

CHAPTER 3

CATIONIC-CELLULOSE NANOFIBERS: PREPARATION AND DYEABILITY WITH ANIONIC REACTIVE DYES FOR APPAREL APPLICATION

3.1 INTRODUCTION

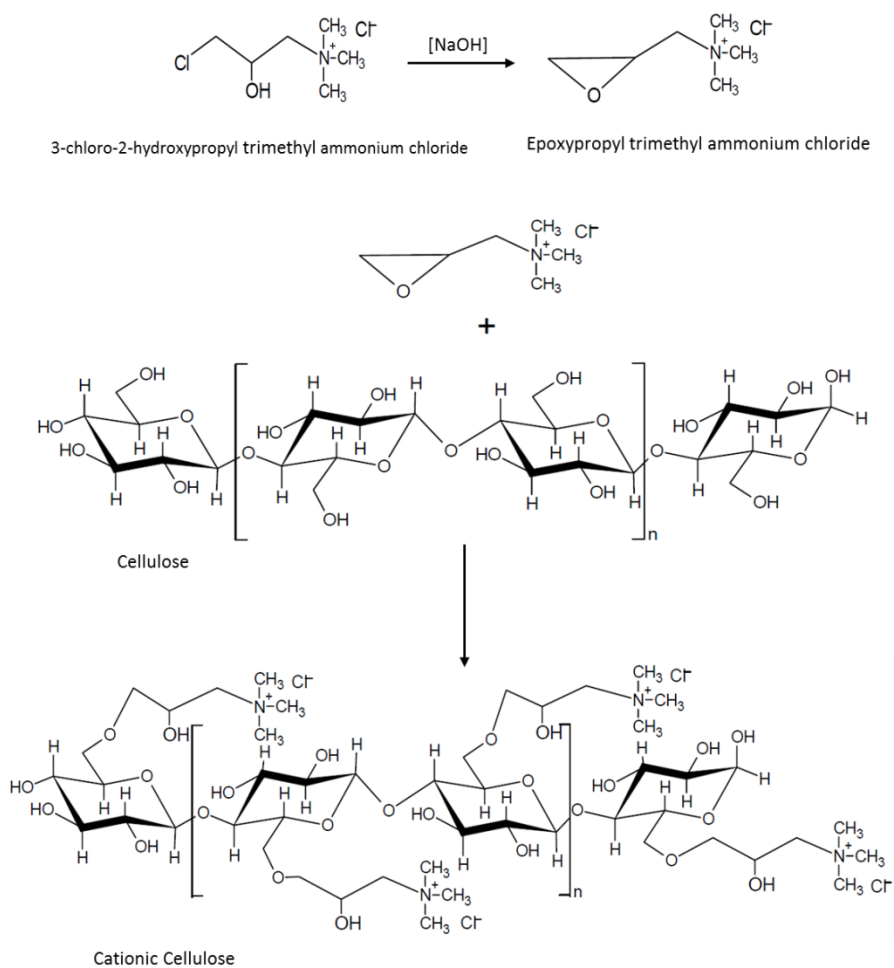
Fashion and casual apparel of cellulose based have widely been used by a consumer due to its outstanding properties of breathability, air permeability, hygroscopicity, no static electricity, biodegradability [1-3] and show interesting physical properties such as a low density together with high mechanical characteristics [4]. These cellulosic apparel are marketed in the form of white, dyed or printed according the end-user's requirement. Cellulose nanofibers have been reported to be used in several technical fields [5-8]. Nanofibers exhibit even better breathability than the conventional cellulosic apparel due to having a small pore size between nanofibers [9] and high porosity [10]. Therefore, nanofibers have a great potential for use as apparel; and have attracted a great deal of interest recently. Kim et al. described garment breathability, thermal insulation, antibacterial and mold properties of nanofibers [11]. Lee et al. [12] & Lee et al. [13] produced nanofiber on a mass scale for apparel use successfully. They demonstrated that nanofibers exhibit very good comfort properties and have excellent durability without loss of mechanical properties when subjected to laundering. Waterproof breathable nanofibers show the best combination of waterproofing and breathability as compared

to the conventional fabric systems [9]. Another study showed very good performance by fabric laminated by polyurethane nanofibers [14].

The current research trend in nanofibers as apparel use is increasing gradually. The past research was mainly focused within the functional properties only and to the best of our knowledge aesthetic properties of cellulose nanofibers are not investigated to date. We prepared colored cellulose and cationic-cellulose nanofibers via electrospinning and post treatment, and dyed with anionic reactive dyes for potential use as apparel. There always been a choice to dye cellulose with reactive dyes, direct dyes, sulfur dyes and vat dyes, however, reactive dyes have become a prime choice for coloring cellulosic textiles, because they provide a wide range of inexpensive brilliant colors with excellent washing fastness [15,16]. It is well know that the dye fixation of the reactive dye obtained on the cellulosic materials between 60–80%, the rest of the unfixed dye is drained into effluent during washing-off that may pose an environmental hazard [17]. The anionic character of Reactive dyes is due to the presence of water solubilizing sulfonate groups (SO_3^-). In fact, cellulose also acquires a negative surface charge in water, which lowers the dye affinity to the cellulose fiber, so high concentration of sodium sulfate or sodium chloride (30-100 g/L) in the dyebath are desired to exhaust the dye onto cellulose surface; this lead to another serious environmental hazard as a large amount of electrolyte containing effluent is discharged [18]. A good dyer puts his effort to prevent dye from being hydrolyzed and try to obtain dyed goods with minimum loss of dye. Therefore, dyer always attempt to improve color yield and higher dye fixation during cellulosic dyeing but has remained a challenge. Over recent years, cationizing cellulose by the cationic agent

has been increasing and show significant advantages in terms of improved dyeing properties [17, 20-22]. Among many cationizing agents, the 3-chloro-2-hydroxypropyltrimethylammonium chloride (CHPTAC) has attained much interest in cationization of cellulose because it is commercially available, less toxicity and very good reactivity [23-26]. Chemically cationized cellulose is usually produced by the etherifying reaction of cellulose with the quaternary ammonium cationizing reagents, such as 2,3-epoxypropyltrimethylammonium chloride (Scheme 3.1) [18,27,28]. This compound is usually formed in situ from the reaction of CHPTAC with sodium hydroxide (see Scheme 3.1).

Here, we describe preparation of Cationic-cellulose nanofibers for enhanced color yields and dye fixations, and provide comparison between dyed cellulose nanofibers and cationic-cellulose nanofibers. The dyed nanofibers were characterized by color yield (K/S), colorimetric properties by L^* , a^* , b^* , C^* and h° with ΔE^*_{CMC} , color fastness properties, FTIR and FE-SEM analysis.



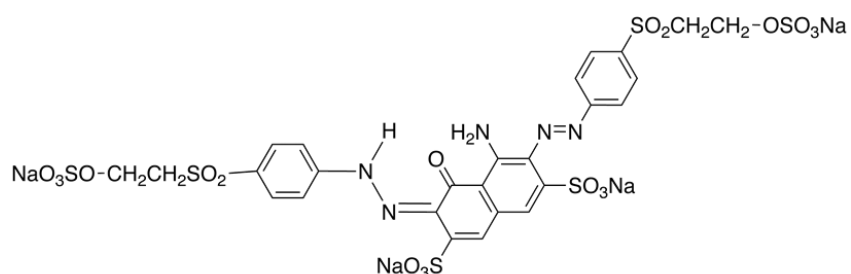
Scheme 3.1 Reactions of CHPTAC showing cationization of cellulose nanofibers [27]

3.2 EXPERIMENTAL

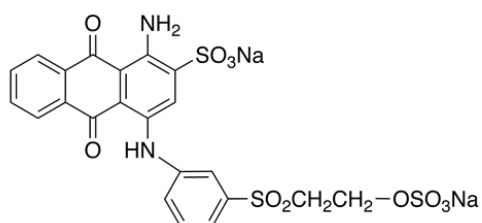
3.2.1 Materials

Cellulose acetate, CA (39.8% acetyl content having average Mw = 30 kDa) was obtained from Aldrich Chemical Company, and used without further purification. The cationizing agent namely, 3-chloro-2-hydroxypropyl trimethylammonium chloride solution, CHPTAC (60 wt% in H₂O, Mw = 188, Aldrich) was used to cationize cellulose nanofibers. Three

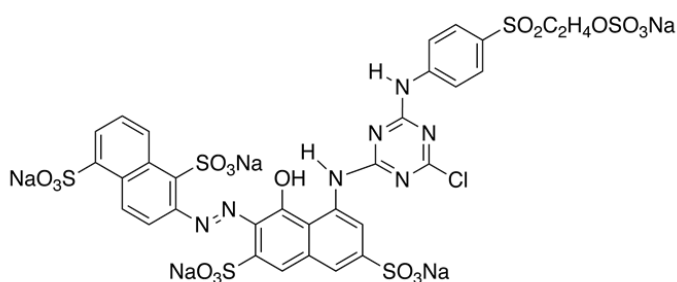
dyes were used namely, C.I. Reactive black 5 (*Vinylsulfone*), C.I. Reactive blue 19 (*Vinylsulfone*), and CI reactive red 195 (*Monoazo-monochlorotriazine+ Vinylsulfone*), supplied by the Sumitomo Chemical Company, Ltd., Japan. The corresponding dye structures for each class are given in Figure 3.1. Sodium Sulfate decahydrate (Glauber's salt, ACS reagent grade, Aldrich) and other Analar grade auxiliaries were used in this work include sodium hydroxide; sodium carbonate and acetic acid.



CI Reactive Black 5



CI Reactive Blue 19



CI Reactive Red 195

Fig. 3.1 Dye structures of reactive dyes.

3.2.2 Preparation of cationic-cellulose nanofibers

Cellulose is well known for its insolubility to most solvents; therefore, cellulose acetate nanofibers were produced via electrospinning and then deacetylated to convert into regenerated cellulose. The cellulose nanofibers were further treated with the cationic agent to form cationic-cellulose nanofibers. CA nanofibers were electrospun according to our previous work [29]. Briefly, electrospinning was performed using a high-voltage power supply (Har-100*12, Matsusada Co., Tokyo, Japan). A CA solution of 17 % by weight prepared in Acetone/ Dimethyl formamide (DMF) with 2:1 by weight was supplied through a plastic syringe attached to a capillary tip with an inner diameter of 0.6mm. A copper wire connected to a positive electrode was inserted into the CA solution and a negative electrode was connected to a metallic drum. The distance between the capillary tip and the collector was fixed at 15cm and the supplied voltage was set at 12.5 kV. Electrospun nanofibers were collected onto a rotating drum and removed after the average thickness of the CA nanofibers web was obtained in the range 60-70 μm . The diameter of nanofibers obtained in the range of 200-800 nm. The nanofiber webs were air dried for at least 48 hours before deacetylation and cationization treatment. To convert cellulose acetate into cellulose, deacetylation was carried out in 0.05M NaOH aqueous solution for 30 hours at room temperature and rinsed-off thoroughly in distilled water until the pH of nanofiber webs reached to 7. Finally, all cellulose nanofiber samples were dried at 50°C for 4 hours [29].

Cellulose nanofibers were cationized by a two-bath pad-bake process; the optimized parameters for cationization were followed [18]. All samples were dipped through the

CHPTAC/NaOH solutions, squeezed to a wet pick up of approximately 100% and baked in an oven (EYELA SLI-220) at 60°C for 6 minutes. Wherein, the molar ratio of CHPTAC to NaOH was 1:1. Finally, cationic-cellulose nanofiber were washed thoroughly to remove unfixed traces of CHPTAC and dried before a reactive dye application.

3.2.3 Dyeing of cellulose and cationic-cellulose nanofibers

All nanofiber web samples were dyed by batchwise method using a liquor-to-good ratio of 50:1 in glass tubes followed by heating in an oven with precise control of time and temperature. Dyeings were carried out to study the effect of temperature (10-80°C), dyeing time (10-80 minutes) and dye concentrations (1, 3 and 5% omw). The dye and sodium sulfate were added in liquor as the dyeing started while sodium carbonate was added after 10 minutes. In case of cationic-cellulose nanofibers, the dyeing was carried out without an addition of salt. To remove unfixed dye from dyed nanofibers, soaping-off with 2g/l Nonionic detergent (Hostpal AE Liq., Clariant) was carried out at boil for 10 minutes using 50:1 liquor-to-good ratio.

3.2.4 Color measurements. Color yield was determined by calculating corresponding K/S values from the reflectance values (%R) for each dyed cationic-cellulose nanofibers and cellulose nanofibers samples using a Konica-Minolta Spectrophotometer CM-3600d under illuminant D65, employing 10° standard observer with a UV component included and specular component excluded. The CIELAB colorimetric co-ordinates L^* , a^* , b^* , C^* and h° , and ΔE^*_{CMC} were also measured. The samples were folded so as to realize four thicknesses. The relative color strengths (the K/S values) were assessed using Equation 1:

$$K/S = (1-R^2)/2R \quad (1)$$

where R = decimal fraction of the reflectance of the dyed fabric, K = absorption coefficient and S = scattering coefficient.

The extent of covalent bonding of the dye molecule with cellulose is generally determined by the extent of dye fixation, % F . The Equation 2 as described in our previous work was used to determine the absorbed dye fixation for each dyed sample [30].

$$\% F = (K/S)_a / (K/S)_b \quad (2)$$

where, F is the dye fixation in percentage and $(K/S)_a$ and $(K/S)_b$ are after and before wash K/S of dyed samples.

3.2.5 FTIR spectroscopy. The chemical structure of cationic-cellulose and cellulose nanofibers before and after dyeing was analyzed on FTIR spectroscopy. (IR Prestige- 21 by Shimadzu, Japan).

3.2.6 FE-SEM. The morphology of nanofibers before and after dyeing was examined in FE-SEM (S-5000 by Hitachi, Japan) with the accelerating voltage of 20 kV.

3.2.7 Color fastness tests. Color fastness tests were performed for both dyed cellulose and cationic-cellulose nanofibers. Color fastness to washing was performed in Gyrowash (James H. Heal Co., UK) according to ISO 105- CO3 and Color fastness to light was performed in Apollo (James H. Heal Co., UK) according to ISO 105- BO2.

3.3 RESULTS AND DISCUSSION

3.3.1 Effect of temperature on color yield and dye fixation

Before presenting dyeability and performance comparison between cationic-cellulose and cellulose nanofibers, the dyeing parameters such as temperature and time were optimized. The cellulose nanofibers were dyed with 1% of CI Reactive Black 5. Figure 3.2a shows the effect of temperature on color yield and dye fixation for cellulose nanofibers. The color yield of CI reactive black 5 increased rapidly with increasing dyeing temperature from 30°C to 50°C and gradually until 60°C but decreased slowly at 70°C and 80°C. Increasing dyeing temperature lowers the substantivity ratio which reduced the final color yield [31].

The substantivity ratio is the most influential factor governing fixation efficiency. Figure 3.2a shows a gradual increment in dye fixation as the temperature was increased; a maximum of 85% dye fixation was achieved at 70°C and 80°C that reveals that the minimum dye hydrolysis of about 15% can be expected at this point. An increase of dyeing temperature lowers the substantivity ratio and may accelerate the rate of hydrolysis of the dye; both of these effects reduce fixation efficiency [31]. The rates of diffusion into and reaction with the nanofibers were also accelerated, however, these factors both favor fixation of the dye. It is worth considering the optimum dyeing temperature of 60°C because of higher yield though the dye fixation was slightly lower than at higher temperatures but that can further be improved by optimizing dyeing time.

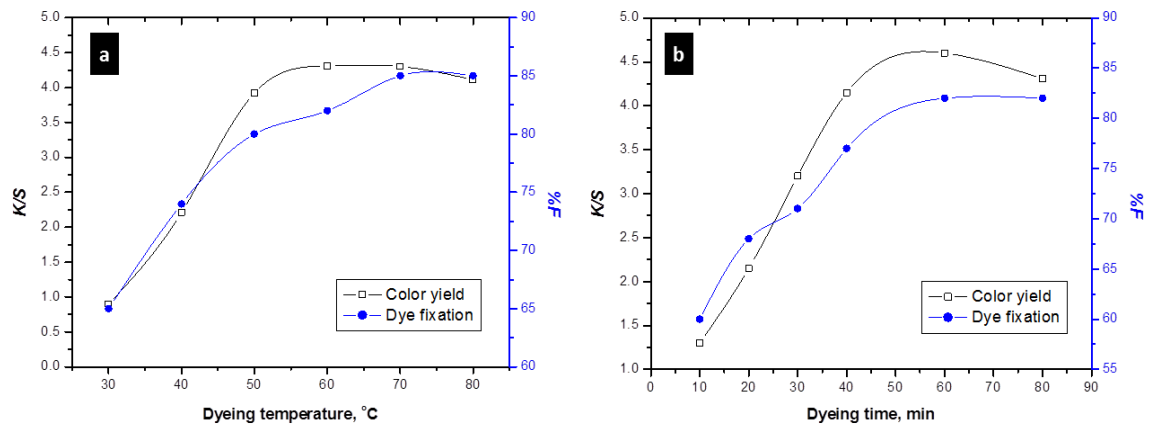


Fig. 3.2 Effect of temperature (a) and effect of time (b) on color strength (K/S) and dye fixation (%F) of CI reactive black 5 (dyeing time 80 min, dye concentration 1% omw).

3.3.2 Effect of time on color yield and dye fixation

Figure 3.2b shows the effect of dyeing time obtained at 60°C (the optimized temperature) on the color yield of the cellulose nanofibers. Color yield increased sharply until 60 minutes dyeing time but decreased slightly when dyeing was lasted for 80 minutes. The reason for this may be the dye hydrolyses at prolonged dyeing time. The %F profile as depicted in Figure 3.2b, increased as the dyeing time was increased, these results commensurate with the color yield values obtained. Like the temperature, dyeing time is one of the most influencing parameters for assessing dyeability of nanofibers. Color yield obtained at the dyeing time of 60 minutes was higher than 80 minutes, whereas %F showed no further increase at 80 minutes dyeing time; dye hydrolyses could be a contributing factor to this. Therefore, 60 minutes dyeing time was selected for further study.

3.3.3 Comparison of build-up property and dye fixation between cationic-cellulose and cellulose nanofibers

As discussed earlier, the anionic reactive dye has poor substantivity towards cellulose as cellulose adopts anionic charges when immersed in water [17]. The repulsive charges between cellulose surface and the reactive dye can be overcome by either electrolyte addition into dyebath or surface modification of cellulose. Therefore, a substantial quantity of electrolyte (sodium sulfate) was added to cellulose nanofibers and no electrolyte was added to cationic-cellulose nanofibers.

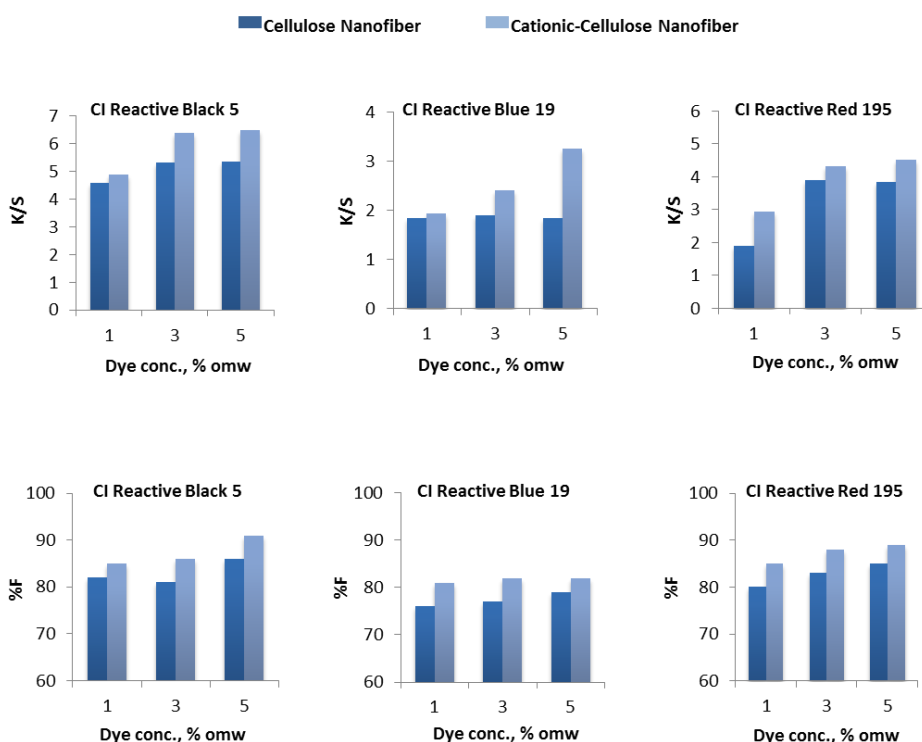


Fig. 3.3 Build-up and dye fixation (%F) of three dyes each at (1%; 3%; 5% omw) dye concentrations obtained for cellulose and cationic-cellulose nanofibers (dyeing temperature 60 °C and dyeing time 60 min).

Figure 3.3 shows a build-up property and %F of cationic-cellulose nanofibers and directly compared with cellulose nanofibers each dyed with three different dyes such as CI reactive black 5, CI reactive blue 19 and CI reactive red 195. Irrespective to the type of dye, higher color yield and %F obtained for cationic-cellulose nanofibers than the cellulose nanofibers. A build-up characteristic of each dye was investigated measuring K/S values at each dye concentrations (1%, 3% and 5%) used. The black 5 is amongst the most successful of all reactive dyes having four solubilizing groups in the precursor form of CI reactive black 5 (Figure 3.1) confer high solubility but unusually low substantivity. This dye is almost symmetrical in structure and when the sulfate ester groups are lost by 1,2 elimination, the substantivity for cellulose is enhanced and the bis(vinylsulfone) structure formed shows highly efficient fixation under alkaline conditions (Shore 1995). Build-up of CI reactive black 5 for cationic-cellulose and cellulose nanofibers revealed that there was a significant increase in K/S when dye concentration was increased from 1% to 3%, and no enhancement in K/S was obtained at higher dye concentration of 5%. This indicates that the dyeing at 3% dye concentration reached near to fiber saturation. Comparing the build-up results for Cationic-cellulose nanofibers with cellulose nanofibers, it could be observed that at all dye concentrations; K/S of the former was higher than the latter. This may be due to a higher ionic attraction between dye anion and cationic-nanofibers leading to higher dye absorption. The extremely attractive bright blue hue combined with an excellent light fastness of CI reactive blue 19 (Figure 3.1) remained unchallenged by competing blue reactive dyes for many years. The aqueous solubility of this structure is inherently low; depending only on the 2-sulfonate group after 1,2-elimination of the sulfate ester has taken place. This has led to poor reproducibility and levelling problems, but nevertheless this dye has remained second only to CI reactive black 5 in terms of market share amongst reactive dyes [32]. The build-up of CI reactive blue 19 demonstrated a very poor on cellulose nanofibers over the dye concentrations used whereas a

linear relationship obtained on cationic-cellulose nanofibers. The results showed that the cationization of cellulose nanofibers significantly enhanced the K/S of around 4.9%, 27% and 76% for dye concentrations of 1%, 3% and 5% respectively. CI reactive red 195 is a unique class of reactive containing two dissimilar reacting groups. The reaction of a dichlorotriazine dye with an arylamine containing a 2- sulfatoethylsulfone grouping is the preferred route to mixed bifunctional reactive dyes capable of reacting with cellulose either via a monochlorotriazine moiety or a vinylsulfone group (Figure 3.1). Both reactive systems can contribute to the fixation process but the relatively greater reactivity of the vinylsulfone group ensures that most of the fixation arises via this function. The build-up of CI reactive red 195 was higher on cationic-cellulose nanofibers than on cellulose nanofibers. There was no further increase in K/S of cationic-cellulose and cellulose nanofibers when dye concentration was increased from 3% to 5%, however, the Cationic-cellulose yielded higher K/S than the cellulose nanofibers, for instance, about 21%, 10% and 16% K/S enhancement at 1%, 3% and 5% dye concentrations respectively.

The dye fixation %F was investigated for each dye that corresponds to the degree of dye fixation to cellulose structure. Figure 3.3 depicts %F for each CI reactive black 5, CI reactive blue 19 and CI reactive red 195. Irrespective to dye concentrations used, the %F of all three dyes obtained for the cationic-cellulose was higher than the cellulose nanofibers. For instance, CI reactive black 5 and CI reactive red 195 on cationic-cellulose nanofibers achieved dye fixation values of 85%-91% and 85%-89% respectively. A relatively lower dye fixation of 81%-82% achieved for CI reactive blue 19 compared to CI reactive black 5 and CI reactive red 195 in case of cationic-cellulose nanofibers. In general,

the higher color yields obtained for cationic-cellulose nanofibers without electrolyte addition that may be due to the ionic attraction between the quaternary ammonium groups of CHPTAC and anionic sites of the dyes.

3.3.4 Colorimetric data of dyed nanofibers

When the shade of the dyed cationic-cellulose nanofibers was compared visually, showed a noticeable shade difference compared to cellulose nanofibers samples. To compare the shade difference between cationic-cellulose nanofibers and cellulose nanofibers, the color difference (ΔE^*_{cmc}) was calculated using the measured values of CIELAB L^* , a^* , b^* , C^* and h° . Color differences between cationic-cellulose nanofibers and cellulose nanofibers by Colorimetric data obtained for each dye are shown in Figure 3.4 (a-c).

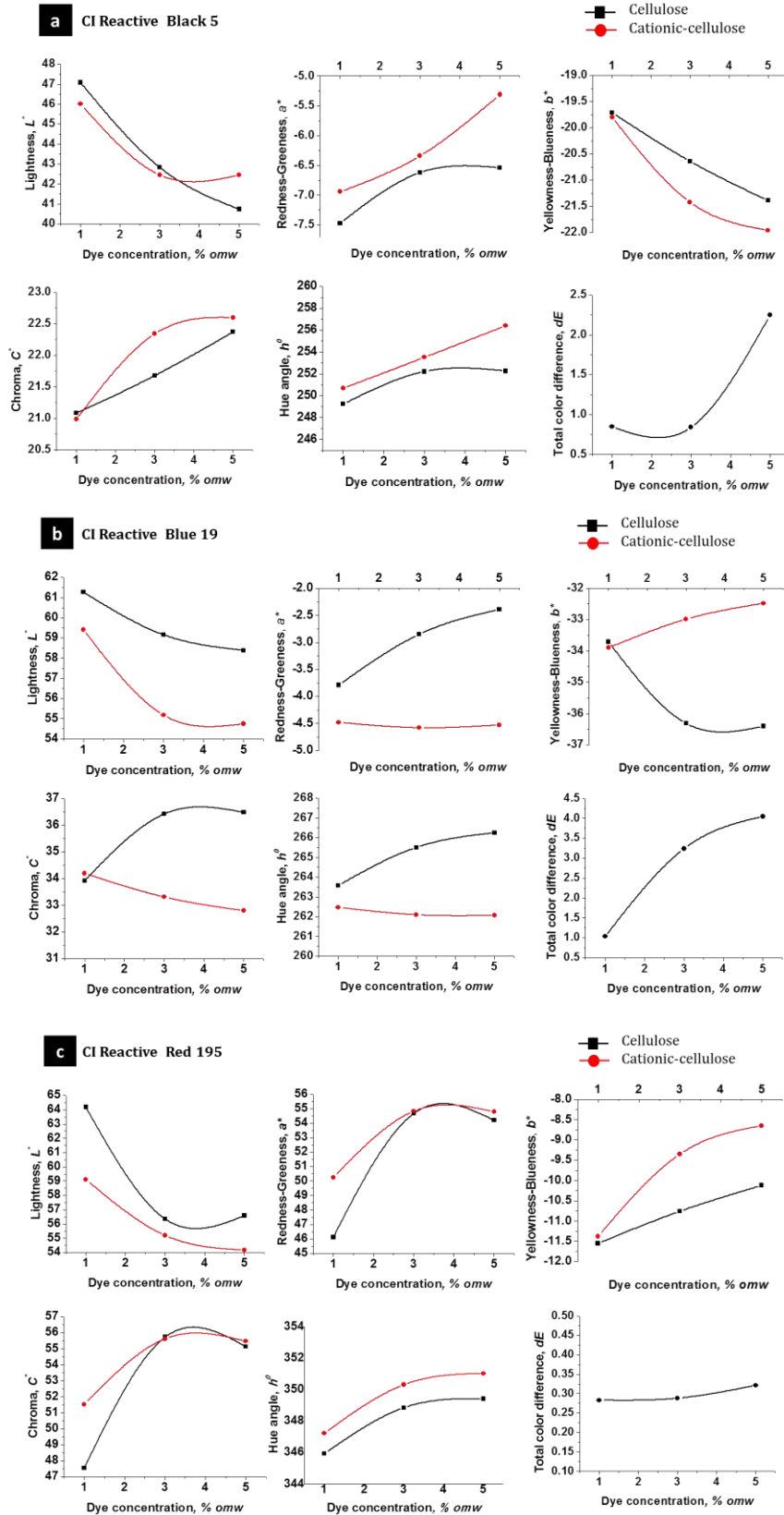


Fig. 3.4 (a) Color difference for CI reactive black 5. (b) Color difference for CI reactive blue 19. (c) Color difference for CI reactive red 195.

CI Reactive Black 5

Referring Figure 3.4(a), Cationic-cellulose nanofibers became darker until the dye concentration of 3% and remain consistent at 5% dye concentration while cellulose nanofibers showed linear decrement of Lightness value demonstrating that samples became darker as the dye concentration was increased. The tonal differences were studied by Cartesian coordinates a^* and b^* showed that the tone of cationic-cellulose nanofibers shifted towards a redder region in coordinate a^* and towards a bluer region in coordinate b^* as the dye concentration was increased. In addition, the tonal differences were also investigated using Polar coordinates C^* and h° . Higher C^* value suggested that the cationic-cellulose nanofibers were brighter than the cellulose nanofibers at higher dye concentrations. The total color difference was calculated using ΔE_{CMC} formulae [30] that quantify total color deviations from reference. ΔE_{CMC} for cationic-cellulose nanofibers was calculated against reference cellulose nanofibers and as expected, data demonstrated that the cationic-cellulose nanofibers went beyond commercial factor set at 1.0 and significantly increased at dye concentrations of 5%. The major contributing factor to this difference was a significant difference between cationic-cellulose nanofibers and cellulose nanofibers samples in a^* value at 5% dye concentration.

CI Reactive Blue 19

Referring Figure 3.4(b), the L^* of cationic-cellulose nanofibers obtained was relatively darker than the cellulose nanofibers as the dye concentration was increased. The

Cartesian coordinates a^* and b^* showed a significant difference between cationic-cellulose nanofibers and cellulose nanofibers; the results demonstrated that the tone of cationic-cellulose nanofibers samples shifted towards a redder region in coordinate a^* and a yellower region in coordinate b^* as the dye concentration was increased. In contrast to cationic-cellulose nanofibers, the cellulose nanofibers showed no significant change in coordinate a^* but significantly shifted towards a bluer region in coordinate b^* as the dye concentration was increased. The tonal differences using Polar coordinates C^* and h° demonstrated that the Chroma, C^* of cationic-cellulose nanofibers resulted lower values than the cellulose nanofibers signifying dullness of cationic-cellulose nanofibers samples as the dye concentration was increased. On the other hand, cellulose nanofibers became brighter as the dye concentration was increased. This suggests that the increasing dye concentration of CI reactive blue 19 produced dullness in cationic-cellulose nanofibers. Since the differences between cationic-cellulose nanofibers and cellulose nanofibers were big in all coordinates (L^* , a^* , b^* , C^* and h°) at 3% and 5% dye concentration, therefore, ΔE^*_{CMC} of cationic-cellulose nanofibers was expectedly high at higher dye concentrations.

CI Reactive Red 195

Referring Figure 3.4(c), the cellulose nanofibers did not show any further decrement in L^* value at an extent the cationic-cellulose nanofibers showed at the dye concentration of 5%. This suggests that color darkness was enhanced in cationic-cellulose nanofibers as the dye concentration was increased from 3% to 5%. The Cartesian coordinate a^* showed a relatively no significant difference between cationic-cellulose nanofibers and

cellulose nanofibers at dye concentrations of 3% and 5%; the results for both cationic-cellulose nanofibers and cellulose nanofibers demonstrated that the tone shifted towards a redder region. It has less effect on sample appearance due to the fact that the samples were dyed with red hue dyes. The results of cationic-cellulose nanofibers in coordinate b^* showed a tone shifting towards a yellower region as the dye concentration was increased. In fact, the yellowness imparted a brightness in the both cationic-cellulose nanofibers and cellulose nanofibers. The increment of C^* value at higher dye concentrations indicate samples become brighter. The results of C^* and b^* are well in agreement. Except the coordinate b^* , all coordinates (L^* , a^* , C^* and h°) found to have small color differences between cationic-cellulose nanofibers and cellulose nanofibers, this is the reason why ΔE^*_{CMC} of cationic-cellulose nanofibers achieved within commercial factor 1.0 and consistent at all dye concentrations.

3.3.5 Structural feature of nanofibers

The change in chemical structure of dyed and undyed nanofibers is described in Figure 3.5. The characteristic adsorption peaks of cellulose acetate attributed to the vibrations of the acetate group C=O at 1745, C-CH₃ at 1375 and C-O-C at 1235 cm⁻¹ disappeared and an absorption peak O-H at 3500 cm⁻¹ increased, as shown in Figure 3.5a. This substantiates a complete conversion of cellulose acetate nanofibers into cellulose nanofibers. FT-IR spectra of all samples showed characteristic cellulose peaks around 1,000–1,200 cm⁻¹. Other characteristic bands related to the chemical structure of cellulose were the hydrogen-bonded O-H stretching at 3,550–3,100 cm⁻¹, the C-H stretching at 2,917 cm⁻¹, and the C-H wagging at 1,316 cm⁻¹. Cationic-cellulose nanofibers

(Figure 3.5c) has an obvious new peak at $1,491\text{ cm}^{-1}$ (C-N) compared to cellulose nanofibers (Figure 3.5b), which attributed to quaternary ammonium groups [21]. These results indicated that the reaction has successfully converted cellulose into cationic-cellulose. Two additional bands appeared at 875 cm^{-1} and 925 cm^{-1} which attributed to an asymmetrical ring stretching of the epoxy ring of un-reacted CHPTAC [33]. It is difficult to identify the dye interaction with nanofibers due to small ratio of dye concentration to nanofiber mass, however, the spectra of cationic-cellulose nanofibers retained to cellulosic form after being dyed with CI reactive black 5, (Figure 3.5d & 3.5e). The FTIR spectra of CI reactive blue 19 and CI reactive red 195 were similar to that of CI reactive black and therefore, omitted. This suggests the cationization was an interim product before dye was applied and we may expect structural properties of dyed Cationized-nanofiber as that of the dyed cellulose nanofibers.

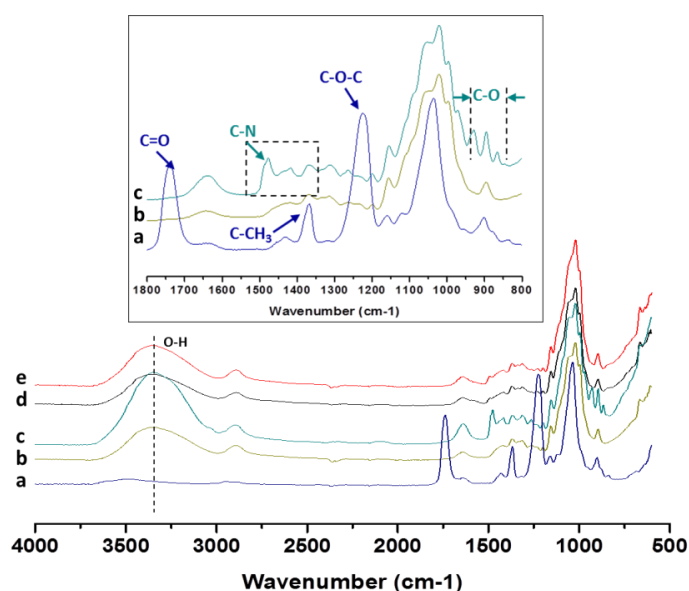


Fig. 3.5. FTIR spectra: (a) CA, (b) CA-DA, (c) cationic cellulose, (d) cellulose dyed with CI reactive black 5, (e) cationic-cellulose dyed with CI reactive black 5

3.3.6 Surface morphology of nanofibers

The Figure 3.6 (a-g) shows SEM images of cationic-cellulose nanofibers and cellulose nanofibers each undyed and dyed nanofibers and the inset images are FE-SEM images. Referring Figure 3.6, the cationic-cellulose nanofibers (b) became irregular slightly than the cellulose nanofibers (a) after being cationization treatment but again retained their regularity after dyeing with each dye class; refer images (c) through (h). The SEM images show a very good stability and regularity of nanofibers even after dyeing in aqueous solution. Therefore, it is inferred that the dyeing process does not affect morphology of cationic-cellulose nanofibers and cellulose nanofibers. Besides, surface smoothness of nanofibers (see inset FE-SEM images) unaffected throughout various wet treatments such as, deacetylation, cationization, dyeing and washing-off process.

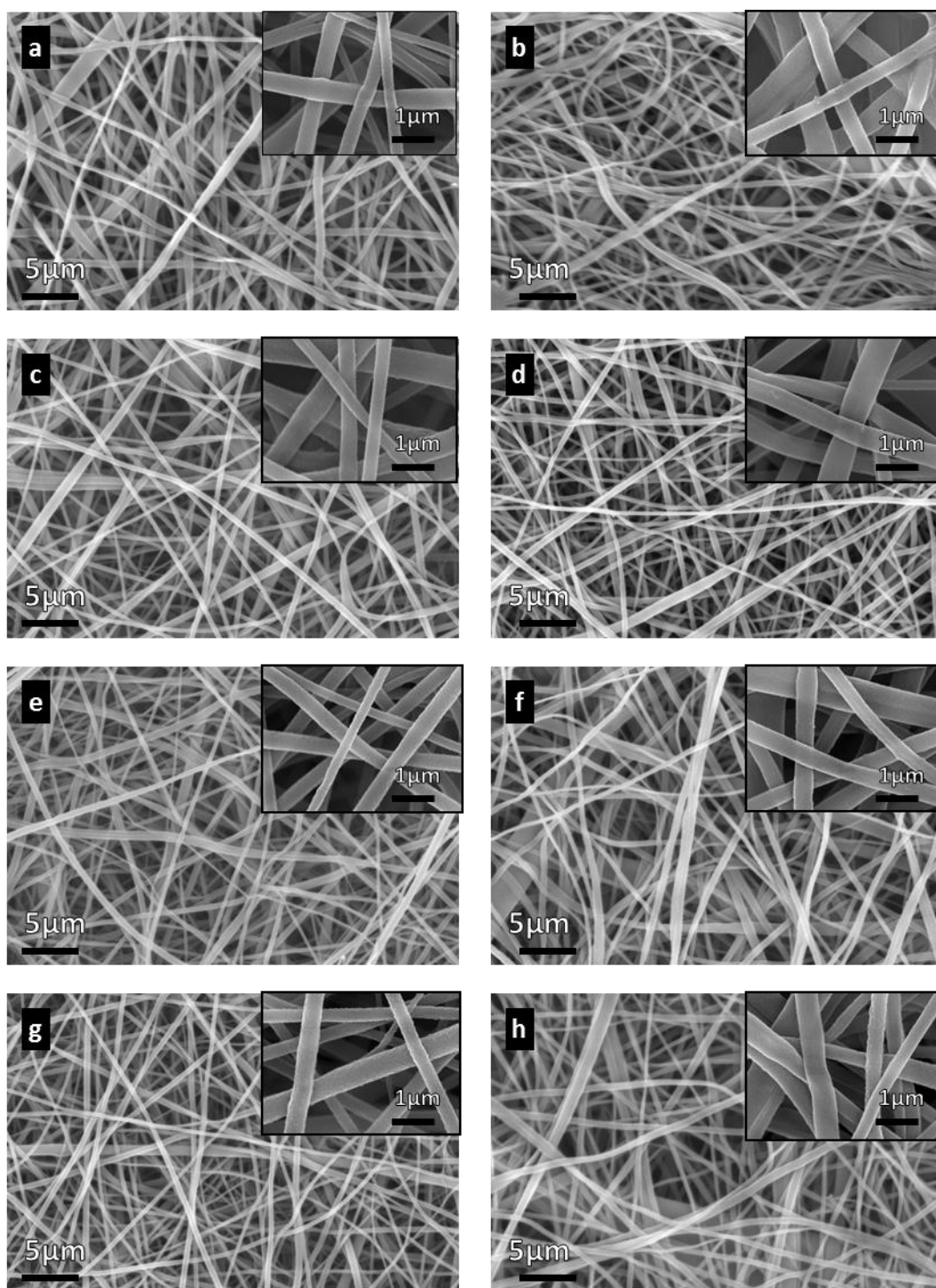


Fig. 3.6 SEM images (a, c, e and g) cellulose and (b, d, f and h) cationic-cellulose nanofibers; inset are FE-SEM images; (a and b) undyed, (c and d) dyed with CI reactive black 5, (e and f) dyed with CI reactive blue 19 and (g and h) dyed with CI reactive red 195

3.3.7 Color fastness performance of nanofibers

Table 3.1 outlines the color fastness to washing test according to ISO 105/C03. Irrespective to the class of dye used, the dyed cationic-cellulose nanofibers qualifies well along with the dyed cellulose nanofibers and showed superior staining ratings on each component of a multifiber strip. The reason for this may be due to the ionic interaction that took part in addition to covalent bonding between dye and the cationic-cellulose nanofibers and thus reduced the removal of dyes from the nanofibers during the washing. The shade change rating of 4-5 obtained in both cases cationic-cellulose nanofibers and cellulose nanofibers that are good to excellent. The results obtained from wash fastness test confirm that the dye fixation was very good on cationic-cellulose nanofibers as well as on cellulose nanofibers. It could be safely concluded that the cationic-cellulose nanofibers can significantly be preferred over cellulose nanofibers for dyeing based on the advantages discussed earlier.

Table 3.1 Color fastness to washing test ISO 105/C03 and color fastness to light test ISO 105/BO2

Sample	Dye class	Light fastness	Change of shade	Staining on multifiber					
				CT	CO	PA	PES	PAC	CV
Cationic-Cellulose nanofibers ¹	CI Reactive black 5	3-4	4-5	5	5	5	5	5	5
	CI Reactive blue 19	5-6	4-5	5	5	5	5	5	5
	CI Reactive red 195	3-4	4-5	5	5	5	5	5	5
Cellulose nanofibers ¹	CI Reactive black 5	3-4	4-5	5	4-5	4-5	5	5	4-5
	CI Reactive blue 19	5-6	4-5	5	4-5	4-5	5	5	4-5
	CI Reactive red 195	3-4	4-5	5	4-5	4-5	5	5	4-5

¹Dyeing conditions: Dye concentration 3%, temperature 60°C and time 60 min

The color fastness to light was performed according to ISO 105/BO2 and the results are summarized in Table 3.1. The Light fastness ratings in all cases were found reasonably good keeping dark shades in consideration. There was no difference obtained between cationic-cellulose nanofibers and cellulose nanofibers in the case of all three dyes used. Interestingly, the color fastness to light for CI reactive blue 19 was found to have very good ratings for both cationic-cellulose nanofibers and cellulose nanofibers samples due to having anthraquinone chromogen.

3.4 CONCLUSION

The cationic-cellulose and cellulose nanofibers can effectively be dyed with commercially available reactive dyes by batchwise method. The cationic-cellulose nanofibers demonstrated potential advantages over cellulose nanofibers due to enhanced color yield and higher dye fixation without addition of electrolyte. Built-up property of each dye showed improvement at all dye concentrations in case of cationic-cellulose nanofibers. Except CI reactive blue 19, it was observed that there was no significant improvement in color yield and dye fixation at the dye concentration of 5%. Excellent color fastness to washing results were achieved for both dyed cellulose and cationic-cellulose nanofibers. Despite the number of wet treatments, the morphology of nanofibers remains structurally stable, smooth and regular. The cellulose based colored and breathable nanofibers paved the way toward novel apparel applications and can potentially be considered as future apparel for surgical gowns, institutional articles, casual and fashion.

3.5 REFERENCES

[1] Schurz, J. (1999). A bright future for cellulose. *Progress in Polymer Science*, 24(4), 481–483.

[2] Klemm, D., Heublein, B. Fink, H.-P., & Bohn, A. (2005). Cellulose: Fascinating Biopolymer and Sustainable Raw Material. *Angewandte Chemie International Edition*, 44(22), 3358–3393.

[3] Klemm, D., Kramer, F., Moritz, S., Lindstrom, T., Ankerfors, M., Gray, D., & Dorris, A. (2011). Nanocelluloses: A New Family of Nature-Based Materials. *Angewandte Chemie International Edition*, 50(24), 5438–5466.

[4] Berlioz, S., Molina-Boisseau, S., Nishiyama, Y., & Heux, L. (2009). Gas-Phase Surface Esterification of Cellulose Microfibrils and Whiskers. *Biomacromolecules* 10(8), 2144–2151.

[5] Filpponen, I., Kontturi, E., Nummelin, S., Rosilo, H., Kolehmainen, E., Ikkala, O., & Laine, J. (2012). Generic Method for Modular Surface Modification of Cellulosic Materials in Aqueous Medium by Sequential “Click” Reaction and Adsorption. *Biomacromolecules* 13(3), 736–742.

[6] Iwamoto, S., Isogai, A., & Iwata, T. (2011). Structure and Mechanical Properties of Wet-Spun Fibers Made from Natural Cellulose Nanofibers. *Biomacromolecules*, 12(3), 831–836.

[7] Ishii, D., Saito, T., & Isogai, A. (2011). Viscoelastic Evaluation of Average Length of Cellulose Nanofibers Prepared by TEMPO-Mediated Oxidation. *Biomacromolecules*, 12(3), 548–550.

[8] Ifuku, S., Nogi, M., Abe, K., Handa, K., Nakatsubo, F., & Yano H. (2007). Surface Modification of Bacterial Cellulose Nanofibers for Property Enhancement of Optically Transparent Composites: Dependence on Acetyl-Group DS. *Biomacromolecules*, 8(6), 1973–1978

[9] Yoon, B., & Lee, S. (2011). Designing waterproof breathable materials based on electrospun nanofibers and assessing the performance characteristics. *Fibers and Polymers*, 12(1), 57-64.

[10] Maa, Z., Kotakia, M., & Ramakrishna S. (2005). Electrospun cellulose nanofiber as affinity membrane. *Journal of Membrane Science*, 265(1–2), 115–123.

- [11] Kim, B. S., Kimura, N., Kim, H. K., Watanabe, K., & Kim, I. S. (2011). Thermal insulation, antibacterial and mold properties of breathable nanofiber-laminated wallpapers. *Journal of Nanoscience and Nanotechnology*, 11(6), 4929-4933.
- [12] Lee, S., Kimura, D., Yokoyama, A., Lee, K. H., Park, J. C., & Kim, I. S. (2009). The Effects of Laundering on the Mechanical Properties of Mass-produced Nanofiber Web for Use in Wear. *Textile Research Journal*, 79(12), 1085-1090.
- [13] Lee, S., Kimura, D., Lee, K. H., Park, J. C., & Kim, I. S. (2010). The Effect of Laundering on the Thermal and Water Transfer Properties of Mass-produced Laminated Nanofiber Web for Use in Wear. *Textile Research Journal*, 80 (2), 99-105.
- [14] Kang, Y. K., Park, C. H., Kim, J., & Kang, T. J. (2007). Application of electrospun polyurethane web to breathable water-proof fabrics. *Fibers and Polymers*, 8(5), 564-570.
- [15] Wang, H., & Lewis, D. M. (2002). Chemical modification of cotton to improve fibre dyeability. *Coloration Technology*, 118(4), 159–168.
- [16] Xie, K. L., Hou, Ai. Q., & Wang, X. J. (2008). Dyeing and diffusion properties of modified novel cellulose with triazine derivatives containing cationic and anionic groups. *Carbohydrate Polymers*, 72(4), 646–651.

[7] Xie, K. L., Liu, H., & Wang, X. J. (2009). Surface modification of cellulose with triazine derivative to improve printability with reactive dyes. *Carbohydrate Polymers*, 78(3), 538–542.

[18] Wang, L., Ma, W., Zhang, S., Teng, X., & Yang, J. (2009). Preparation of cationic cotton with two-bath pad-bake process and its application in salt-free dyeing. *Carbohydrate Polymers*, 78(3), 602–608.

[19] Ma, W., Zhang, S. F., Tang, B. T., & Yang, J. Z. (2005). Pretreatment of cotton with poly(vinylamine chloride) for salt-free dyeing with reactive dyes. *Coloration Technology*, 121(4), 193–197.

[20] Zhang, S. F., Ma, W., Ju, B. Z., Dang, N. Y., Zhang, M., Wu, S. L., & Yang, J. (2005). Continuous dyeing of cationised cotton with reactive dyes. *Coloration Technology*, 121(4), 183–186.

[21] Zhang, M., Ju, B. Z., Zhang, S. F., Ma, W., & Yang, J. Z. (2007). Synthesis of cationic hydrolyzed starch with high DS by dry process and use in salt-free dyeing. *Carbohydrate Polymers*, 69(1), 123–129.

- [22] Zhang, F., Chen, Y. Y., Lin, H., Wang, H., & Zhao, B. (2008). HBP-NH₂ grafted cotton fiber: Preparation and salt-free dyeing properties. *Carbohydrate Polymers*, *74*(2), 250–256.
- [23] Song, Y., Sun, Y., Zhang, X., Zhou, J., & Zhang, L. (2008). Homogeneous Quaternization of Cellulose in NaOH/Urea Aqueous Solutions as Gene Carriers. *Biomacromolecules*, *9*(8), 2259–2264.
- [24] Song, Y., Wang, H., Zeng, X., Sun, Y., Zhang, X., Zhou, J., & Zhang, L. (2010). Effect of Molecular Weight and Degree of Substitution of Quaternized Cellulose on the Efficiency of Gene Transfection. *Bioconjugate Chemistry*, *21*(7), 1271-1279.
- [25] Song, Y., Zhang, J., Gan, W., Zhou, J., & Zhang, L. (2010). Flocculation Properties and Antimicrobial Activities of Quaternized Celluloses Synthesized in NaOH/Urea Aqueous Solution. *Industrial & Engineering Chemistry Research*, *49*(3), 1242-1246.
- [26] You, J., Zhou, J., Li, Q., & Zhang, L. (2012). Rheological Study of Physical Cross-Linked Quaternized Cellulose Hydrogels Induced by β -Glycerophosphate. *Langmuir*, *28*(11), 4965–4973.
- [27] Hauser P. J. (2000). Reducing pollution and energy requirements in cotton dyeing, *Textile Chemist and Colorist & American Dyestuff Reporter*, *32*(6), 44-48.

[28] Montazer, M., Malek, R., & Rahimi, A. (2007). Salt free reactive dyeing of cationized cotton. *Fibers and Polymers*, 8(6), 608-612.

[29] Khatri, Z., Wei, K., Kim, B. S., & Kim, I. S. (2012). Effect of deacetylation on wicking behavior of co-electrospun cellulose acetate/polyvinyl alcohol nanofibers blend. *Carbohydrate Polymer*, 87(3), 2183-2188.

[30] Khatri, Z., Memon, H. M., Khatri, A., & Tanwari, A. (2011). Cold Pad-Batch dyeing method for cotton fabric dyeing with reactive dyes using ultrasonic energy. *Ultrasonics Sonochemistry*, 18(8), 1301-1307.

[31] Shore J. (1995). Dyeing with reactive dyes. In Shore J. (Ed.), *Cellulosic dyeing* (pp. 189-245). United Kingdom: Society of Dyers and Colourists.

[32] Shore J. (2002). Chemistry of reactive dyes. In Shore J. (Ed.), *Colorants and Auxiliaries* (pp. 356-443). United Kingdom: Society of Dyers and Colourists.

[33] Robert, M. S., Francis, X. W., & David, J. K. (2005). *Spectrometric Identification of Organic Compounds*. (7th Ed.). United States: John Wiley and Sons Inc.

CHAPTER 4

PAD DYEING OF CELLULOSE ACETATE NANOFIBERS WITH DISPERSE DYES

4.1 INTRODUCTION

The growing application of nanofibers in various fields led the nanofibers research intense in terms of exploring multifunctional properties. The prominent and potential applications of nanofibers are in filter membranes [1], biosensors [2,3], wound dressings [4], tissue engineering scaffolds [5], drug delivery systems [6,7], protective clothing [8,9] and nanofibrous composites [10]. Cellulose Acetate (CA) nanofibers have unique absorption properties and therefore they have been considered a suitable candidate for applications such as CA nanofibers with photochromic property [11], antimicrobial property [12], substrate for biosensor [13], highly porous membrane [14] etc. Beside, its technical application, a few patents and papers on nanofibers apparel have been appeared recently. Lee, 2009 produced nanofiber in mass scale for apparel use successfully [15,16]. The results indicated that the nanofiber web had excellent durability without loss of mechanical properties when subjected to laundering. It has been shown that the nanofibers apparel demonstrated better breathable, thermal insulation, antibacterial and mold properties [17]. Nanofibers also exhibit very good comfort having thermal and water transfer properties [15]. Yoon & Lee have found better waterproofing

and breathability was achieved in mass-produced nanofiber layered fabric system as compared to the conventional fabric systems [18]. Some studies showed a very good performance by fabric laminated by polyurethane nanofibers [19]. Based on the current research trend in nanofibers as apparel use, the researchers mainly focused on their functional properties only and to the best of our knowledge aesthetic properties are not investigated to date. It is well known that disperse dyes have the affinity towards the CA polymer [20].

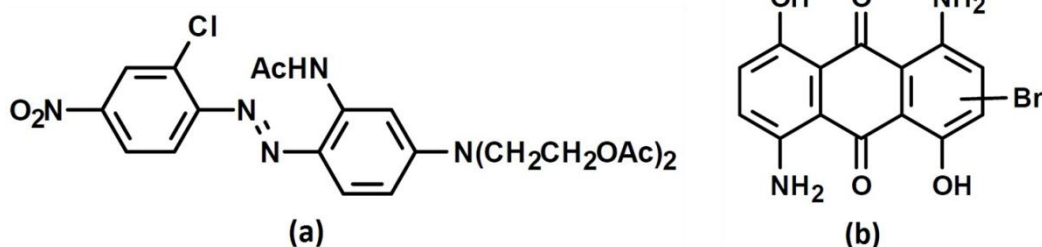
In this report, we investigated the dyeability and dyeing properties of CA nanofibers web with disperse dyes to produce colored nanofibers for apparel use. We electrospun CA nanofibers from polymer solution and then dyed nanofiber webs with disperse dyes by pad-dry-bake method. The dyed nanofibers were evaluated for color yield (K/S), colorimetric values, color fastness, tensile properties and SEM analysis.

4.2 EXPERIMENTAL

4.2.1 Materials

Cellulose acetate, CA (39.8% acetyl content having an average $M_w = 30$ kDa) was obtained from Aldrich Chemical Company, and used without further purification. Commercial disperse dyes, Clariant's Foron Rubine S-GFL 150 (CI Disperse Red 167:1, high energy level) and Foron Blue E-BL (CI Disperse Blue 56, low energy level), were used. The dye structures are shown in Figure 4.1. The selection criteria of dyes included process

compatibility, commercial usage, variety of energy levels and color. Laboratory grade



acetic acid was used for adjusting dyebath pH.

Figure 4.1 Dye structures of (a) CI Disperse Red 167:1 and (b) CI Disperse Blue 56

4.2.2 Electrospinning

CA nanofibers were electrospun according to our previous work [21]. Briefly, A high-voltage power supply (Har-100*12, Matsusada Co., Tokyo, Japan) was used for electrospinning. A CA solution of 17% by weight prepared in Acetone/ Dimethyl formamide (DMF) with 2:1 by weight was supplied through a plastic syringe attached to a capillary tip with an inner diameter of 0.6mm with the supplied voltage of 12.5 kV. Electrospun nanofibers were collected onto a rotating drum and removed after the average web thickness of 60 μm was obtained. Nanofibers samples were cut into 5 cm \times 5 cm and were conveniently handled during padding, baking and washing. The average thickness of all nanofibers webs were measured by Digital Micrometer MCD 130-25 with measuring sensitivity of 1 μm . The nanofiber webs were air dried for at least 48 hours before dyeing.

4.2.3 Dyeing of nanofibers

The nanofiber web samples were dyed by padding (two dip-two nip, 100% liquor pick-up) on a Rapid laboratory horizontal padding mangle (with 30 g/L dye in a dyebath having pH of 5 (adjusted using acetic acid)). The samples were air dried at ambient temperature of around 35°C using fan for 20 min, followed by baking on a Rapid laboratory mini-dryer for 60 sec, and finally given a gentle rinse with warm then cold water. The wash was given in water bath and continued until no dye bleeding was observed. Dyeings were carried out to study the effect of variation in the magnitudes of baking temperature (80-180°C), baking time (0–120 sec) and dye concentration (10–50 g/L).

4.2.4 Measurements

Color yield (K/S) value and $CIE L^* a^* b^* C^*$ and h^o coordinates at the maximum absorption peak were measured on a Gretag Macbeth CE-7000A spectrophotometer (settings: 8.4 mm sample aperture, illuminant D65, UV included, the specular component included, reflectance mode and 1964 (10°) CIE Supplementary Standard Observer). The color yield after rinsing (K/S) was obtained as the final color yield. The nanofibers samples were folded twice so as to realize four thicknesses while presenting to spectrophotometer for color measurement. The color fastness to washing (ISO 105-C10:2006), hot pressing (ISO 105 – X11) and light (ISO 105-B02) were performed on dyed samples [22-24].

The morphology of dyed and undyed nanofibers were examined in SEM (S-3000N by Hitachi, Japan) with an accelerating voltage of 30 kV. Mechanical property of the

nonwoven nanofibers was performed according to ASTM D-638 using a universal testing machine (TENSILON RTC1250A, A&D Company, Ltd, Japan). The crosshead speed was set at 5.0 mm/min.

4.3 RESULTS AND DISCUSSION

4.3.1 Effect of baking temperature

The CA nanofibers were dyed with two different classes of disperse dyes viz. high and low energy level (sublimation fastness). As the glass transition (T_g) of cellulose acetate nanofibers is around 190°C [25], therefore, the maximum baking temperature employed was 180°C. As was expected, Figure 4.2a shows that the color yield increased with increasing the baking temperature. The related effect of temperature can also be seen on the color depth (in terms of lightness, L^*) and Chroma (C^*) in Figure 4.2; where decreased L^* values (Figure 4.2b) indicating the sample darkness with increasing baking temperature while increasing C^* values (Figure 4.2c) indicating the color saturation with increasing baking temperature. The increase in color yield for CI Disperse Blue 56 was gradual. However, the same was the case for CI Disperse Red 167:1 only up to 140°C after which the rate of increase was notably higher. This may be because the Red 167:1 is a high energy level dye having comparatively bigger dye molecular size. This indicates that the proper diffusion of dyes in the nanofiber in a short dwell-time of dye fixation (i.e.60 sec), hence the definite color development on the nanofiber, was achieved at temperatures above 140°C.

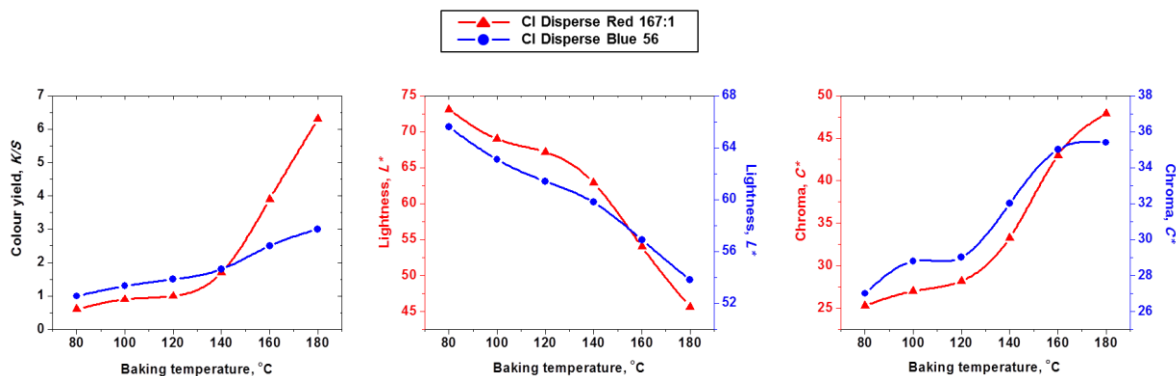


Figure 4.2. Effect of baking temperature on (a) colour yield (K/S), (b) lightness (L*) and (c) chroma (C*). For those plots with two y-axes, the right scale corresponds to CI Disperse Blue 56 measurements, the left scale corresponds to CI Disperse Red 167:1 measurements

4.3.2 Effect of baking time

The effect of baking time at 180°C on the color yield of samples dyed with 30 g/L CI Disperse Red 167:1 and CI Disperse Blue 56 is shown in Figure 4.3. Color yield increased with increasing baking time up to 90 sec for Red 167:1 and to 60 sec for Blue 56. The final color yield of the CI Disperse Blue 56 was achieved earlier than that of the CI Disperse Red 167:1. CI Disperse Blue 56 gives lower color yield may be due to its lower tinctorial strength than the CI Disperse Red 167:1. Other reason of lower color yield may be attributed due to more ready sublimation away from the substrate into the environment during baking. The rapid increase in the color yield of red dyed substrate by increase in baking temperature and time may be because the dye being larger in size starts diffusing

at certain level of substrate swelling that was achieved above 140°C and for more than 30sec.

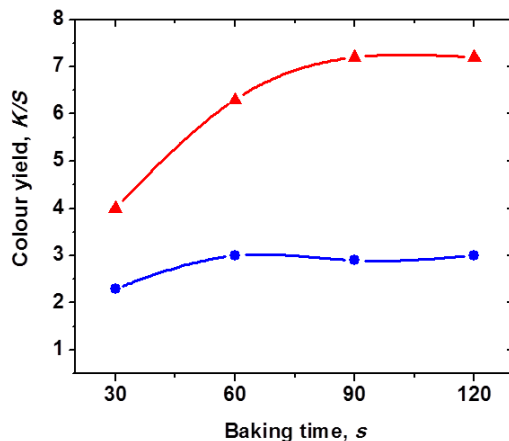


Figure 4.3 Effect of baking time on colour yield

4.3.3 Effect of dye concentration

Figure 4.4 shows the effect of dye concentrations from 10 to 50 g/L on the color yield of the samples dyed and baked at 180°C for 120 sec. As was expected, the color yield increased with increasing dye concentration for both the CI Disperse Red 167:1 and the CI Disperse Blue 56. The colorimetric results of the same shown in Figure 4.4 are conformed to the color yield results. For both dyes, the lightness (L^*) of the dyed samples decreased, thus the color depth increased, with increasing dye concentration.

CIELAB colorimetric data of each dye is shown in Figure 4.4. Referring Figure 4.4, CI disperse red 167:1 and CI disperse blue 56 showed almost a linear decrement of Lightness values (L^*) indicating that the samples became darker as the dye concentration was increased. The Cartesian coordinate a^* decreased, meaning the dyed sample became greener, with increasing CI disperse red 167:1 concentration whereas the sample dyed with CI disperse blue 56 became redder with increasing dye concentration. The coordinate b^* on the other hand, demonstrates that both dyes shifted towards a yellow region as the dye concentration was increased. Furthermore, the Polar coordinates C^* and h° were also investigated to determine the brightness and hue respectively. The saturation value C^* decreased in case of CI disperse red 167:1 at higher dye concentration indicating the samples became duller, whereas CI disperse blue 56 became brighter until the dye concentration of 40 g/L.

These results are well in agreement with the lightness values obtained for both dyes. The CI disperse red 167:1 and CI disperse blue 56 showed a change of h° angle as the dye concentration was increased. Over the dye concentrations used, significant shifts from 2° to 14° (red to yellow) and from 264° to 274° (blue to red) were observed in CI disperse red 167:1 and CI disperse blue 56 respectively.

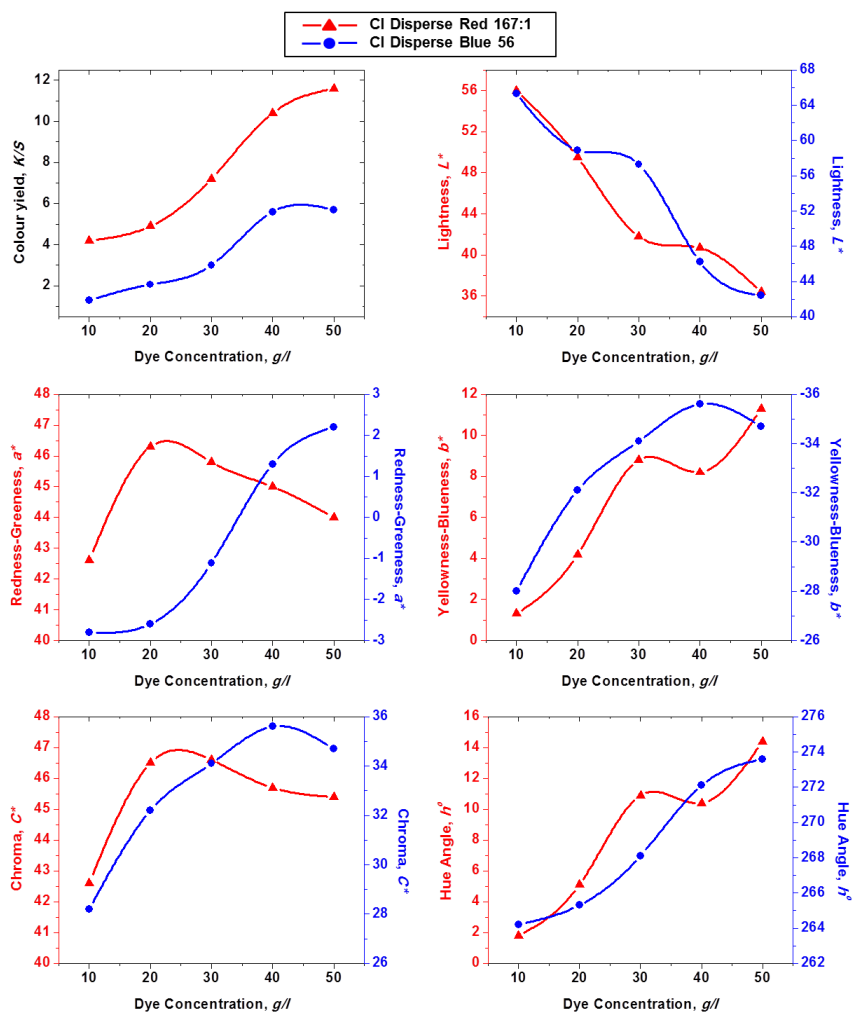


Figure 4.4 Effect of dye concentration on colour yield and colorimetric values. For those plots with two y-axes, the right scale corresponds to CI Disperse Blue 56 measurements, the left scale corresponds to CI Disperse Red 167:1 measurements

4.3.4 Color fastness properties

The light and hot pressing fastness results of the samples dyed with 30 g/L of both dyes at baking temperature of 180°C for 120 sec are given in Table 4.1. The light fastness

obtained with both dyes was good being grade 5 on the blue wool reference scale. The hot pressing of the sample dyed with CI Disperse Red 167:1 was generally better than that of the sample dyed with CI Disperse Blue 56. This may be because the Red 167:1 is high energy level dye and has bigger molecular size, thus sublimates at lesser extent. The washing test of dyed CA nanofibers was performed to assess the color fastness properties. Irrespective to the type of dye used, the washing results showed a color change of 4/5 that is very good to excellent ratings while the staining on adjacent cotton fabric was fair to good.

Table 4.1 Color fastness of dyed nanofibres

Dye Samples ^a	Color yield (K/S)	Light Fastness	Hot Pressing Fastness (Dry)	
		Blue Wool Reference	Color Change	Staining
30 g/l CI Disperse Red 167:1	7.2	5	4/5	3/4
30 g/l CI Disperse Blue 56	3.0	5	4/5	2/3

^a Baking temperature: 180 °C; baking time: 120 s

4.3.5 Morphology of dyed CA nanofibers

The Figure 4.5 (a-c) shows SEM images of undyed nanofibers and dyed (30 g/l dye, 180°C, 120 sec) nanofibers and the inset images are macroscopic photographs. The images revealed that the morphology of dyed nanofibers remained identical to that of the undyed nanofibers, indicating good resistance to wet and heat treatments carried out

during dyeing. The nanofibers remains smooth and regular even after dyeing followed by dye padding and baking at 180°C.

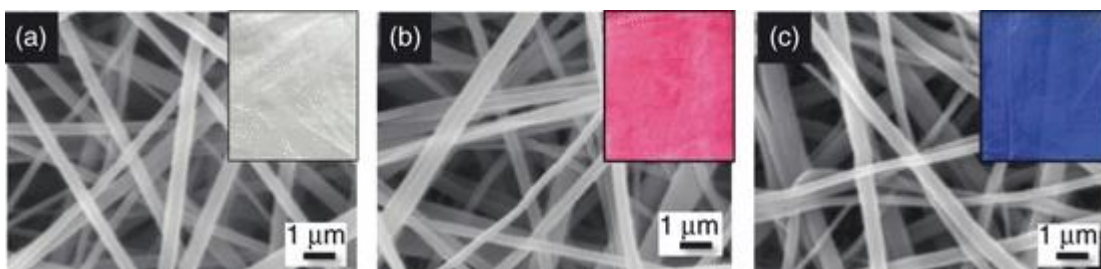


Figure 4.5 SEM images of cellulose acetate nanofibres: (a) without dye, (b) dyed with CI Disperse Red 167:1 and (c) dyed with CI Disperse Blue 56. Inset images are macroscopic photographs of dyed webs of cellulose acetate nanofibres

4.3.6 Mechanical property

The Figure 4.6 demonstrates Young's Moduli of undyed CA nanofibers and dyed CA nanofibers. The results revealed that Young's Moduli of dyed CA nanofibers increased around three-fold than the undyed CA nanofibers. This suggests the dyed samples became stiffer than the undyed samples. The increased Young's moduli of the dyed CA nanofibers were mainly due to the heat treatment during baking process. This was confirmed by pad bake treatment of 'blank sample' (just water-without dye).

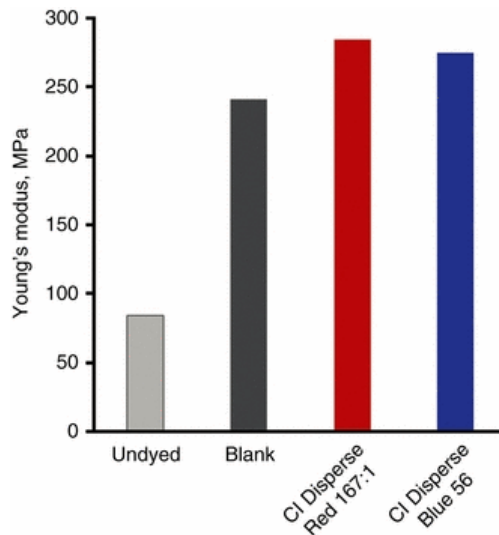


Figure 4.6 Young's moduli of undyed, blank and dyed Cellulose acetate nanofibres

4.4 CONCLUSION

The dyeing of CA nanofibers can effectively be dyed with disperse dyes by pad-dry-bake method. The dyeing results were mainly dependent on baking temperature and the dye class used. It was generally observed that the high energy level dye, CI Disperse Red 167:1, had better color yield and color fastness results than the low energy level dye, CI Disperse Blue 56. Besides successful dyeability and good color fastness results (washing, light and hot pressing), Young's modulus of dyed nanofibers increased around three times than the undyed CA nanofibers, therefore, proposed colored nanofibers worth considering for aesthetically pleasing apparel as well as for casual apparel use.

4.5 REFERENCES

- [1] Daels, N., De Vrieze, S., Sampers, I., Decostere, B., Westbroek, P., Dumoulin, A., ... & Van Hulle, S. W. H. (2011). Potential of a functionalised nanofibre microfiltration membrane as an antibacterial water filter. *Desalination*, 275(1), 285-290.
- [2] Huang, J., Liu, Y., & You, T. (2010). Carbon nanofiber based electrochemical biosensors: A review. *Analytical Methods*, 2(3), 202-211.
- [3] Lu, X., Zhou, J., Lu, W., Liu, Q., & Li, J. (2008). Carbon nanofiber-based composites for the construction of mediator-free biosensors. *Biosensors and Bioelectronics*, 23(8), 1236-1243.
- [4] Khil, M. S., Cha, D. I., Kim, H. Y., Kim, I. S., & Bhattarai, N. (2003). Electrospun nanofibrous polyurethane membrane as wound dressing. *Journal of Biomedical Materials Research Part B: Applied Biomaterials*, 67(2), 675-679.
- [5] Ki, C. S., Kim, J. W., Hyun, J. H., Lee, K. H., Hattori, M., Rah, D. K., & Park, Y. H. (2007). Electrospun three-dimensional silk fibroin nanofibrous scaffold. *Journal of Applied Polymer Science*, 106(6), 3922-3928.

[6] Yoo, H. S., Kim, T. G., & Park, T. G. (2009). Surface-functionalized electrospun nanofibers for tissue engineering and drug delivery. *Advanced drug delivery reviews*, 61(12), 1033-1042.

[7] Luu, Y. K., Kim, K., Hsiao, B. S., Chu, B., & Hadjiargyrou, M. (2003). Development of a nanostructured DNA delivery scaffold via electrospinning of PLGA and PLA-PEG block copolymers. *Journal of controlled release*, 89(2), 341-353.

[8] Gibson, P., Schreuder-Gibson, H., & Rivin, D. (2001). Transport properties of porous membranes based on electrospun nanofibers. *Colloids and Surfaces A: Physicochemical and Engineering Aspects*, 187, 469-481.

[9] Gorji, M., Jeddi, A. A., & Gharehaghaji, A. A. (2012). Fabrication and characterization of polyurethane electrospun nanofiber membranes for protective clothing applications. *Journal of Applied Polymer Science*, DOI: 10.1002/app.36611.

[10] Wang, C., Li, Y., Ding, G., Xie, X., & Jiang, M. (2012). Preparation and characterization of graphene oxide/poly (vinyl alcohol) composite nanofibers via electrospinning. *Journal of Applied Polymer Science*, DOI: 10.1002/app.37656.

[11] Shuiping, L., Lianjiang, T., Weili, H., Xiaoqiang, L., & Yanmo, C. (2010). Cellulose acetate nanofibers with photochromic property: Fabrication and characterization. *Materials Letters*, 64(22), 2427-2430.

[12] Son, W. K., Youk, J. H., & Park, W. H. (2006). Antimicrobial cellulose acetate nanofibers containing silver nanoparticles. *Carbohydrate Polymers*, 65(4), 430-434.

[13] Wang, X., Kim, Y. G., Drew, C., Ku, B. C., Kumar, J., & Samuelson, L. A. (2004). Electrostatic assembly of conjugated polymer thin layers on electrospun nanofibrous membranes for biosensors. *Nano Letters*, 4(2), 331-334.

[14] Celebioglu, A., & Uyar, T. (2011). Electrospun porous cellulose acetate fibers from volatile solvent mixture. *Materials Letters*, 65(14), 2291-2294.

[15] Sumin, L., Kimura, D., Yokoyama, A., Lee, K., Park, J. C., & Kim, I. (2009). The effects of laundering on the mechanical properties of mass-produced nanofiber web for use in wear. *Textile Research Journal*, 79(12), 1085-1090.

[16] Sumin, L., Kimura, D., Lee, K. H., Park, J. C., & Kim, I. S. (2010). The Effect of Laundering on the Thermal and Water Transfer Properties of Mass-produced Laminated Nanofiber Web for Use in Wear. *Textile Research Journal*, 80(2), 99-105.

[17] Kim, B. S., Kimura, N., Kim, H. K., Watanabe, K., & Kim, I. S. (2011). Thermal Insulation, Antibacterial and Mold Properties of Breathable Nanofiber-Laminated Wallpapers. *Journal of Nanoscience and Nanotechnology*, 11(6), 4929-4933.

[18] Yoon, B., & Lee, S. (2011). Designing waterproof breathable materials based on electrospun nanofibers and assessing the performance characteristics. *Fibers and Polymers*, 12(1), 57-64.

[19] Kang, Y. K., Park, C. H., Kim, J., & Kang, T. J. (2007). Application of electrospun polyurethane web to breathable water-proof fabrics. *Fibers and Polymers*, 8(5), 564-570.

[20] Choi, J. H., & Towns, A. D. (2001). Acetate dyes revisited: high fastness dyeing of cellulose diacetate and polyester—polyurethane. *Coloration Technology*, 117(3), 127-133.

[21] Khatri, Z., Wei, K., Kim, B. S., & Kim, I. S. (2011). Effect of deacetylation on wicking behavior of co-electrospun cellulose acetate/polyvinyl alcohol nanofibers blend. *Carbohydrate Polymers*, 87 (3), 2183-2188.

[22] ISO Standard Catalogue, *TC 38 Textiles*, ISO 105-C10: Colour fastness to washing with soap or soap and soda (2006).

[23] ISO Standard Catalogue, *TC 38 Textiles*, ISO 105-X11: Colour fastness to hot pressing (1994)

[24] ISO Standard Catalogue, *TC 38 Textiles*, ISO 105-B02: Colour fastness to artificial light: Xenon arc fading lamp test (1994).

[25] Tang, C., Chen, P., & Liu, H. (2008). Cocontinuous cellulose acetate/polyurethane composite nanofiber fabricated through electrospinning. *Polymer Engineering & Science*, 48(7), 1296-1303.

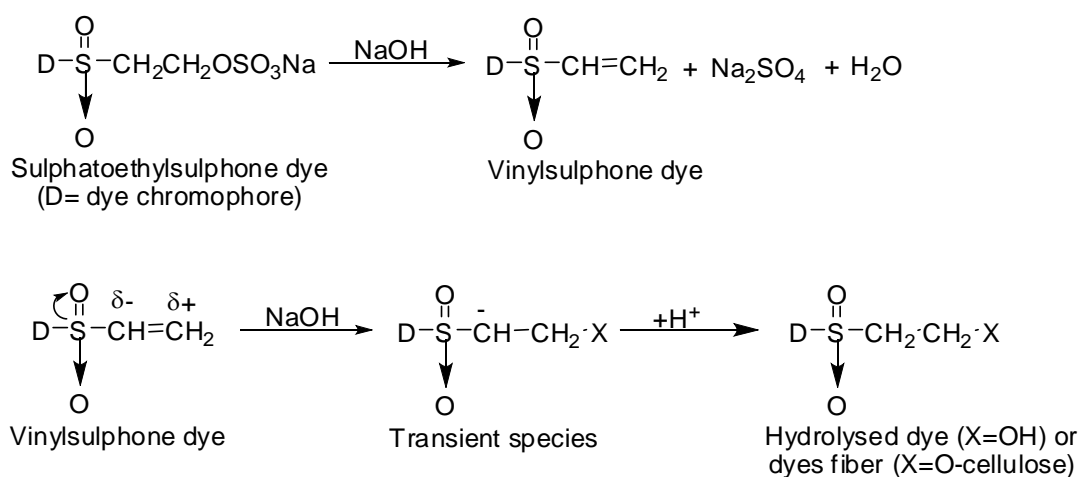
CHAPTER 5

DYEING OF CELLULOSE NANOFIBERS FOR IMPROVING COLOR YIELDS BY DUAL PADDING METHOD

5.1 INTRODUCTION

A great deal of research is underway to develop nonwoven fabrics based on electrospun nanofibers, because electrospinning is currently the only technique capable of producing continuous nanofibers from variety of polymers. The functional characteristics of electrospun nanofibers for apparel application have been reported [1-7]. Our group has just initiated to develop colored nanofibers; our series of recent work includes dyeability of cationic cellulose nanofibers with reactive dyes [8] and dyeing of cellulose acetate nanofibers with disperse dye [9] which extend the scope and versatility of nanofibers fabric. The difficult part in nanofiber dyeing is the final color yield obtained which approximately is four to five times lower than the conventional fibers. The transition from microfiber to nanofiber nonwovens leads to significant changes in the transport processes of the material as a result of the dramatic reduction in the pore dimensions and the large increase in the inner surface area [10]. The surface area of cellulose acetate nanofibers has been reported to be $3.5 \text{ m}^2/\text{g}$ [11], thirteen times higher than the conventional fibers and twice as high as super-microfibers [12]. The reason for lower color yield is mainly due to the higher surface area of nanofibers and their ability to

scatter more light. Therefore, we attempt to improve color yield of dyed nanofibers by simple dual padding method. In comparison to batchwise dyeing, the pad dyeing method has enormous advantages such as continuous process; higher dye fixation yield due to the less amount of water is needed and high amount of dye can be used [14]. We employed pad dyeing method in our work using padding step twice instead of once. Cellulose nanofibers were produced by electrospinning cellulose acetate nanofibers followed by deacetylation in alkaline bath. The cellulose nanofibers were dyed with CI reactive black 5 by single padding and dual padding; and the effect of dye concentrations on color yield dye fixation and color fastness have been investigated. The dyed nanofibers were further characterized by FTIR, WAXRD and FE-SEM analysis.



Scheme 5.1. Reaction mechanism of CI reactive black 5 with cellulose (Shore 2002)

5.2 EXPERIMENTAL

5.2.1 Materials

Cellulose acetate, CA (39.8% acetyl content having average Mw = 30 kDa) was obtained from Aldrich Chemical Company, and used without further purification. A commercial reactive dye was used namely, CI Reactive Black 5 (*Vinylsulfone*), supplied by Jay Chemical India; the corresponding dye structure is given in Fig.5.1. Sodium carbonate and Urea were used of Analar grade.

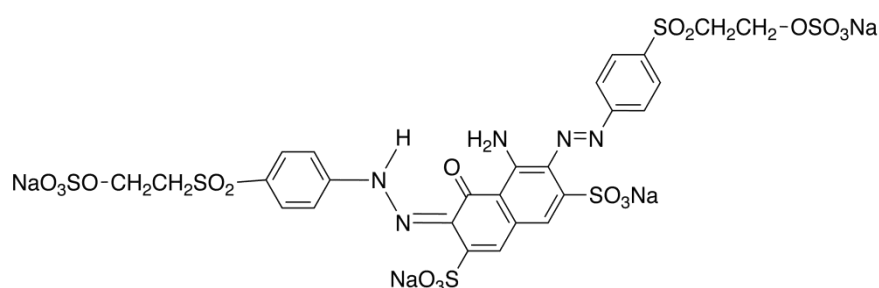


Fig. 5.1 Dye structure of CI reactive black 5

5.2.2 Preparing Cellulose nanofibers

Cellulose nanofibers were prepared by electrospinning of Cellulose Acetate (CA) nanofibers followed by deacetylation to remove acetyl groups. CA nanofibers were electrospun according to our previous report [13]. Briefly, A high-voltage power supply (Har-100*12, Matsusada Co., Tokyo, Japan) was used for electrospinning. CA solution of 17% by weight prepared in Acetone/ Dimethyl formamide (DMF) with 2:1 by weight was supplied

through a plastic syringe attached to a capillary tip with an inner diameter of 0.6mm with supplied voltage of 12.5 kV. The distance between the capillary tip and the collector was fixed at 15cm. Electrospun nanofibers were collected onto a rotating metallic drum/collector and removed after the average thickness of CA nanofibers of 60 μm was obtained. The nanofiber webs were air dried for at least 48 hours before deacetylation and dyeing. To convert cellulose acetate into cellulose, deacetylation was carried out at room temperature by soaking nanofibers in 0.05M NaOH aqueous solution for 30 hours and rinsed-off thoroughly in distilled water until the pH of nanofiber webs reached to 7. Finally, all cellulose nanofiber samples were dried at 50°C for 4 hours [14].

5.2.3 Dyeing of nanofibers

The nanofibre web samples were dyed by padding (two dip-two nip, 100% wet pick-up) through a dyebath solution using Rapid laboratory horizontal padding mangle. Dyebath containing 30 g/L dye, 25-30 g/L sodium carbonate, 50g/L Urea and 2 g/L sodium alginate. The samples were air dried followed by baking on a Rapid laboratory mini-dryer and finally, washing-off was carried out by exhaust method followed by (cold rinse \rightarrow warm rinse \rightarrow soaping-off \rightarrow warm rinse \rightarrow cold rinse). The soaping-off was carried out for 15 min at boil using contained 2 g/l Nonionic detergent (Hostpal AE Liq., Clariant). The liquor-to-good ratio was set to 50:1 during soaping. Baking temperature (100-180°C) and baking time (0–120 sec) were optimised prior to study the effect of dyeing concentrations on color yield. Dyeing experiments were followed by two sequences first, single padding of white nanofibers and second, double padding of dyed nanofibers. The dye concentrations for single padding were selected (20, 30, 40, 60 and 80 g/L), whereas,

the selected dyed nanofibers 20, 40 and 60 g/L were further double padded with 20, 40 and 60 g/L respectively. In addition, each of the dyed nanofibers (20, 40 and 60 g/L) were also double padded with 80 g/L of dye.

5.2.4 Color measurement and testing

Color strength (K/S) value and $CIE L^* a^* b^* C^*$ and h° coordinates [15] at the maximum absorption peak were measured on a Gretag Macbeth CE-7000A spectrophotometer (settings: 8.4 mm sample aperture, illuminant D65, UV included and specular component included). The K/S after soaping was obtained as the final color yield. Color fastness to washing was performed in Gyrowash (James H. Heal Co., UK) according to ISO 105-C10:2006 and color fastness to light was performed in Apollo (James H. Heal Co., UK) according to ISO 105-BO2 (20 hours).

5.2.5 Characterization

The chemical structure of CA nanofibers before and after dyeing was analysed for FTIR spectroscopy on an IR Prestige- 21 by Shimadzu, Japan. The wide-angle X-ray diffraction (WAXD) experiments were performed at room temperature with hybrid nanofiber samples using a Rotaflex RTP300 (Rigaku.Co., Japan) X-ray diffractometer operating at 50 kV and 200 mA. Nickel-filtered $Cu K_\alpha$ radiation was used for the measurements, along with an angular range of $5 < 2\theta < 30^\circ$. The morphology of undyed and dyed nanofibres were examined on an FE-SEM (S-5000 by Hitachi, Japan) with the accelerating voltage of 20 kV.

5.3 RESULTS AND DISCUSSION

5.3.1 Effect of dye concentration in single padding

Fig. 5.2 shows the effect of dye concentrations on color yield and dye fixation of nanofibers dyed with CI reactive black 5. Number of trials were undertaken to optimize baking temperature and baking time (data not shown), which concluded 120 °C and 90 sec as optimum baking temperature and baking time respectively. Color yield increased with increasing dye concentration from 20 g/L to 80 g/L, indicating a very good build up property on cellulose nanofibers. However, the dye fixation achieved maximum of 90% until the dye concentration of 40 g/L. The decreased dye fixation at 60 g/L and 80 g/L concentrations may be due to the dye hydrolysis[14].

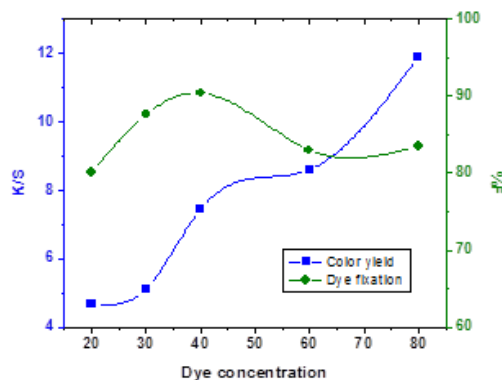


Fig. 5.2 Effect of dye concentration on color yield and dye fixation

In addition to K/S values, the colorimetric values (L^* , a^* , b^* , C^* and h^o) were measured for each dye concentration used tabulated in Table 5.1. As expected, the lightness value L^* decreased as the dye concentration was increased indicating the dyed nanofibers

became darker, the results are well in agreement with the K/S obtained. The negative a^* designate for the greenness and positive for the redness. In this case, consistently decreasing negative a^* with increasing dye concentration showed that a tone of dyed nanofibers shifting towards a redder region. On the other hand, negative b^* designated for blueness and positive for the yellowness. Since the CI reactive black 5 is bluer in tone, this is the reason why negative b^* obtained for all dye concentration; this is well demonstrated by the hue angle h^o that show all values within blue region. Decreasing C^* values with increasing dye concentration describes the dyed nanofibers became duller.

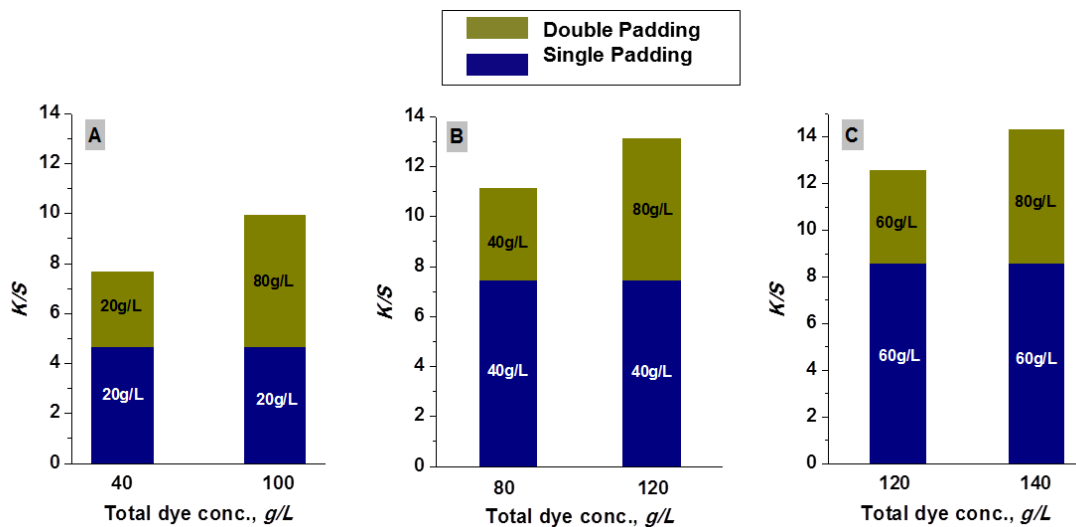


Fig. 5.3 Effect of dual padding on color yield

Table 5.1 Effect of dye concentration on colorimetric values

Dye conc. g/L	L*	a*	b*	C*	h°
20	43.55	-3.51	-19.55	19.87	259.82
30	41.40	-3.37	-18.62	19.34	259.76
40	35.82	-1.12	-19.30	18.92	266.69
60	32.87	0.20	-18.88	18.88	270.60
80	27.69	2.36	-17.34	17.50	277.76

5.3.2 Effect of dye concentration in dual padding

The surface area of cellulose acetate nanofibers has been reported to be 3.5 m²/g [20], 13 times higher than the conventional fibers and twice as high as super-microfibers (Bai et al., 2005). Our results show that the nanofibers exhibit lower K/S values than the conventional cotton fibers; this is mainly due to the higher surface area of nanofibers and their ability to scatter more light. For instance, cellulose nanofibers and cotton fabric were dyed with 20 g/L of CI reactive black 5, the K/S value obtained were 4.68 and 16.05 respectively. Our results are well in agreement with the report on dyeing of super-microfibers. It is worth noting that the dye concentration cannot be further increased in single padding, as the dye fixation value reduced significantly at dye concentration of 80 g/L. We, therefore, considered double padding of the dyed nanofibers with aim to investigate the extent of color yield enhancement. Fig. 5.3(A-C) is a stack plot for single and double padding which shows the extent of color yield enhanced by double padding

at various dye concentrations. It can be seen from the Fig. 5.3 enhancement of color yield is dependent upon the dye concentration used during the single padding. Comparing double paddings of 20 g/L, 40 g/L and 60 g/L in Fig. 5.3 A, B, and C, it was noticed that despite being higher dye concentration of 60 g/L, the color yield obtained was almost equal to the color yield of 20 g/L. The obvious reason for this may be the lesser dye sites available, as most of the surface area of nanofibers may be occupied by dye molecules, but this was true when the high amount dye was used during the single padding. Irrespective to the dye concentration used, doubling padding generally contributed a better enhancement in color yield. More interestingly, the dye fixation obtained for all double paddings were excellent between 80-90%. In addition to K/S values, the reflectance (%R) were measured for each double padded nanofiber sample and compared to their corresponding single paddings.

In Fig. 5.4 A, B and C, the CI reactive black 5 gives two reflectance values, one broad and low in the wavelength region between 360-500 nm and second sharp and high in the wavelength region between 700-750 nm. In comparison to single paddings, all double paddings show same with lower reflectance profile over the wavelength (360-750 nm) in comparison to single paddings. This indicates that the double paddings exhibit deeper of color than the single paddings.

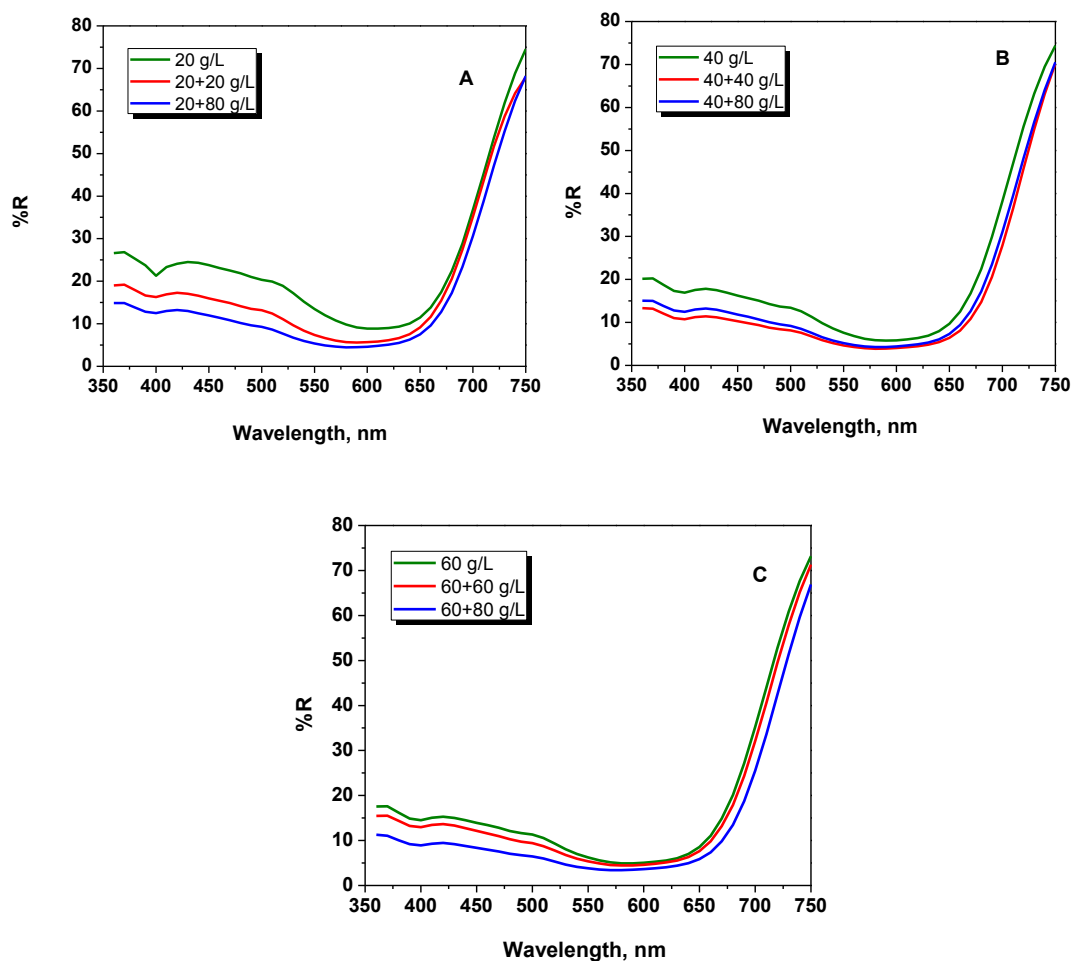


Fig. 5.4 Reflectance curves of CI reactive black 5

5.3.3 Color fastness properties

Table 5.2 shows color fastness results for nanofibers of single and double paddings with lower and higher dye concentrations. Single padding with 20 g/L shows a very good shade change and staining ratings among all other samples. The higher concentration of single padding with 80 g/L affected just half rating on shade change. The washing fastness results for double paddings were encouraging despite of very high dye

Table 5.2 Color fastness to light test ISO 105-BO2 and color fastness to washing test ISO 105-C10:2006

¹ Dye conc. (g/L)	Light fastness (20 hours)	Washing fastness (Change of shade)	² Washing fastness (Staining on multifiber)					
			CT	CO	PA	PES	PAC	Wo
20	2	4	5	5	5	4/5	4/5	4/5
80	2	3/4	5	4	4	4/5	4	3/4
20+20	2	3/4	5	4	4	4	4/5	4
60+80	2	3/4	5	4	4	3/4	4/5	3/4

¹Dyeing conditions: Baking temperature 120°C and baking time 90 sec

²CT, cellulose triacetate; CO, cotton; PA, polyamide; PES, polyester; PAC, polyacrylic; Wo, wool.

concentrations were used. The acceptable ratings for shade change and staining on multifibers indicate that the dye fixation was reasonably good.

The light fastness, on the other hand, was found to be very poor for all dyed nanofibers; this may be due to the small diameter of nanofibers than the conventional nanofibers, the light can easily penetrate into the interior of nanofibers that lead to more photo-fading of dye

5.3.4 Chemical structure of nanofibers

The FTIR spectra of nanofibers before and after dyeing with CI reactive black 5 are demonstrated in Fig. 5.5. The dyed and undyed nanofibers showed characteristic adsorption peaks of cellulose peaks around $1,000\text{--}1,200\text{ cm}^{-1}$. Other characteristic bands related to the chemical structure of cellulose were the hydrogen-bonded OH stretching at $3,550\text{--}3,100\text{ cm}^{-1}$, the CH stretching at $2,917\text{ cm}^{-1}$, and the CH wagging at $1,316\text{ cm}^{-1}$ [16]. The results indicated that the cellulose acetate has been completely converted into cellulose (Fig. 5.5A). In order to elucidate the effect of CI reactive dye, the FTIR spectrum of the dyed nanofibers was compared with that of the undyed cellulose nanofibers (Fig. 5.5A and C). The dyed cellulose nanofibers have an obvious new peaks at $1,744\text{ cm}^{-1}$ (C=O), $1,493\text{ cm}^{-1}$ (C=C), $1,236\text{ cm}^{-1}$ (C-O-C) and $1,047\text{ cm}^{-1}$ (C-OH). In the dye nanofibers Fig.5.5C, the peak $1,236\text{ cm}^{-1}$ corresponds to (C-O-C) became larger than the dye Fig.5.5B; the changes to peak intensity confirm the involvement of OH groups or CH_2OH groups of cellulose with the dye. The strong peak of carbonyl groups at $1,744\text{ cm}^{-1}$ indicates the existence of dye molecule in nanofibers. In comparison to the spectra of dye, the peak at $1,493\text{ cm}^{-1}$ decreased in dyed nanofibers (Fig.5.5C), yet another indication that most of the vinyl sulfone groups in dye may have been involved with the cellulose nanofibers. A small peak at around $1,047\text{ cm}^{-1}$ was depicted in dyed nanofibers, which is assigned to C-OH bending modes [17]

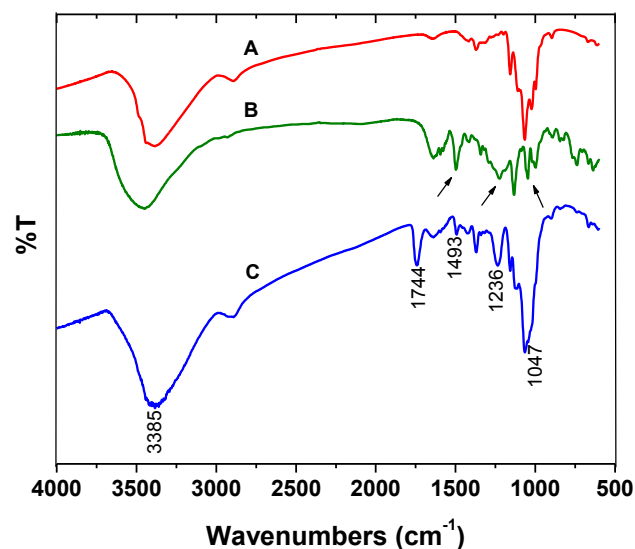


Fig.5.5 FTIR spectra of cellulose nanofibers without dye (A), CI reactive black 5 dye (B) and cellulose nanofibers dyed with CI reactive black 5 (C).

5.3.5 Morphology of Nanofibers

The effect of higher dye concentration on morphology of cellulose nanofibers, we examined nanofibers under FE-SEM. The Fig. 5.6 shows FE-SEM images of cellulose acetate nanofibers (A), undyed cellulose nanofiber (B) and dyed cellulose nanofibers (C); we selected dyed sample of highest dye concentration i.e. double padding of 60+80 g/L. It can be seen from the images that the dyed nanofibers having very smooth morphology and similar to the undyed nanofibers. Since the cellulose acetate was converted in to cellulose by deacetylation, therefore, the image (B) also exhibit similar surface morphology to that of the cellulose acetate nanofibers.

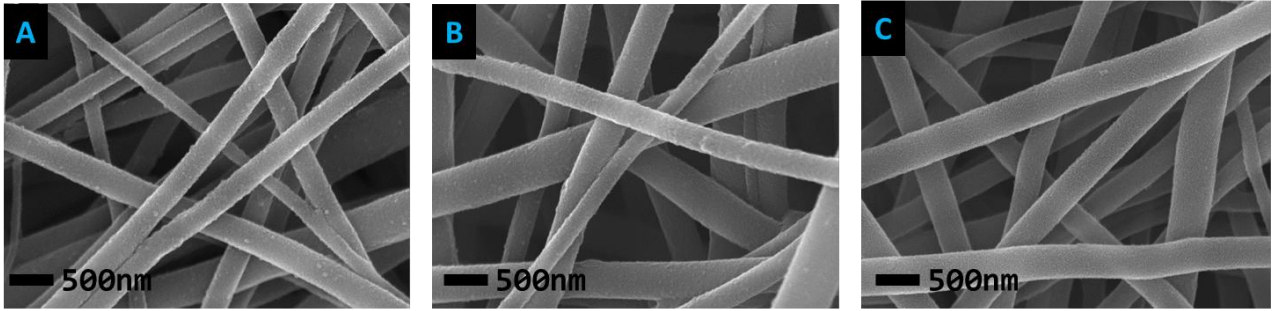


Fig. 5.6 FESEM images of cellulose acetate nanofibers (A), cellulose nanofibers without dye (B) and cellulose nanofibers dyed with CI reactive black 5 (C).

5.4 CONCLUSION

We conclude that the color yield of cellulose nanofibers can significantly be enhanced by dual padding with higher dye concentrations. The degree of color enhancement by dual padding is dependent on the dye concentration used in single padding. The problem of lower dye fixation at 80 g/L dye concentration in single padding was fixed; the dual padding offers improved color yields without affecting dye fixation values (80-90%). Except the light fastness, all dyed nanofibers exhibited a very good washing fastness.

5.4 REFERENCES

[1] Han, X. J., Huang, Z. M., He, C. L., Liu, L., & Wu, Q. S. (2008). Coaxial electrospinning of PC (shell)/PU (core) composite nanofibers for textile application. *Polymer Composites*, 29(5), 579-584.

- [2] Huang, L., Nagapudi, K., Apkarian, R. P., & Chaikof, E. L. (2001). Engineered collagen–PEO nanofibers and fabrics. *Journal of Biomaterials Science, Polymer Edition*, 12(9), 979-993.
- [3]Kang, Y. K., Park, C. H., Kim, J., & Kang, T. J. (2007). Application of electrospun polyurethane web to breathable water-proof fabrics. *Fibers and Polymers*, 8(5), 564-570.
- [4] Ding, B., Li, C., Hotta, Y., Kim, J., Kuwaki, O., & Shiratori, S. (2006). Conversion of an electrospun nanofibrous cellulose acetate mat from a super-hydrophilic to super-hydrophobic surface. *Nanotechnology*, 17(17), 4332-4339.
- [5] Kim, S. H., Nam, Y. S., Lee, T. S., & Park, W. H. (2003). Silk Fibroin Nanofiber. *Electrospinning, Properties, and Structure. Polymer journal*, 35(2), 185-190.
- [6]Yoon, B., & Lee, S. (2011). Designing waterproof breathable materials based on electrospun nanofibers and assessing the performance characteristics. *Fibers and Polymers*, 12(1), 57-64.
- [7] Greiner, A., & Wendorff, J. H. (2007). Electrospinning: a fascinating method for the preparation of ultrathin fibers. *Angewandte Chemie International Edition*, 46(30), 5670-5703.
- [8] Khatri, Z., Mayakrishnan, G., Hirata, Y., Wei, K., & Kim, I. S. (2012a). Cationic-Cellulose Nanofibers: Preparation and Dyeability with Anionic Reactive Dyes for Apparel Application. *Carbohydrate Polymers*. 91 (1), 434-443

- [9] Kim, B. S., Kimura, N., Kim, H. K., Watanabe, K., & Kim, I. S. (2011). Thermal Insulation, Antibacterial and Mold Properties of Breathable Nanofiber-Laminated Wallpapers. *Journal of Nanoscience and Nanotechnology*, 11(6), 4929-4933
- [10] Khatri, Z., Memon, M. H., Khatri, A., & Tanwari, A. (2011b). Cold Pad-Batch dyeing method for cotton fabric dyeing with reactive dyes using ultrasonic energy. *Ultrasonics sonochemistry*, 18(6), 1301-1307.
- [11] Khatri, Z., Khatri, A., Saleem, U., Mayakrishnan, G., Kim, B. S., Wei, K., & Kim, I. S. (2012b). Pad dyeing of cellulose acetate nanofibres with disperse dyes. *Coloration Technology*, DOI 10.1111/j.1478-4408.2012.00409.x
- [12] Khatri Z., Wei K., Kim B. S. and Kim I. S. (2011a). Effect of deacetylation on wicking behavior of co-electrospun cellulose acetate/polyvinyl alcohol nanofibers blend. *Carbohydrate Polymer*, 87(3), 2183-2188
- [13] Sumin, L., Kimura, D., Yokoyama, A., Lee, K., Park, J. C., & Kim, I. (2009). The effects of laundering on the mechanical properties of mass-produced nanofiber web for use in wear. *Textile Research Journal*, 79(12), 1085-1090.
- [14] Sumin, L., Kimura, D., Lee, K. H., Park, J. C., & Kim, I. S. (2010). The Effect of Laundering on the Thermal and Water Transfer Properties of Mass-produced Laminated Nanofiber Web for Use in Wear. *Textile Research Journal*, 80(2), 99-105.
- [15] Shore J. (1995). Dyeing with reactive dyes. In Shore J. (Ed.), *Cellulosic dyeing* (pp. 189-245). United Kingdom: Society of Dyers and Colourists.

[16] Bai, G., & Song, X. Y. (2005). Dyeing properties of polyamide super-microfibre with disperse dyes. *Coloration technology*, 121(6), 329-331.

[17] Chung, C., Lee, M., & Choe, E. K. (2004). Characterization of cotton fabric scouring by FT-IR ATR spectroscopy. *Carbohydrate polymers*, 58(4), 417-420.

CHAPTER 6

PREPARATION AND CHARACTERIZATION OF ELECTROSPUN POLY(ϵ -CAPROLACTONE) -POLY (L-LACTIC ACID) NANOFIBERS TUBES

6.1 INTRODUCTION

The nerve injury within a small nerve gape <6mm can be filled by implanting an extra nerve conduit (blood vessel) [1]. The clinical treatment involves donor nerves obtained from a second operative site of the patient, such as an autologous nerve graft, vein graft, or arterial graft but this technique suffers from donor site injury, shortage of donor tissue and abnormal regeneration. In order to address these issues, various bioengineered nerve grafts have been developed from polymeric materials that have well-tailored properties and dimensions [2].

Biodegradable nanofibrous tubes produced via electrospinning represent a new class of promising scaffolds to support nerve regeneration, because, the electrospinning represents an attractive approach to fabricate nanofibers continuously for neural tissue engineering application [3, 4]. These materials range from naturally derived polymers to non-degradable and biodegradable synthetic polymers [5]. Nerve guide conduits fabricated from biodegradable polymers are preferable to non-biodegradable polymers

because of the obvious advantage of eliminating a second surgery to remove the conduit [2]. So the selectivity of polymer in terms of biodegradability is one of the important parameters to be considered for nerve regeneration. The most widespread Electrospun nanofibers based on biodegradable polymers in neural tissue engineering are poly(ϵ -caprolactone) (PCL) [1, 6], poly (L-lactic acid) (PLLA) [7, 8], poly(l-lactide-co-glycolide) (PLGA)[9], poly(L-lactic acid-co- ϵ -caprolactone) (PLCL) [10], poly (L-lactic acid)- poly (D-lactic acid) PLLA-PDLA [11], poly (DL-lactide-co-glycolide)- poly(ϵ -caprolactone), PLGA-PCL [2], poly(L-lactic acid- ϵ -caprolactone), P(LLA-CL) [12], Silk fibroin (SF) [13]. Blending of biodegradable polymers have attracted recent interest in tissue engineering, as they offer exceptional potential in tailoring physical, biological and mechanical properties [14]. Blending could also serve as an effective route for controlling the properties of the biodegradable polymers.

PCL is commonly found in tissue engineering applications due to its structural and mechanical stability, better permeability and adequate cell binding properties [15, 16]. Owing to its slower biodegradation rates, blending PLA is often considered to enhance biodegradation [17]. PLA has been reported for faster biodegradation but possess low permeability [18]. The clear advantage of blending is that polymer in composition complement over each other, for instance PCL provides a better physical and mechanical stability, and the PLLA enhance the biodegradability. Keeping in view, we attempt to prepare blends of PCL-PLLA nanofibers that have not been investigated in terms of electrospinning nanofibers tubes and characterization, which in our opinion, is an essential preliminary study before the nanofibers tubes undergo for in-vivo or in-vitro

practice. Therefore, the present work deals with the electrospinning nanofibers from PCL-PLLA blends solutions and the resultant nanofibers tubes were characterized. The structure and the morphology electrospun tubes were examined under SEM. All nanofibers tubes were characterized by FTIR, Raman spectroscopy, WAXD and DSC analysis.

6.2 EXPERIMENTAL

6.2.1 Materials

Poly(ϵ -caprolactone) (PCL, Mw 80,000) was purchased from Sigma-Aldrich. A solution of 12% (w/w) PCL was dissolved in 1:9 w/w Dimethylformamide: chloroform. Poly(L-Lactic Acid) (PLLA, Mw 143,000) was purchased from Sigma-Aldrich. 8% (w/w) PLLA solution was prepared by dissolving in 3:1 w/w chloroform: Acetone. Three different blend ratio of PCL-PLLA were prepared as 2:1, 1:1, 1:2 s (w/w) and in addition neat PCL and neat PLLA were also prepared. Each blended polymer solution was mixed at 50 °C for at least 24 hours before electrospinning.

6.2.2 Method

Electrospinning with high-voltage power supply (Har-100*12, Matsusada Co., Tokyo, Japan), capable of generating voltages up to 100 kV, was used as the source of the electric field. The neat PCL, neat PLLA and PCL-PLLA solutions were supplied through a plastic syringe attached to a capillary tip with an inner diameter of 0.6mm. The copper

wire connected to a positive electrode (anode) was inserted into the polymer solution, and a negative electrode (cathode) was attached to a mandrel (collector). The voltage was fixed at 12 kV for all electrospinning solutions. The distance between the capillary tip and the collector was fixed at 12 cm and the plastic syringe was placed at an angle of 10° from the horizontal plane. Electrospun nanofibers were deposited continuously over stainless steel mandrel (diameter of 2 mm) for 120 to 150 minutes. The mandrel was rotated at 1,000 rpm and reciprocated for uniform deposition.

6.2.3 Characterization

The average diameters of nanofibers were analyzed by using Keyence Digital Microscope VH-Z500R at 5000× magnification. The average thickness of scaffold wall was measured by Digital Micrometer MCD130-25 with measuring sensitivity of 1 μm. All specimens were dried in a vacuum oven at 25 °C for a day before use. The morphology of nanofibers tube was examined under scanning electron microscope (SEM, S-3000N by Hitachi, Japan); all samples were sputtered with Pd-Pt before assessment.

The chemical structure of scaffold was analyzed on FTIR spectroscopy (IR Prestige-21 by Shimadzu, Japan). The Raman spectra were recorded with a Raman spectrometer (Hololab 5000, Kaiser Optical Systems Inc., USA), and argon laser at 532 nm, with a Kaiser holographic edge filter. Typically 50 mW of laser light was used at the sample with a × 50 long distance microscope objective. Integration times were around 40 s, and the spectral resolution was 1.2 cm⁻¹. The wide-angle X-ray diffraction (WAXD) pattern measurements were carried out with a fixed anode X-ray generator (Rotaflex RTP300, Rigaku.Co., Japan;

40 kV, 150 mA) with Cu K α radiation ($\lambda = 1.5402 \text{ \AA}$) at a scanning speed of $2\theta=2^\circ/\text{min}$. DSC analyses were performed using a Perkin-Elmer Pyris-1 analyzer. Both the temperature and heat flow were calibrated with a standard indium reference. The weight of nanofibers was maintained within a range of 1-2 mg. All thermal analyses were carried out under a dry nitrogen atmosphere.

6.3 RESULTS AND DISCUSSION

6.3.1 Morphology and structure of nanofibers tubes

Table 6.1 shows diameter of electrospun nanofibers and wall thickness of scaffold obtained for all blends. The duration of electrospinning for each nanofiber tube was between 120-150 minutes. The neat PLLA took little longer time than the neat PCL and PCL-PLLA blends. This may be due to PLLA nanofibers bulkiness that renders the scaffold wall thickness obtained later than that of the PCL nanofibers. The nanofiber diameter decreases with increasing PLLA ratio in the blends.

Table 6.1 Nanofiber diameter and tube wall thickness

PCL:PLLA Nanofibers tubes (blend ratio)	Average diameter of nanofibers (nm)	Tube wall thickness (μm)
1:0	860	55.1
2:1	847	58.42
1:1	812	60.5
1:2	783	62.08
0:1	715	64.7

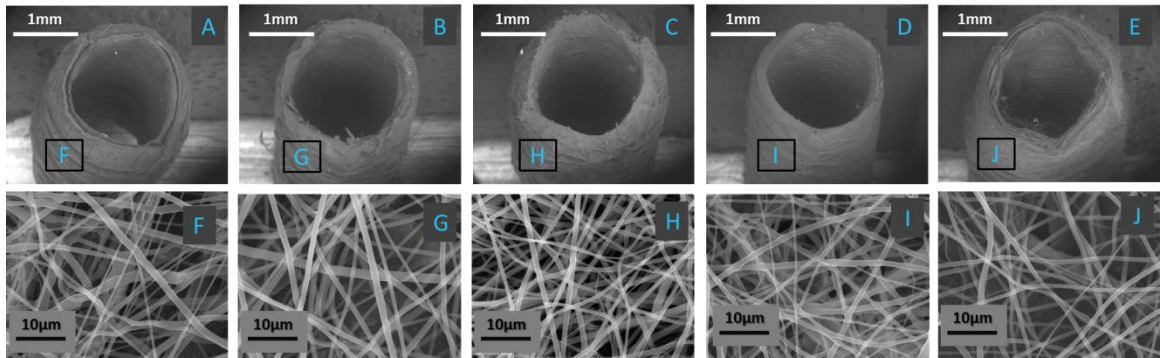


Fig. 6.1 SEM images for nanofiber tubes (A) neat PCL, (B) PCL-PLLA, 2:1, (C) PCL-PLLA, 1:1, (D) PCL-PLLA, 1:2 and (E) neat PLLA; the images F-E are corresponding tube wall surface.

Fig. 6.1 shows SEM images for all nanofibers tubes having inner diameter of approximately 2 mm. In general, the PCL nanofibers had relatively good cohesiveness in nanofibers that led the scaffold compact with cross section close to a circular shape (image A). Whilst the PLLA nanofiber was more bulky with relatively less cohesiveness in nanofibers and therefore, the cross section was physically unstable (image E). It can be seen from the scaffold images (B, C & D) that increasing PCL ratio in the PCL-PLLA blends leads to a better cross sections, physical and structural stability. The morphology of nanofibers of each scaffold surface is shown in Fig. 6.1 (F-J). Irrespective to the type of scaffold, the nanofibers demonstrated smooth morphologies with no beads that were produced via continuous electrospinning.

6.3.2 Chemical structure of PCL-PLLA nanofibers tubes

The FTIR spectra of neat PCL, neat PLLA and their blends nanofibers have been shown in Fig. 6.2 (a-e). The spectrum of neat PCL nanofibers (a) shows characteristic bands of carbonyl stretching $\nu(\text{C=O})$ at around $1,722\text{ cm}^{-1}$, asymmetric COC stretching $\nu_{\text{as}}(\text{COC})$ at $1,238\text{ cm}^{-1}$, OC–O stretching $\nu_{\text{s}}(\text{OC-O})$ at $1,190\text{ cm}^{-1}$ and symmetric COC stretching $\nu_{\text{s}}(\text{COC})$ at $1,164\text{ cm}^{-1}$. The two peaks at $2,945\text{ cm}^{-1}$ and $2,865\text{ cm}^{-1}$ were correspond to asymmetric CH_2 stretching $\nu_{\text{as}}(\text{CH}_2)$ and symmetric CH_2 stretching $\nu_{\text{s}}(\text{CH}_2)$ respectively. The bands at around $1,293\text{ cm}^{-1}$ and $1,157\text{ cm}^{-1}$ are assigned to the backbone C–O and C–C stretching in the crystalline phase (ν_{cr}) and in the amorphous phase (ν_{am}) respectively [19].

On the other hand, the FTIR spectrum of neat PLLA nanofibers (e) was also obtained. The main characteristic peaks at $1,750\text{ cm}^{-1}$ carbonyl stretching $\nu(\text{C=O})$, $1,452\text{ cm}^{-1}$ (the bending of CH_3) and $1,382\text{ cm}^{-1}$ (the symmetric deformation of CH_3). Moreover, the bands at $1,267\text{ cm}^{-1}$, $1,180\text{ cm}^{-1}$ and $1,082\text{ cm}^{-1}$ in neat PLLA nanofibers are assigned to the stretching of ether group $\nu(\text{COC})$ [20].

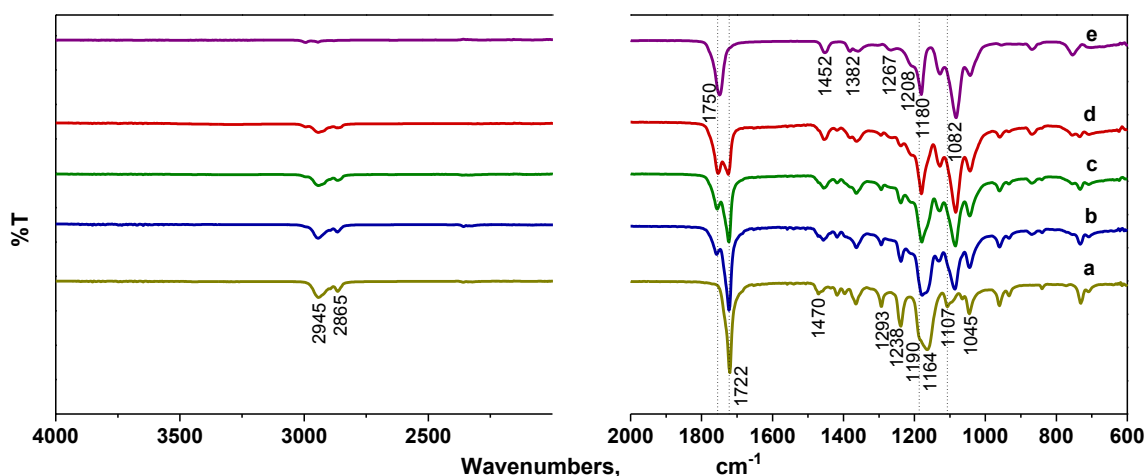


Fig. 6.2 FT-IR spectra for (a) neat PCL, (b) PCL-PLLA, 2:1, (c) PCL-PLLA, 1:1, (d) PCL-PLLA, 1:2 and (e) neat PLLA.

The spectra of the PCL-PLLA nanofibers blends (Fig. 6.2 b, c and d), show characteristic peaks of both PCL and PLLA with varying degree of intensities corresponding to the ratio of PCL to PLLA that indicates that the polymer blending is homogeneous. There was no new peak or peak-shift observed other than the characteristic peaks of PCL and PLLA nanofibers, which confirms that the PCL-PLLA blend nanofibers have retained their corresponding chemical structure. Considering the peaks appearance and intensities in the spectra of PCL-PLLA nanofibers blend, the blend ratio of PCL-PLLA 2:1 (Fig. 6.2 b) show PCL dominating characteristics while the blend ratio of PCL-PLLA 1:2 (Fig. 6.2 d) show PLLA dominating characteristics.

As a matter of fact that the molecular vibrations are inactive in FTIR, therefore, Raman spectra were taken to supplement FTIR spectra. It can be seen from the Raman spectra (Fig. 6.3) that the heights of Raman peaks vary linearly with the ratio of PCL and PLLA. The spectra of neat PLLA nanofibers show CH_3 asymmetric stretching at $3,002\text{ cm}^{-1}$ and CH_3 symmetric stretching at around $2,947\text{ cm}^{-1}$ [21], whilst the neat PCL nanofibers show obvious bands at $2,917\text{ cm}^{-1}$ and $2,872\text{ cm}^{-1}$, which correspond to C-H stretching. Likewise the FTIR spectra of PCL-PLLA blend nanofibers, the Raman spectra showed both characteristics of PCL and PLLA. In case of nanofibers blends, the broadening of peak at $1,443\text{ cm}^{-1}$ is appeared due to CH_3 asymmetric deformation in PLLA and CH_2 vibration in PCL.

6.3.3 Crystallinity of PCL-PLLA nanofibers tubes

Apart from the general characterization, some authors describe crystallinity by taking the peak intensities [22-24]. It is quite obvious from the Fig. 6.3 a ($3,200\text{-}2,700\text{ cm}^{-1}$) and b ($1,800\text{-}800\text{ cm}^{-1}$) that a few peak intensities in Raman spectra are significantly higher than the FTIR spectra. Briefly, the Raman peak at $1,725\text{ cm}^{-1}$ corresponds to the crystalline component of the carbonyl vibration in PCL, which is very sensitive to the degree of crystallinity [24] and on contrary the peak at $1,774\text{ cm}^{-1}$ corresponds to the amorphous component of the carbonyl vibration in PLLA [21]. Two crystalline Raman peaks were observed at $2,917\text{ cm}^{-1}$ and $2,878\text{ cm}^{-1}$ (νCH) in PCL. A few more crystalline domains appeared at $1,443\text{ cm}^{-1}$ and $1,420\text{ cm}^{-1}$ (δCH_2), $1,305\text{ cm}^{-1}$ and $1,284\text{ cm}^{-1}$

(ωCH_2), and at $1,110\text{ cm}^{-1}$ (skeletal stretching), 914 cm^{-1} (νCC of C-COO group), [24]. Owing to the better crystallinity of the neat PCL than the neat PLLA, the Raman spectra of the PCL-PLLA nanofibers blends show varying degree of crystallinity that is actually governed by increasing ratio of PCL in the blends.

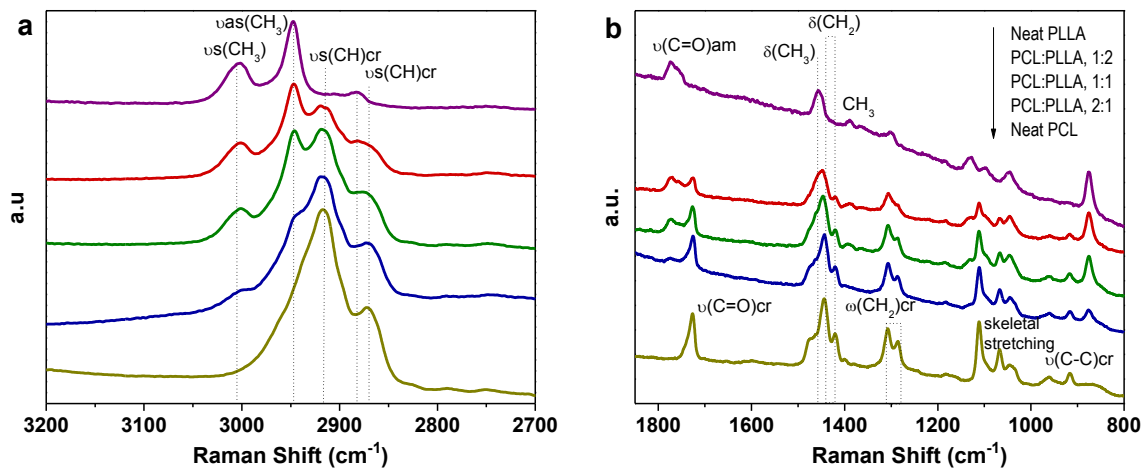


Fig. 6.3 Raman spectra for neat PCL, neat PLLA and their blends.

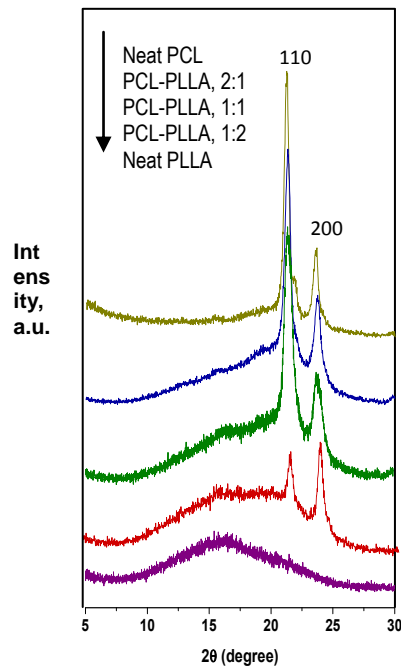


Fig. 6.4 XRD patterns for neat PCL, neat PLLA and their blends.

Fig. 6.4 presents the X-ray diffraction patterns of the PCL-PLLA nanofibers blends vs. that of the neat PCL and neat PLLA nanofibers. The neat PCL nanofibers showed two main peaks at Bragg angles $2\theta = 21.4^\circ$ and 23.8° , which attributed to the diffraction of the (110) lattice plane and the (200) lattice plane of semi-crystalline PCL, respectively [25]. On contrary, XRD pattern of neat PLLA nanofibers did not exhibit a crystalline nature; these results are well in agreement with previous report [11, 17, 26]. The reason for lower crystallinity is due to the nature of electrospinning process where quick stretching driven by a high electric field, and as a consequence, the PLLA chains don't get chance to arrange regularly and fit into crystalline lattices within such a short time (less than 0.1 s) [27]. Besides, substantial peaks at $2\theta = 21.4^\circ$ and 23.8° observed in the PCL-PLLA nanofibers blends by increasing PCL ratio in the blends. These peaks corresponded to the diffraction of PCL crystals. This may be the reason why PCL-PLLA nanofibers nerve guides have a better physical and mechanical stability than the neat PLLA nerve guide. It is worth to be noted that the handling of neat PLLA nerve guide was difficult in comparison to neat PCL and PCL-PLLA nerve guides.

6.3.4 Differential scanning calorimetry

Differential scanning calorimetry (DSC) thermograms were employed to investigate compatibility of PCL-PLLA nanofibers blends and shown in Fig. 6.5. The neat PLLA nanofibers displayed glass transition temperature (T_g) at 69.3°C , crystallizing temperature (T_c) at 82.6°C and melting temperature (T_m) at 176.5°C . The T_m of neat PCL

nanofibers displayed at 58.2 °C. It was noticed that the T_g region of PLLA overlaps significantly with the melting range of PCL, however, a recrystallization of PLLA was observed in two blends of PCL-PLLA (1:2 and 1:1) at 73.7°C, which was about 10 °C lower than the T_c of the neat PLLA nanofibers. This phenomenon supports the possible alignment and orientation of chains in PCL-PLLA blends. In addition, the PCL-PLLA nanofibers blends exhibit two melting peaks at 58.2 °C and 178.3 °C; the second peak, however, slightly higher than the melting peak of the neat PLLA nanofibers [17]. The recrystallization is relatively dependent on the PLLA ratio in the PCL-PLLA blends. Based on the results obtained, we can infer that recrystallization caused by segmental mobility in the PCL-PLLA blends (1:2 and 1:1) can be enhanced by keeping the PCL ratio less than or equal to the PLLA. Our results are well in agreement with the previous reports [28, 29].

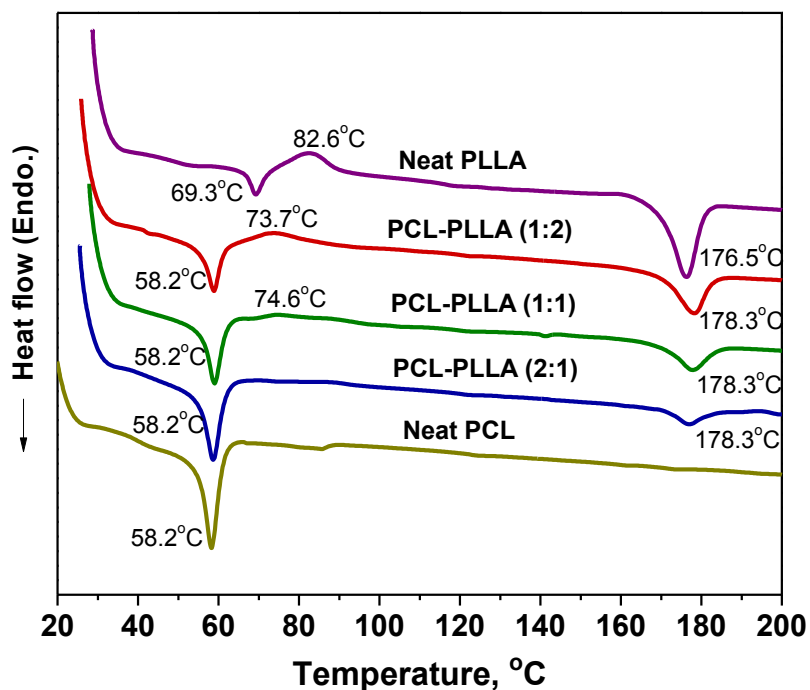


FIG. 6.5 DSC THERMOGRAMS FOR NEAT PCL, NEAT PLLA AND THEIR BLENDS.

6.4 CONCLUSION

The nerve guides of PCL and PLLA with various ratios were successfully fabricated via electrospinning. Except neat PLLA, all blends of PCL-PLLA and neat PCL showed a better morphology in terms of good structural stability and formability. More deposition time was required to obtain a reasonable nerve wall thickness as the PCL ratio was increased. FTIR study revealed that the PCL-PLLA blend nanofiber exhibit characteristic peaks of both PCL and PLLA. Raman and XRD studies demonstrated that crystallinity of the PCL-PLLA blends can be improved by increasing PCL ratio. The PCL and PLLA have very good compatibility as revealed by DSC; moreover, the recrystallization was observed in PCL-PLLA blends ratio of 1:2 and 1:1. Based on morphology of nanofibers tubes and characterization of PCL-PLLA, we conclude that these biomaterials may be a better substrate for further in-vivo or in-vitro investigation. Moreover, the biocompatibility of PCL and PLLA make these materials viable in tissue engineering.

6.4 REFERENCES

- [1] Ku, S. H., & Park, C. B. (2010). Human endothelial cell growth on mussel-inspired nanofiber scaffold for vascular tissue engineering. *Biomaterials*, 31(36), 9431-9437.
- [2] Panseri, S., Cunha, C., Lowery, J., Del Carro, U., Taraballi, F., Amadio, S., ... & Gelain, F. (2008). Electrospun micro-and nanofiber tubes for functional nervous regeneration in sciatic nerve transections. *BMC biotechnology*, 8(1), 39.

[3] Ramakrishna, S., Jose, R., Archana, P. S., Nair, A. S., Balamurugan, R., Venugopal, J., & Teo, W. E. (2010). Science and engineering of electrospun nanofibers for advances in clean energy, water filtration, and regenerative medicine. *Journal of materials science*, 45(23), 6283-6312.

[4] Xie, J., MacEwan, M. R., Schwartz, A. G., & Xia, Y. (2010). Electrospun nanofibers for neural tissue engineering. *Nanoscale*, 2(1), 35-44.

[5] Wang, S., & Cai, L. (2010). Polymers for fabricating nerve conduits. *International Journal of Polymer Science*, 2010.

[6] Lee, S. J., Oh, S. H., Liu, J., Soker, S., Atala, A., & Yoo, J. J. (2008). The use of thermal treatments to enhance the mechanical properties of electrospun poly (ϵ -caprolactone) scaffolds. *Biomaterials*, 29(10), 1422-1430.

[7] Yang, F., Murugan, R., Ramakrishna, S., Wang, X., Ma, Y. X., & Wang, S. (2004). Fabrication of nano-structured porous PLLA scaffold intended for nerve tissue engineering. *Biomaterials*, 25(10), 1891-1900.

- [8] Patra, S. N., Easteal, A. J., & Bhattacharyya, D. (2009). Parametric study of manufacturing poly (lactic) acid nanofibrous mat by electrospinning. *Journal of materials science*, 44(2), 647-654.
- [9] Bini, T. B., Gao, S., Wang, S., & Ramakrishna, S. (2006). Poly (l-lactide-co-glycolide) biodegradable microfibers and electrospun nanofibers for nerve tissue engineering: an in vitro study. *Journal of materials science*, 41(19), 6453-6459.
- [10] Tian, L., Prabhakaran, M. P., Ding, X., Kai, D., & Ramakrishna, S. (2012). Emulsion electrospun vascular endothelial growth factor encapsulated poly (l-lactic acid-co- ϵ -caprolactone) nanofibers for sustained release in cardiac tissue engineering. *Journal of Materials Science*, 1-10.
- [11] Zong, X., Kim, K., Fang, D., Ran, S., Hsiao, B. S., & Chu, B. (2002). Structure and process relationship of electrospun bioabsorbable nanofiber membranes. *Polymer*, 43(16), 4403-4412.
- [12] Xu, C. Y., Inai, R., Kotaki, M., & Ramakrishna, S. (2004). Aligned biodegradable nanofibrous structure: a potential scaffold for blood vessel engineering. *Biomaterials*, 25(5), 877-886.

[13] Marelli, B., Alessandrino, A., Farè, S., Freddi, G., Mantovani, D., & Tanzi, M. C. (2010). Compliant electrospun silk fibroin tubes for small vessel bypass grafting. *Acta Biomaterialia*, 6(10), 4019-4026.

[14] Carfi Pavia, F., La Carrubba, V., & Brucato, V. (2009). Tuning of biodegradation rate of PLLA scaffolds via blending with PLA. *International Journal of Material Forming*, 2:713

[15] Hollister, S. J. (2005). Porous scaffold design for tissue engineering. *Nature materials*, 4(7), 518-524.

[16] Gross, R. A., & Kalra, B. (2002). Biodegradable polymers for the environment. *Science*, 297(5582), 803-807.

[17] Zeng, J., Chen, X., Liang, Q., Xu, X., & Jing, X. (2004). Enzymatic Degradation of Poly (L - lactide) and Poly (ϵ - caprolactone) Electrospun Fibers. *Macromolecular bioscience*, 4(12), 1118-1125.

[18] Kim, K., Yu, M., Zong, X., Chiu, J., Fang, D., Seo, Y. S., ... & Hadjiargyrou, M. (2003). Control of degradation rate and hydrophilicity in electrospun non-woven poly (D, L-lactide) nanofiber scaffolds for biomedical applications. *Biomaterials*, 24(27), 4977-4985.

- [19] Elzein, T., Nasser-Eddine, M., Delaite, C., Bistac, S., & Dumas, P. (2004). FTIR study of polycaprolactone chain organization at interfaces. *Journal of colloid and interface science*, 273(2), 381-387.
- [20] He, J., Qin, Y., Cui, S., Gao, Y., & Wang, S. (2011). Structure and properties of novel electrospun tussah silk fibroin/poly (lactic acid) composite nanofibers. *Journal of Materials Science*, 46(9), 2938-2946.
- [21] Furukawa, T., Sato, H., Murakami, R., Zhang, J., Noda, I., Ochiai, S., & Ozaki, Y. (2006). Raman microspectroscopy study of structure, dispersibility, and crystallinity of poly (hydroxybutyrate)/poly (l-lactic acid) blends. *Polymer*, 47(9), 3132-3140.
- [22] He, Y., & Inoue, Y. (2000). Novel FTIR method for determining the crystallinity of poly (ϵ - caprolactone). *Polymer international*, 49(6), 623-626.
- [23] Taddei, P., Tinti, A., & Fini, G. (2001). Vibrational spectroscopy of polymeric biomaterials. *Journal of Raman Spectroscopy*, 32(8), 619-629.
- [24] Hartman, O., Zhang, C., Adams, E. L., Farach-Carson, M. C., Petrelli, N. J., Chase, B. D., & Rabolt, J. F. (2010). Biofunctionalization of electrospun PCL-based scaffolds with perlecan domain IV peptide to create a 3-D pharmacokinetic cancer model. *Biomaterials*, 31(21), 5700-5718.

[25] Meng, Z. X., Zheng, W., Li, L., & Zheng, Y. F. (2010). Fabrication and characterization of three-dimensional nanofiber membrane of PCL–MWCNTs by electrospinning. *Materials Science and Engineering: C*, 30(7), 1014-1021.

[26] Liu, D., Yuan, X., & Bhattacharyya, D. (2012). The effects of cellulose nanowhiskers on electrospun poly (lactic acid) nanofibres. *Journal of Materials Science*, 1-7.

[27] Reneker, D. H., Yarin, A. L., Fong, H., & Koombhongse, S. (2000). Bending instability of electrically charged liquid jets of polymer solutions in electrospinning. *Journal of Applied physics*, 87(9), 4531-4547.

[28] Yang, J. M., Chen, H. L., You, J. W., & Hwang, J. C. (1997). Miscibility and Crystallization of Poly (L-lactide)/Poly (ethylene glycol) and Poly (L-lactide)/Poly (EPSILON.-caprolactone) Blends. *Polymer journal*, 29(8), 657-662.

[29] Kim, C. H., Cho, K. Y., Choi, E. J., & Park, J. K. (2000). Effect of P (ILA - co - ε CL) on the compatibility and crystallization behavior of PCL/PLLA blends. *Journal of applied polymer science*, 77(1), 226-231.

SUMMARY

The effect of deacetylation was evaluated with respect to wicking rate. Three nanofibers webs were prepared, out of which the CA/PVA (10%) nanofibers blend demonstrates faster and more uniform wicking rate as compared to the CA/PVA (15%) nanofibers blends and CA without PVA nanofibers webs. The blending of PVA nanofibers significantly decreases the wicking rate if not deacetylated. After deacetylation, all types of nanofibers webs used in this study showed overall enhanced wicking rate. The vertical capillary method provides a better understanding of wicking behavior than the water contact angle of nanofibers webs. FTIR data showed no chemical reaction between CA nanofibers and PVA nanofibers. The deacetylation had significantly affected the nanofibers web thickness, which brought a positive change in terms of increase in nanofibers network as study showed by SEM analysis. Such type of nanofibers webs can be used where the faster wicking is desired such as, biosensor strips and other medical

The cationic-cellulose and cellulose nanofibers can effectively be dyed with commercially available reactive dyes by batchwise method. The cationic-cellulose nanofibers demonstrated potential advantages over cellulose nanofibers due to enhanced color yield and higher dye fixation without addition of electrolyte. Built-up property of each dye showed improvement at all dye concentrations in case of cationic-cellulose nanofibers. Except CI reactive blue 19, it was observed that there was no significant improvement in color yield and dye fixation at the dye concentration of 5%. Excellent color fastness to washing results were achieved for both dyed cellulose and cationic-cellulose nanofibers. Despite the number of wet treatments, the morphology of nanofibers remains structurally stable, smooth and regular. The cellulose based

colored and breathable nanofibers paved the way toward novel apparel applications and can potentially be considered as future apparel for surgical gowns, institutional articles, casual and fashion.

The dyeing of CA nanofibers can effectively be dyed with disperse dyes by pad-dry-bake method. The dyeing results were mainly dependent on baking temperature and the dye class used. It was generally observed that the high energy level dye, CI Disperse Red 167:1, had better color yield and color fastness results than the low energy level dye, CI Disperse Blue 56. Besides successful dyeability and good color fastness results (washing, light and hot pressing), Young's modulus of dyed nanofibers increased around three times than the undyed CA nanofibers, therefore, proposed colored nanofibers worth considering for aesthetically pleasing apparel as well as for casual apparel use.

We conclude that the color yield of cellulose nanofibers can significantly be enhanced by dual padding with higher dye concentrations. The degree of color enhancement by dual padding is dependent on the dye concentration used in single padding. The problem of lower dye fixation at 80 g/L dye concentration in single padding was fixed; the dual padding offers improved color yields without affecting dye fixation values (80-90%). Except the light fastness, all dyed nanofibers exhibited a very good washing fastness.

The nerve guides of PCL and PLLA with various ratios were successfully fabricated via electrospinning. Except neat PLLA, all blends of PCL-PLLA and neat PCL showed a better morphology in terms of good structural stability and formability. More deposition time was required to obtain a reasonable nerve wall thickness as the PCL ratio was increased. FTIR study revealed that the PCL-PLLA blend nanofiber exhibit characteristic peaks of both PCL and PLLA.

Raman and XRD studies demonstrated that crystallinity of the PCL-PLLA blends can be improved by increasing PCL ratio. The PCL and PLLA have very good compatibility as revealed by DSC; moreover, the recrystallization was observed in PCL-PLLA blends ratio of 1:2 and 1:1. Based on morphology of nanofibers tubes and characterization of PCL-PLLA, we conclude that these biomaterials may be a better substrate for further in-vivo or in-vitro investigation. Moreover, the biocompatibility of PCL and PLLA make these materials viable in tissue engineering.

ACCOMPLISHMENTS

JOURNAL PUBLICATIONS

1. **Zeeshan Khatri**, Kai Wei, Byoung-Suhk Kim, Ick-Soo Kim, Effect of deacetylation on wicking behavior of co-electrospun cellulose acetate/polyvinyl alcohol nanofibers blend, *Carbohydrate Polymers*, 87 (3), 2183-2188, (2012).

2. **Zeeshan Khatri**, Gopiraman Mayakrishnan, Yuichi Hirata, Kai Wei, Ick-Soo Kim, Cationic-Cellulose Nanofibers: Preparation and Dyeability with Anionic Reactive Dyes for Apparel Application, *Carbohydrate Polymers*, 91 (1), 434-443, (2013).

3. **Zeeshan Khatri**, Awais Khatri, Umaima Saleem, Gopiraman Mayakrishnan, Byoung-Suhk Kim, Kai Wei, and Ick-Soo Kim, Pad dyeing of cellulose acetate nanofibers with disperse dyes, *Coloration Technology*, 129 (2), 159–163, (2013).

4. **Zeeshan Khatri**, Rabia Almas Arain, Abdul Waha Jatoy, Gopiraman Mayakrishnan, Kai Wei and Ick-Soo Kim, Dyeing of cellulose nanofibers for improving color yields by dual padding method, *Cellulose*, 20 (3), 1469-1476. (2013).

5. **Zeeshan Khatri**, Gopiraman Mayakrishnan, Kai Wei, Ick-Soo Kim, Characterization of poly(ϵ -caprolactone)/poly(L-lactic acid) nanofibers tubes prepared via electrospinning, *Journal of Materials Science*. 48 (10), 3659-3664 (2013)

6. Gopiraman Mayakrishnan, S Ganesh Babu, **Zeeshan Khatri**, Kai Wei, M Endo, R Karvembu and Ick Soo Kim, Facile and Homogeneous Decoration of RuO₂ Nanorods on Graphene Nanoplatelets for Transfer Hydrogenation of Carbonyl Compounds *Catalysis Science and Technology*, 3 (6), 1485-1489 (2013)

7. Gopiraman Mayakrishnan, Fujimori Kazushige, **Zeeshan Khatri**, Byoung-Suhk Kim, Ick-Soo Kim, Structural and mechanical properties of cellulose acetate/graphene hybrid nanofibers: spectroscopic investigations *Express Polymer Letters*, 7 (6), 554-563 (2013)

8. Mayakrishnan Gopiraman, Sundaram Ganesh Babu , **Zeeshan Khatri**, Wei Kai, Yoong Ahm Kim, Morinobu Endo, Ramasamy Karvembu and Ick Soo Kim, An efficient copper oxide nanoparticles over multi-wall carbon nanotubes catalyst for N-arylation of imidazole
Journal of Physical Chemistry- C, Under review (2013)

9. Mayakrishnan Gopiraman, Sundaram Ganesh Babu , **Zeeshan Khatri**, Wei Kai, Yoong Ahm Kim, Morinobu Endo, Ramasamy Karvembu and Ick Soo Kim, Dry Synthesis of Easily Tunable Nano Ruthenium Supported on Graphene – Novel Nanocatalysts for Aerial Oxidation of Alcohols and Transfer Hydrogenation of Ketones
Carbon, 62, 135–148 (2013)

10. Shamshad Ali, **Zeeshan Khatri**, Kyung Wha Oh, Ick-Soo Kim and Seong Hun Kim, Preparation and characterization of hybrid Polycaprolactone/Cellulose ultrafine fibers via Electrospinning
Carbohydrate Polymers, Under review (2013)

11. **Zeeshan Khatri**, Yotaro Nakajima, Imran Khatri, Gopiraman Mayakrishnan, Kai Wei and Ick-Soo Kim, Cell Adhesion Behavior of Electrospun Poly(ϵ -caprolactone) -Poly (L-Lactic Acid) Nanofibers Scaffold
Materials Letters, Submitted (2013)

LIST OF CONFERENCE PRESENTATIONS

- 1. Zeeshan Khatri**, Ick Soo Kim, Byoung Suhk Kim, Kyu-Oh Kim and Nakashima Ryu, Electrospun Polycaprolactum Nanofiber Tubes- Preparation and Characterization
NanoTech Conference and Expo 2011, Boston, MA, United States, 13-16 June 2011. [POSTER]
- 2. Ja-Lam Gu, Zeeshan Khatri**, Byoung-Suhk Kim, Myung-Seob Khil, Hak-Yong Kim and Ick-Soo Kim, Fabrication of Kenaf-based Composite Nanofiber via Electrospinning
Nano Korea (KINTEX), South Korea, 24-26 August 2011. [POSTER]
- 3. Zeeshan Khatri**, Wei Kai, Byoung Suhk Kim and Ick Soo Kim, Effect of Deacetylating on Wicking Rate of Co-electrospun Cellulose Acetate/ Polyvinyl Alcohol Nanofiber Blends
4th International Symposium on High-Tech Fiber Engineering for Young Researcher, Shinshu University, Ueda city, Nagano, Japan, August 29- September 4, 2011. [ORAL]
- 4. Zeeshan Khatri**, Umaima Saleem, Muhammad Hanif Memon and Ick Soo Kim, Ionic crosslinking of hospital green fabric using cationic glycerin
ATC-11, Daegu, South Korea, November 1-4, 2011. [ORAL]
- 5. Zeeshan Khatri**, Kai Wei, Byoung-Suhk Kim and Ick-Soo Kim, Coloration of cationic-cellulose nanofiber with reactive dyes,
6th ICAFTM, Ueda, Nagano, Japan, 7-9 December 2011. [POSTER]
- 6. Zeeshan Khatri**, Byoung-Suhk Kim, Kyu-Oh Kim and Ick-Soo Kim, Cellulose acetate nanofibers- a water permeable membrane with enhanced wicking
2nd Nanotoday, Hawaii, United States, 11-15 December 2011. [POSTER]
- 7. Zeeshan Khatri**, Byoung-Suhk Kim and Ick-Soo Kim, Ultrasonic assisted dyeing of cotton fabric- Enhanced dyeing rate without thermal energy
2nd International Conference EESD 2012, Pakistan, Feb 27-29, 2012. [ORAL]
- 8. Zeeshan Khatri**, Byoung-Suhk Kim and Ick-Soo Kim, Electrospun polycaprolactone/ poly(L-Lactide Acid) nanofibers tubes- Biodegradable polymers for nerve regeneration
2nd International Conference EESD 2012, Pakistan, Feb 27-29, 2012. [ORAL]
- 9. Zeeshan Khatri** and Ick-Soo Kim, Colored Nanofiber-preparation and dyeability for apparel application
Nanofiber 2012, Tokyo Institute of Technology, Japan, June 4-5, 2012. [ORAL]
- 10. Zeeshan Khatri**, Kai Wei and Ick-Soo Kim Photochromic nanofibers- preparation and characterization
Hybrid Materials 2013, Sorrento (near Naples), Italy, March 3-7, 2013 [POSTER]

11. Zeeshan Khatri, Kai Wei and Ick-Soo Kim, Nanofibers- preparation and potential application
4th International Conference on Textile and Clothing, Pakistan, March 28-30, 2013. [ORAL]

12. Zeeshan Khatri, Kai Wei, Ick-Soo Kim, Nanofibers preparation and potential applications,
ICTC 2013, Lahore, Pakistan, 28-31 March 2013. [ORAL- Video conference]

13. Zeeshan Khatri, Kai Wei and Ick-Soo Kim, Photochromic Nanofibers
2013 AATCC International Conference, South Carolina, United States April 9-11, 2013 [ORAL]

14. Shamshad Ali, **Zeeshan Khatri**, Kyung-Wang Oh, Ick-Soo Kim, Seong-Hun Kim,
Preparation and Characterization of Polycaprolactone-Cellulose Hybrid Sub-microfibers
The International Textile Conference, Daegu, South Korea, 16-18 April 2013.

15. Shamshad Ali, **Zeeshan Khatri**, Kyung-Wang Oh, Ick-Soo Kim, Seong-Hun Kim, Fabrication
of Ultrafine Polycaprolactone-Cellulose Fibrous Membranes
ATC-12, Shanghai, China. 23-26 October 2013.

PATENTS

1. 特願 2012-170687 車載ランプ用通気防水膜
2. 特願 2012-170688 電子部品用通気防水膜